universität wien

DISSERTATION

Species-Specific Evolving Regions in the Human and Chimpanzee Genomes

angestrebter akademischer Grad

Doktor der Naturwissenschaften (Dr. rer.nat.)

Verfasser:	Ricardo de Matos Simões
Matrikel-Nummer:	648262
Dissertationsgebiet (lt. Studienblatt):	Molekularbiologie
Betreuer:	Univ.-Prof. Dr. Arndt von Haeseler

Wien, im Juni 2010

... ontogeny does not recapitulate phylogeny: it creates it.

Walter Garstang (1922)

Abstract

Comparative analyses of the human and chimpanzee transcriptomes aim at the identification of genes whose expression pattern has changed since both species last shared a common ancestor. This approach complements the search for genes with altered function in compiling the catalogue of genetic changes responsible for the distinct phenotypes of the contemporary species. However, gene expression analyses are ultimately dependent on the availability of tissue samples. Embryonic tissues from chimpanzees are rare, if available at all. Thus, changes in the gene expression pattern in these early stages of ontogenesis, which potentially play a key role in differential development, are likely to be missed. Here I present a bioinformatics approach to identify candidates that may be expressed in a species-specific manner. Specifically, I have searched for genes in the human and chimpanzee genomes of which evolutionary sequence change shows signs of different extents of transcription-coupled-repair in the two species. Human, chimpanzee and rhesus branch-specific substitution matrices were estimated for 12,596 non-overlapping sliding windows 125 Kb in size representing the transcribed fraction in a human-chimpanzee-rhesus genome alignment. Applying a novel test statistic, 717 transcribed regions were identified in which the estimated branch-specific substitution models differ significantly between humans and chimpanzees. More specifically, it is shown that the two species differ mainly in their relative rates of $A \leftrightarrow G$ and $T \leftrightarrow C$ substitutions, and in the rate ratio of the two transition types. This pattern is expected when transcription-coupled-repair acts to different extents on the corresponding genes in the two species and provides initial evidence that these genes may be differentially expressed during early stages of human and chimpanzee development. A subsequent Gene Ontology enrichment analysis of the corresponding genes revealed an enrichment for embryonic developmental processes such as anatomical structure development (e.g., skeleton, spinal cord, brain, gut), neurogenesis, signal transduction and regulation processes for transcription, translation and replication.

Contents

Chapter 1

Introduction

Humans and their closest living relatives, the chimpanzees, separated from their last common ancestor only about 5 million years ago. Since then substitutions have driven the divergence of the two genomes such that now on average 1.2% of compared bases between humans and chimpanzees differ (CSAC, 2005). The small genetic difference of the two contemporary species is contrasted by the markedly distinct phenotypes. It was therefore hoped that those genetic changes are identifiable that account for the major phenotypic changes during the evolution of humans and chimpanzees. However, despite numerous attempts (e.g., Varki and Altheide, 2005), no major breakthrough has yet been achieved. Only a handful of genetic changes in protein coding sequences have been detected that are suspected of having a major impact on the evolution of the species phenotype (e.g., Vallender and Lahn, 2004). Accordingly, the question was raised as to whether it is indeed substitutions in the protein sequences that played a major role during the evolution of the species. Alternatively, changes in the pattern of gene expression may be the driving force of phenotypic evolution (King and Wilson, 1975). Meanwhile, a number of comparative studies have been performed on the transcriptomes of humans and chimpanzees and identified a catalogue of genes that are differentially expressed in the two species (Enard *et al.*, 2002; Caceres *et al.*, 2003; Uddin *et al.*, 2004; Khaitovich *et al.*, 2005). Genome-wide transcriptome comparisons between humans and chimpanzees using microarrays have been performed in a variety of studies (Enard *et al.*, 2002; Khaitovich *et al.*, 2005; Gilad *et al.*, 2006; Marvanova *et al.*, 2003; Caceres *et al.*, 2003; Karaman *et al.*, 2003; Uddin *et al.*, 2004). The first published study compared human and chimpanzee gene expression in liver and brain tissues (Enard *et al.*, 2002). Among the differentially expressed genes in brain tissues a higher fraction of genes were

upregulated in humans compared to chimpanzees. In the other tissues such a trend was not observed. The study of Khaitovich *et al.* (2005) reported that in testis the largest number of differentially expressed genes were found compared to other tissues. Brain tissues showed the least gene expression differences between humans and chimpanzees. Gene expression differences were observed to be correlated with sequence divergence of the encoded proteins. Tissue-specific genes seem to show more expression divergence than genes that have no tissue specific expression patterns.

The measurement of gene expression using microarrays is limited by high noise levels due to technical difficulties, e.g., in the hybridization procedures and also biological fluctuations of the observed gene expression levels. For example the measurement of individual gene expression levels are not constant and can differ depending on variables such as gender (Reinius *et al.*, 2008), tissue types and different environments throughout various developmental stages, where the individual tissue and specific cell types emerge (Khaitovich *et al.*, 2006).

Comparative gene expression analysis between humans and chimpanzees are restricted to adult tissues. Gene expression changes during early embryogenesis that may be responsible for the observed differences of the phenotypes between humans and chimpanzees have therefore not been considered. Due to ethical reasons gene expression analyses from embryonic tissue samples of humans and chimpanzees are not feasible. An experimental approach may therefore miss differences of genes active early in embryonic development since the required samples are not available; moreover, subtle changes in the gene expression level may be overlooked due to too stringent cut-offs.

Here, a bioinformatics approach is proposed to predict genes whose expression is likely to have changed during human and chimpanzee evolution. To this end, we utilize the proposed influence of transcription-coupled-repair on the substitution pattern in transcribed sequences (Green, 2003). Genes that are differentially expressed in the two species should be subject to different extents of transcription-coupled-repair, and thus should differ in their rates and patterns of DNA sequence change. In general, DNA sequences of humans and chimpanzees are believed to evolve with the same evolutionary rates and the same substitution model (Ebersberger *et al.*, 2002; Webster *et al.*, 2003). Exceptions to this assumption have been described (Ebersberger and Meyer, 2005), but a genome-wide analysis of this aspect has not been conducted.

The study that was conducted in this thesis aims to identify differences in the sub-

stitution model between humans and chimpanzees that are exclusively derived from a different extend of the $A \rightarrow G$ substitution rate and are presumed to result from species-specific differences in the transcription-coupled repair on the respective genomic regions. The thesis will describe a pipeline how to extract alignment fractions from a multiple genome alignment and outline the datasets that were used for the analyses. In the second part the extent of the influence of transcriptional processes in the human genome is analyzed. In detail, a Likelihood-Ratio-Test is conducted to test for the strand symmetry between substitution rates between a transcribed and a non-transcribed alignment fraction. The strand-specific substitution rates are then compared between both datasets. The third part describes the Single-Branch-Test to identify genomic regions in the human and chimpanzee genomes, where the homogeneity between the human and chimpanzee substitution models is rejected. The substitution patterns in the identified genomic regions are then further studied for differences in strand-specific substitution patterns. In the fourth part a Gene Ontology enrichment analysis is conducted on the set of candidate genes located within the identified transcribed genomic regions. The final part describes evaluation study for the Single-Branch-Test on simulated data.

Chapter 2

Genome alignment and metadata

In this chapter I describe details about the human-chimpanzee-rhesus genome alignment that was used in this study. The concepts how publicly available genome alignments are built are briefly introduced. Finally, the pipeline I developed to handle such data for genome-wide studies is described.

2.1 Mammalian genome alignment

The prerequisite for a genome-wide phylogenetic or comparative analysis between species is an accurate multiple sequence alignment of their entire genomes. A genomic multiple sequence alignment describes the lineup of corresponding nucleotides between three or more homologous sequences. In the case of comparing entire genomes between species, the collinearity of the sequences is usually not given, due to rearrangements such as inversions and translocations of genomic segments. Homologous segments need to be identified and individually aligned by a local alignment. The strategies that are currently developed for this purpose are based on a local or combined local-global alignment approach described in the following.

The UCSC Genome Browser (Karolchik *et al.*, 2007) provides a multiZ (Blanchette *et al.*, 2004) multiple genome alignment from several vertebrate species that were generated by a local alignment approach (Miller *et al.*, 2007). All local pairwise alignments between the genomes are identified using BlastZ (Schwartz *et al.*, 2003). In a subsequent filtering step, segments of collinear local alignments are constructed for each pair of genomes (Kent *et al.*, 2003). MultiZ is based on a progressive alignment strategy, where

sequences are sequentially aligned to form a multiple sequence alignment according to a predefined guide tree. In each step pairwise or multiple alignments are combined, where the corresponding alignment sites are matched by a reference sequence that is present in both alignments. The resulting multiple sequence alignment is projected along a defined reference genome and represents any nucleotide from a genome in at most one alignment block.

The local-global approach starts with the identification of local homologous sequence segments between the individual genomes. Subsequently, the segments are aligned using a global alignment strategy. More precisely, all local alignments between two genomes are identified first. The best scoring subset of pairwise local alignments is then selected to create a rearrangement map, where syntenic regions are identified and aligned using a global alignment method (Green *et al.*, 2003). The strategy is based on a progressive alignment according to a predefined phylogenetic tree. At each step the genomes are progressively aligned to an ancestral genome sequence that is estimated for each node in the tree. The resulting alignments are then joined using the ancestral genome as reference. Thus, this method does not depend on the choice of a certain reference genome. This strategy is for example implemented in the VISTA Genome Pipeline (Dubchak *et al.*, 2009) that provides a multiple genome alignment between vertebrates and other genomes.

Another reference free genome alignment strategy forms the basis of the Ensembl Genome Browser (Flicek *et al.*, 2008). The procedure described in Paten *et al.* (2008) first identifies local pairwise alignments between all genomes. In the next step a graph-based approach is used to order the alignments into consecutive multiple sequence segments. These segments are subsequently globally aligned. The advantage of this method is that neither the underlying phylogenetic relations of the genomes nor a predefined reference genome is required.

For the genome-wide comparative study between the human and chimpanzee genomes a pipeline was developed to efficiently extract fractions from genome alignments. Here, the pipeline is described using the UCSC multiZ genome alignment (Miller *et al.*, 2007) containing the genomes of human, chimpanzee and rhesus. However, any other of the introduced publicly available alignments can be processed with this pipeline as well.

2.1.1 Genome sequences

The genome sequences of human (hg18, finished), chimpanzee (pt2, draft, 6x coverage) and rhesus (rheMac2, draft, 5.1x coverage) were obtained from the UCSC Genome Browser database (Karolchik *et al.*, 2007). We compressed and indexed the genome sequences from each chromosome using "faToNib" (Kent *et al.*, 2003) to decrease storage. From the NIB-encoded sequences, segments are extracted using "nibFrag" (Kent *et al.*, 2003).

2.1.2 Sequence quality

Most algorithms to call nucleotides from Sanger DNA sequence traces assign an error probability to a called nucleotide. The definition of a quality value q is given by (Ewing and Green, 1998):

$$q = -10 \cdot log_{10}(p) \tag{2.1}$$

The quality value q is computed for a given error probability p. For example the quality value q of 40 denotes a base-call with an error probability p of 1/10000 (0.01%).

The genome sequences from rhesus and chimpanzee are in draft status, and thus errors due to low sequence quality must be taken into account. The quality files corresponding to the rhesus genome[1] and the quality files corresponding to the chimpanzee genome[2] were therefore retrieved. The quality sequence file from chimpanzee chromosome 1 contains about 249 million quality values and uses about 670 Mb of disk-space stored as plain-text. The size and format of the file is inconvenient for retrieving quality sequence segments from a given genomic region of interest. To facilitate an instant access to the quality information for any genomic region of interest the quality files were indexed and compressed.

Quality information is stored as values varying from 0 to 99. Storing a quality value in ASCII format (text format) requires at most 3 bytes; an one-digit or two-digit integer and a space character as delimiter. However, a single byte can store an unsigned number ranging from 0 to 255 and is thus sufficient to encode a given quality value. Removing

[1] `ftp://hgdownload.cse.ucsc.edu/goldenPath/rheMac2/bigZips/rheMac2.qual.qv.gz`
[2] `ftp://hgdownload.cse.ucsc.edu/goldenPath/panTro2/bigZips/chromQuals.zip`

also the space delimiter, the quality file can be reduced to a storage volume $\sim 30\%$ of the original size. The quality files for each of the chimpanzee and rhesus chromosomes were compressed and indexed individually (Figure 2.1 A). The compression and extraction of the quality information was done with the perl functions pack() and unpack(), respectively. The program to compress and index the quality files "qualToqib.pl" and for the extraction of a quality value sequence "qFrag.pl" were kindly provided by Sascha Strauss.

2.1.3 Genome alignment

I retrieved a multiple genome alignment of 28 vertebrate species including human, chimpanzee and rhesus from the UCSC Genome Browser[3]. The genome alignment is referenced to each human chromosome and is provided in a MAF format (multiple alignment format). Multiple aligned sequence segments are called alignment "blockset". Every blockset contains the start and end coordinates, strand orientation and the corresponding aligned sequence for each particular species. From this blocksets other species than human, chimpanzee and rhesus were discarded (Figure 2.1 B).

I wanted to eliminate effects caused by sequencing errors in the chimpanzee and rhesus draft genomes in subsequent analyses. Therefore only nucleotides were considered with a quality value of at least 40. The threshold was chosen since it resembles almost the quality of the human genome. Each human chromosome MAF file is split into chunks and masked in parallel to accelerate the procedure (Figure 2.1 B). In the next step (Figure 2.1 C) the quality masked MAF files are rejoined.

The program "maf2fasta"[4] was used to format the quality masked alignments into a fasta format for each human chromosome. Here, the list of blocksets are formatted into a linear multiple alignment along the entire human chromosome sequence string. Subsequently, all columns with a gap position in the aligned human sequence were removed from the alignments using "deleterefgap.c" (Figure 2.1 C). The resulting human genome projected sequences were separately compressed and indexed for each human chromosome. The indexed position of an alignment column for the three aligned sequences corresponds to the indexed position of an nucleotide in a human chromosome.

[3] `ftp://hgdownload.cse.ucsc.edu/goldenPath/hg18/multiz28way/`
[4] `http://www.bx.psu.edu/miller_lab/`

2.2 Transcribed regions in the human genome

The transcribed sequence positions in the human genome sequence were identified using the information provided by Ensembl (build 50). The Ensembl (Hubbard *et al.*, 2007) annotation of human genome transcript coordinates were retrieved using the biomaRt package (Durinck *et al.*, 2005). The information of genomic transcripts were reformatted and compressed into a linear representation. This facilitated the identification whether an individual sequence position is transcribed.

A sequence string was defined that assigns the annotation of human genomic transcripts along the entire human chromosome sequences. The annotation of a transcript is described by the start position in the genome, genomic end position and the orientation of the coding strand. We define "0" for a human sequence position which has no annotation to a transcript, "1" and "-1" for a transcribed position on the "+" or the complementary "-" strand respectively. Nucleotide positions transcribed on both strands were represented by a "0". The string is created by the the program "transARRAY.c", which takes the genomic coordinates and chromosome sizes of each chromosome as input. Further, this sequence is indexed and compressed into a 1-byte char using the perl pack() function and extracted with the perl unpack() function by the perl scripts "traARRAY2tip.pl" and "tipFrag.pl" (Figure 2.2 B).

2.3 Genome alignment window extraction

In this section I describe the procedure to obtain alignment fractions from the processed human referenced multiple genome alignment. The transcribed fractions of 125 Kb alignment windows were extracted and oriented such that the coding strand is in '+'

Figure 2.1 ***(following page)*****:** Compression and indexing of a human-chimpanzee-rhesus genome alignment projected along the human genome sequence. A) The genome sequence quality files of chimpanzee and rhesus are compressed and indexed for each individual chromosome. B) Human, chimpanzee and rhesus aligned blocksets in the MAF files are extracted from the 28-way alignment and split into chunks for parallelized quality masking of the chimpanzee and rhesus sequences. C) The MAF files for each chromosome are rejoined and reformatted into a linear multiple sequence alignment along the human chromosome sequences. All alignment columns with a gap in the human sequence are removed. The aligned sequences of human, chimpanzee and rhesus projected along a human chromosome are separately compressed.

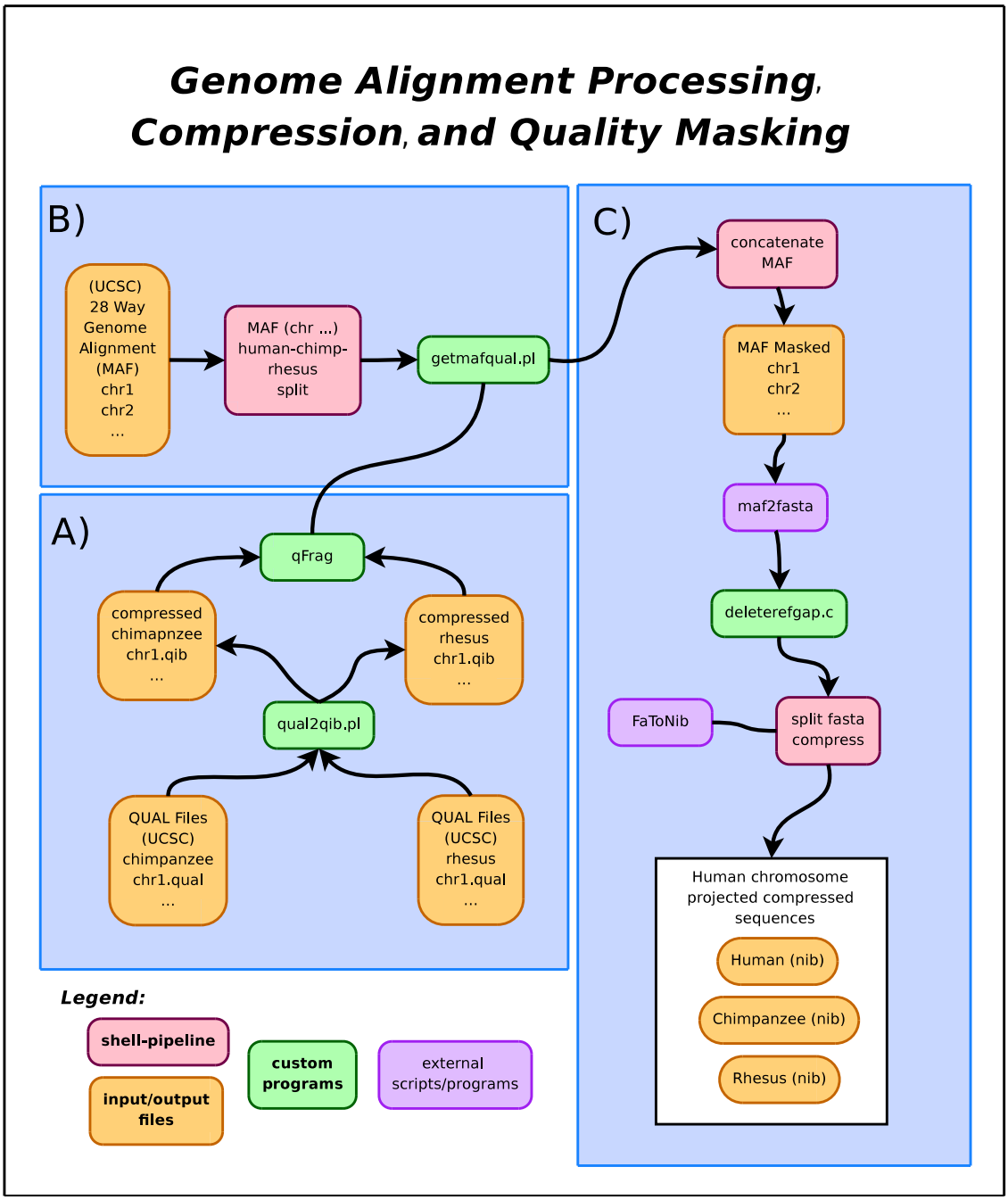
Genome Alignment Processing, Compression, and Quality Masking
B)
(UCSC) 28 Way Genome Alignment (MAF) chr1 chr2 ...
MAF (chr ...) human-chimp-rhesus split
getmafqual.pl
A)
qFrag
compressed chimapnzee chr1.qib ...
compressed rhesus chr1.qib ...
qual2qib.pl
QUAL Files (UCSC) chimpanzee chr1.qual ...
QUAL Files (UCSC) rhesus chr1.qual ...
C)
concatenate MAF
MAF Masked chr1 chr2 ...
maf2fasta
deleterefgap.c
FaToNib
split fasta compress
Human chromosome projected compressed sequences
Human (nib)
Chimpanzee (nib)
Rhesus (nib)
Legend:
shell-pipeline
input/output files
custom programs
external scripts/programs

orientation. First, an input file was created with human referenced coordinates for each alignment window with the script "hg_cutter.pl". Then the input file is split to extract the alignment windows in a parallel manner using the script "getTRFwindow.pl". The string defining the transcript annotation along the chromosomes is extracted to identify the non-transcribed sequence positions and the orientation of a transcribed sequence position. Alignment columns corresponding to the non-transcribed human nucleotides were discarded (Figure 2.2 A).

Further, the alignment fraction of non-overlapping windows of 125 KB, 250 KB, 500 KB and 1000 KB in size were extracted. An input file was created with human referenced coordinates for each alignment window according to a window size with the script "hg_cutter.pl". The input file is split to extract the alignment windows in a parallel manner using the script "getwindow.pl". (Figure 2.2 C).

2.4 Transcribed and non-transcribed alignment fraction

The extraction of the datasets corresponding to the alignment fraction of individual genes and further subsets of the transcribed regions such as from exon, intron, repeats, intergenic flanking regions of genes and a dataset with excluded CpG related transitions are described in the following. The exon coordinates of genes in the human genome were obtained from Ensembl (build 50). In total, 24,890 human-chimpanzee-rhesus alignments according to the genomic transcript start and end location of human genes were extracted using the described pipeline in Figure 2.3.

A subset of alignments was defined that accounted for genes that are expressed in

Figure 2.2 ***(following page)*:** Extraction procedures for the transcribed fraction (A, B) and entire fraction (C) of windows from the human projected human-chimpanzee-rhesus genome alignment. **A)** The genomic transcript annotation for each human chromosome is used to construct a compressed sequence, which assigns whether a nucleotide is transcribed or non-transcribed in the human genome. **B)** For the 125 Kb windows the corresponding transcribed fractions are extracted in coding strand orientation and alignment columns corresponding to non-transcribed genomic regions are discarded. **C)** The entire fraction of non-overlapping alignment windows of sizes 125 Kb, 250 Kb, 500 Kb and 1 Mb are extracted from the compressed aligned human, chimpanzee and rhesus sequences.

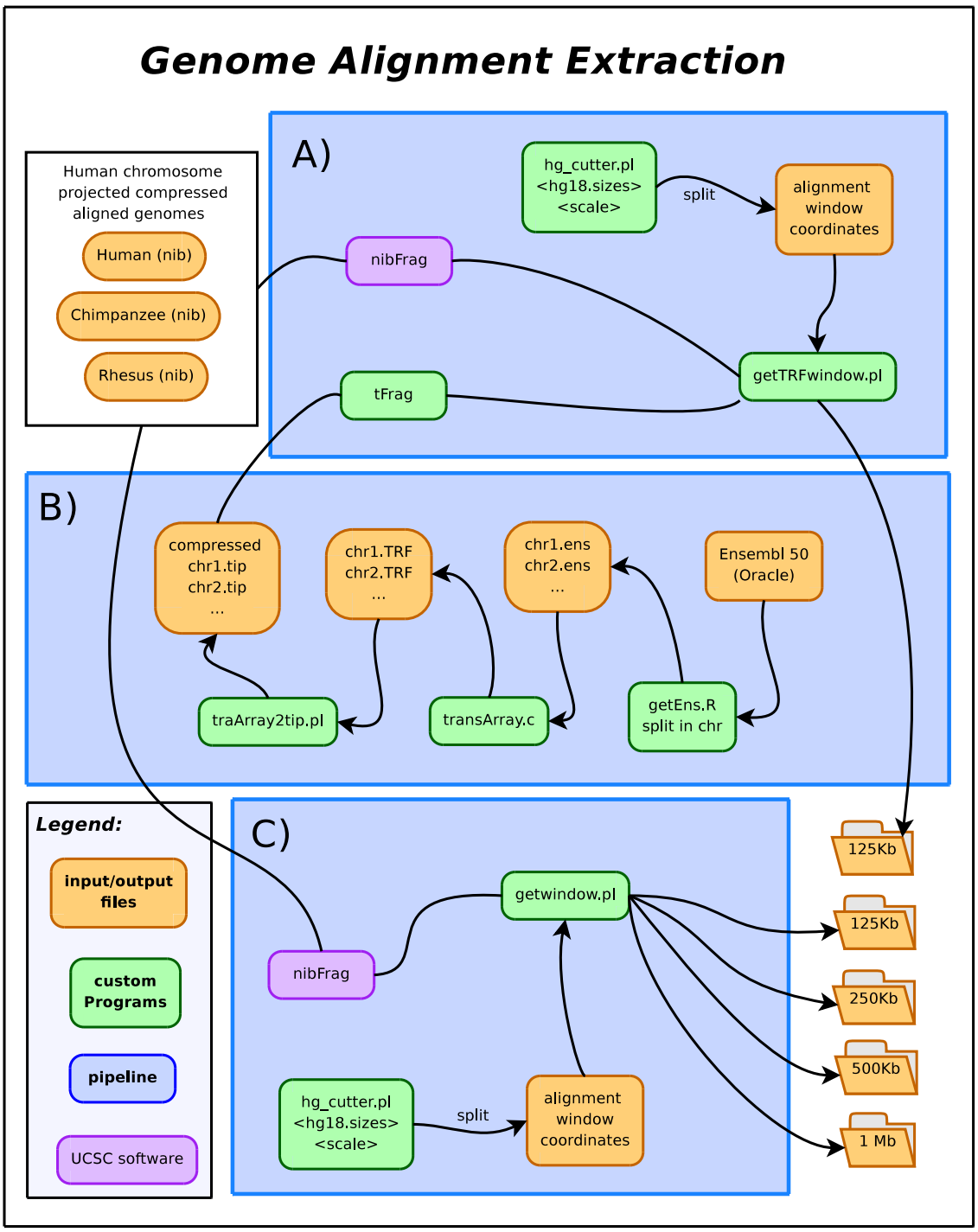
Genome Alignment Extraction
A)
Human chromosome projected compressed aligned genomes
Human (nib)
Chimpanzee (nib)
Rhesus (nib)
hg_cutter.pl <hg18.sizes> <scale>
split
alignment window coordinates
nibFrag
tFrag
getTRFwindow.pl
B)
compressed chr1.tip chr2.tip ...
chr1.TRF chr2.TRF ...
chr1.ens chr2.ens ...
Ensembl 50 (Oracle)
traArray2tip.pl
transArray.c
getEns.R split in chr
Legend:
input/output files
custom Programs
pipeline
UCSC software
C)
getwindow.pl
nibFrag
hg_cutter.pl <hg18.sizes> <scale>
split
alignment window coordinates
125Kb
125Kb
250Kb
500Kb
1 Mb

the germline. The germline is defined by the line of cells starting from the zygote and leading to mature sperm and egg cells. As gene expression along the germline is not well studied in human, the identification of such genes was realized by obtaining EST sequencing data from tissues that include germline cells. Unigene (Wheeler *et al.*, 2003) provides clustered and annotated collections of transcribed sequences derived from different tissues and species, where the human testis tissue transcriptome data was used to define genes expressed in the germline. The mapping of ensembl gene identifiers to unigene cluster identifiers were retrieved from Biomart (Smedley *et al.*, 2009). In total, 11,285 Human Unigene clusters from testis tissue corresponded to 10,962 Ensembl genes having a primary transcript length $\leq$ 500 Kb. Concatenating the corresponding alignment fractions into a superalignment resulted in 634 Mb gap free alignment columns with unambiguous nucleotides. Then, the alignment fraction corresponding to exons and introns of the germline expressed gene set was extracted. Here, the intron coordinates were computed along the genomic transcript boundaries for each gene in respect to the exon coordinates. The concatenated intron alignment fractions resulted in a total of 588 Mb and the concatenated exon alignment fraction in 46 Mb.

From the defined transcribed regions, the fraction corresponding to 4 categories of interspersed repeats (Smit, 1996) were extracted as well: LINEs (long interspersed nuclear elements), SINEs (short interspersed nuclear elements), DNA transposons and LTRs (long terminal repeats). The coordinates of interspersed repeats in the human genome were obtained from the RepeatMasker (Smit *et al.*, 1996-2004) repository[5].

The alignment fractions corresponding to the 4 categories of interspersed repeats were extracted from the genome alignment and merged into a superalignment for each category. Only the subset of repeat alignment fractions corresponding the germline gene set were considered. The concatenated alignment fractions comprised a total of 75 Mb (LINE), 64 Mb (SINE), 24 Mb (LTR) and 15 Mb (DNA Transposons) gapfree alignment columns with unambiguous nucleotides.

Additionally, a dataset was constructed which represented a non transcribed fraction of the genome alignment. Here, it was assumed that the genomic flanking regions of genes are not transcribed. The 50 Kb flanking regions of the 5' and 3' ends of the genes in the human genome were determined according to the genomic transcript start and end coordinates. The flanking region was extracted from genes with no adjacent gene

[5] `http://www.repeatmasker.org/genomes/hg18/hg18.fa.out.gz`

in the range of 200 Kb defined in Ensembl (further details in table 2.1).

2.5 Discussion

The genome-wide analysis of the substitution processes affecting the human and chimpanzee genomes was based on the multiZ genome alignment provided by the UCSC. First, a versatile tool was developed to extract human, chimpanzee and rhesus alignment fractions corresponding to the coordinates of the human genome that provided the infrastructure for this analysis. Then, the tool was used to extract a number of different datasets for the analysis. The procedure begins with a quality masking of the draft genome sequences of chimpanzee and rhesus. For each human chromosome the corresponding aligned sequences were extracted and stored in an indexed compressed format. The information whether an alignment position corresponds to a human transcript and its direction of transcription was additional stored in an indexed form. This information is extracted to exclude alignment columns corresponding to the non-transcribed alignment fraction.

The presented pipeline can be adapted to any of the publicly available genome alignments. Here, a reference genome needs to be defined, where each nucleotide of the reference genome is aligned to at most one nucleotide in the other genome. The main advantage of the UCSC multiZ genome alignments is that the one to one relation of each human nucleotide to a nucleotide in the other genomes is provided. The sequence quality cut-off was restricted to ≥ 40 for the draft genomes. However, for the sequence quality masking step any other desired cut-off can be defined. For the analysis described in the thesis only the genome of human, chimpanzee and rhesus was considered. The pipeline can also be extended to any number of aligned sequences that are projected along a defined reference genome.

The pipeline was used to extract alignment windows and a variety of subsets from the transcribed fraction or the entire genome alignment. The extracted datasets correspond to (i) individual windows along the genome (sizes ranging from 125 Kb to 1000 Kb), (ii) the transcribed fraction of the 125 Kb windows and (iii) individual genes. Further, the transcribed fraction from introns, exons, the four classes of transposable elements (LINEs, SINEs, DNA transposon and LTRs) were extracted.

Dataset	Description
1) Window alignment fractions:	
1000 Kb	2,176 windows (> 742 Kb) 1.79 Gb
500 Kb	4,321 windows (> 370 Kb) 1.79 Gb
250 Kb	8,608 windows (> 184 Kb) 1.79 Gb
125 Kb	17,138 windows (> 742 Kb) 1.8 Gb
125 Kb transcribed fraction (TRF_{125Kb})	12,596 windows (> 23 Kb) 926 Mb
Gene Transcripts ($TRF_{Transcript}$)	7,292 transcripts (> 23 Kb) 654 Mb
2) Concatenated alignment fractions:	
Unigene (Testis)	10,962 Ensembl genes ($\leq$ 500 Kb)
all unigene transcripts	634 Mb
CpG transitions excluded	574 Mb
Exon	46 Mb
Intron	588 Mb
interspersed repeats:	
LINE	75 Mb
SINE	64 Mb
DNA	15 Mb
LTR	24 Mb
3) non-transcribed	50 Kb intergenic flanking region of genes with no adjacent gene in 200 Kb 7,499 regions 295 Mb

Table 2.1: Overview of the extracted window, transcribed and non-transcribed alignment fractions from the human, chimpanzee and rhesus genome alignment. 1) The sizes shown in brackets denote the defined minimal size for an extracted alignment window. 2) The transcribed fraction corresponds to human germ line expressed genes with a maximal primary transcript size of $\leq$ 500 Kb. For this purpose the genomic locations of Ensembl genes of testes expressed EST sequences represented as Unigene Clusters are used. 3) The non-transcribed fraction corresponds to 50 Kb directly flanking up and downstream regions of genes with no adjacent gene in a distance of 200 KB.

Chapter 3

Modeling the evolution of DNA sequences

This chapter introduces substitution models that are used to describe the process of single nucleotide substitutions in biological sequences.

Mutations drive the molecular evolution of biological sequences such as DNA, RNA and protein sequences. Causes of mutations are replication errors in a dividing cell, chemical mutagens, radiation or viruses and transposons. These events occur in all cells of an organism, but only the mutations that were inherited by germline cells generation after generation are accumulated in contemporary sequences.

The mutations of single nucleotides (point mutations) are distinguished from mutations, that affect whole sections of genomic regions. The mutations of whole genomic sections that are e.g., derived from chromosomal rearrangements, where several consecutive nucleotides are deleted, inserted, translocated (from another genomic region) or duplicated. Point mutations are deletions or insertions of single nucleotides or substitutions of a single nucleotide by another nucleotide.

Sequence evolution is in general investigated by analyzing single nucleotide substitutions inferred from an alignment between sequences. This chapter will introduce Markov models to describe such a substitution process in a stochastic framework. The formulas shown in this chapter are based on Salemi and Vandamme (2003), Felsenstein (2004) and Yang (1994b).

3.1 Markov substitution models

For a given alignment, e.g., between two homologous sequences, the substitution process is in general investigated from the observed substitutions (Figure 3.1).

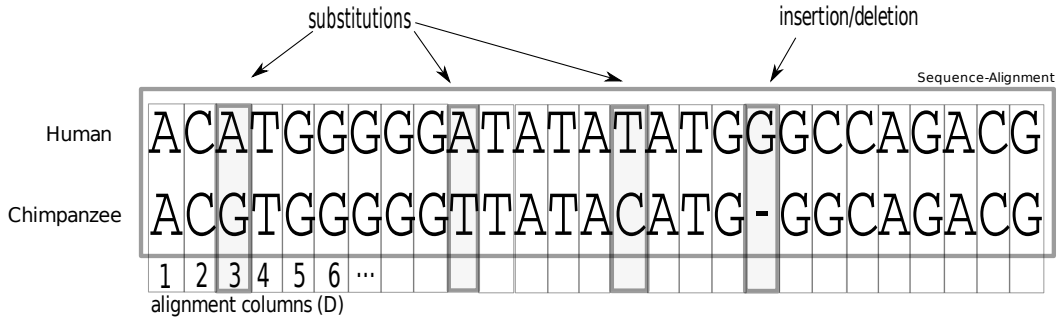

Figure 3.1: Point mutations inferred from a pairwise sequence alignment. Mismatch nucleotides are called substitutions. An insertion/deletion of a single nucleotide is represented by a gap character.

The observable number of substitutions is limited due to a saturation of the substitutions (Figure 3.2). Therefore the number of observed substitutions generally underestimates the actual number of substitutions that have occurred. The saturation of substitutions can be explained by the following scenarios: 1) Backmutation: a substitution of a nucleotide is not observed when a second substitution recovers the initial state of the nucleotide; 2) Multiple substitutions: only one substitution is observed when multiple substitutions occur at the same site; 3) Parallel substitutions: when comparing two homologous sequences a substitution is not observed when the same substitution occurs at the same site in both sequences. To overcome such problems a substitution model is used to describe the evolution of aligned sequences.

Suppose that the rate of changes in DNA sequences from one nucleotide into another follows a Markov process with four states, where each state represents one of the four nucleotides (A, G, C, T). In general, the substitutions described by a Markov model are assumed to occur independently for each site in the sequence. Assume the substitution of a nucleotide to another nucleotide (Figure 3.3) within a DNA sequence X from a time point t_0 to t:

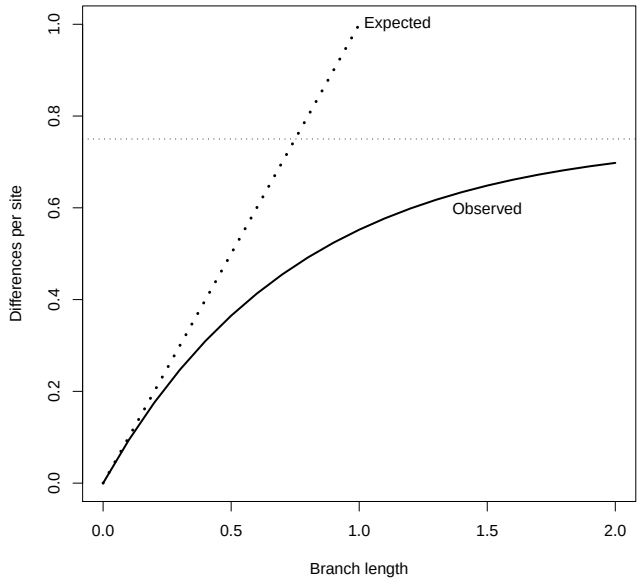

Figure 3.2: The number of observed differences and expected number of substitutions per site (branch length) between two DNA sequences. The observed differences are defined by the mismatch characters per site observed between two homologous sequences and the expected number of substitution per site (branch length) is estimated. The saturation of observed substitutions between two homologous aligned sequences are shown.The observed number of substitutions (black line) underestimates the expected number of substitutions (dotted line), e.g., due to parallel, multiple and backmutations as explained in the text.

$$X_{t_0} \longrightarrow X_t$$

The substitution model describes the probability $P_{ij}(t)$ to observe nucleotide j at time t, if nucleotide i is present at time t_0. The probability is solely dependent on the initial state without considering the putative changes that occurred within a given time period. The transition probabilities follow an exponential distribution, where the probability for a substitution increases with time t. In general, the transition probabilities from one nucleotide into another are described in a 4×4 matrix $P(t)$:

$$P(t) = \exp(Q(t)) \tag{3.1}$$

The transition probabilities in $P(t)$ are a function of time t and can differ at each sequence position. The rate matrix Q describes the process in an infinitesimal time

interval and therefore does not depend on time.The matrix Q has off-diagonal entries $q_{ij} > 0$ that give the instantaneous substitution rates per unit time at which nucleotide j is replaced by nucleotide i (i $\neq$ j $\in \{A, C, G, T\}$). The diagonal elements of Q are given by

$$q_{ii} = -\sum_{j \neq i} q_{ij} \tag{3.2}$$

such that rows sum up to zero. Let $\pi = (\pi_A, \pi_C, \pi_G, \pi_T)$ be the equilibrium frequency of nucleotide i ($i \in \{A, C, G, T\}$) . The rate matrix Q is typically normalized such that the total rates of changes is 1 per unit time by scaling the negative sum of the diagonal components (trace) to 1.

$$-\sum_{i} \pi_i q_{ii} = 1 \tag{3.3}$$

The normalization allows to measure time in expected numbers of substitutions per site.

The transition probability matrix $P(t)$ is computed from the matrix exponential of Q (equation 3.1). There are several approaches to compute the matrix exponential (Moler and Charles, 2003). The most popular method to compute the exponential is the eigenvalue decomposition method (Bailey *et al.*, 1990). Assume that the transition probability matrix $P(t)$ has a spectral decomposition:

$$P(t) = U \cdot diag(e^{\lambda_1 t}, e^{\lambda_2 t}, e^{\lambda_3 t}, e^{\lambda_4 t}) \cdot U^{-1} \tag{3.4}$$

The matrix $P(t)$ is described by the product of left 4 eigenvectors in the matrix U, the diagonal matrix of the 4 eigenvalues λ_i and the 4 right eigenvectors in the matrix U^{-1} of Q. The eigenvectors describe the properties of a matrix and are equal between $P(t)$ and Q. The exponential of the matrix is obtained by replacing the eigenvalues λ_i by $e^{\lambda_i t}$. The rate matrix Q can be expressed from equation 3.4 as

$$Q = U \cdot diag(\lambda_1 t, \lambda_2 t, \lambda_3 t, \lambda_4 t) \cdot U^{-1}. \tag{3.5}$$

The substitution process is generalized in a so called Markov process which describes the relative rates of change of the nucleotides along a sequence defined in the rate matrix Q. The substitution model defined in Q is in general restricted to the following

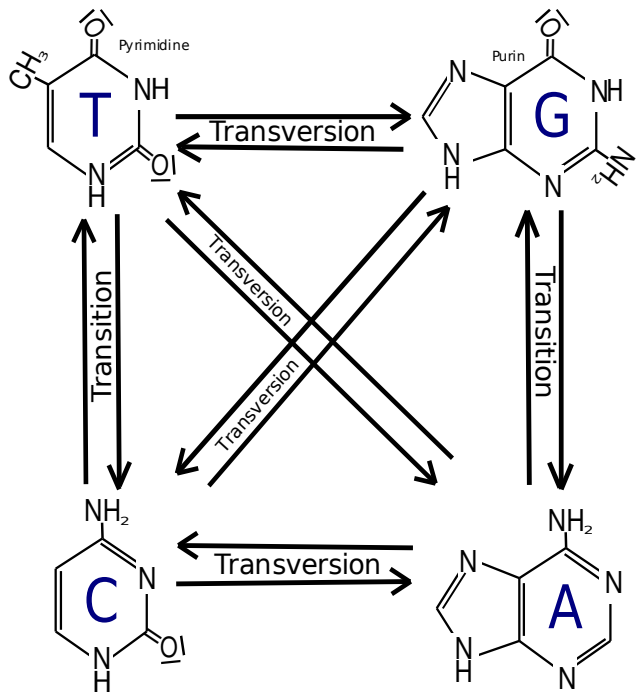

Figure 3.3: Nomenclature for the different types of substitutions. Transitions are substitutions between a purine and a purine nucleotide described by an exchange between a Guanine (G) and a Adenine (A) or a pyrimidine to a pyrimidine nucleotide described by an exchange between a Thymine (T) and a Cytosine (C). The remaining substitutions types are transversions which describe an exchange between purine and pyrimidine nucleotides.

three assumptions: First, the rate of change from nucleotide i to j is independent from any previous state of the nucleotide i. In other words the process is memoryless i.e. independent from any previous event at any site. Second, the homogeneity of the process assumes that the substitution rates remain unchanged over time. Third, the stationarity of the process assumes that the relative nucleotide frequencies $(\pi_A, \pi_C, \pi_G, \pi_T)$ are in equilibrium, i.e., remain unchanged.

3.2 Reversible substitution models

The most commonly used substitution models assume the reversibility of the substitution process. In a reversible model the substitution rate between any nucleotide i to j is the same as the reverse substitution rate from nucleotide j to i:

$$q_{ij} = q_{ji} \tag{3.6}$$

This class of substitution models are called time-reversible substitution models that are introduced in the following.

The general time-reversible model (GTR) describes the evolutionary process by the

following instantaneous rate matrix Q (Lanave *et al.*, 1984):

$$Q = \begin{pmatrix} - & \alpha\pi_C & \beta\pi_G & \gamma\pi_T \\ \alpha\pi_A & - & \delta\pi_G & \varepsilon\pi_T \\ \beta\pi_A & \delta\pi_C & - & \eta\pi_T \\ \gamma\pi_A & \varepsilon\pi_C & \eta\pi_G & - \end{pmatrix} \tag{3.7}$$

The components q_{ij} of matrix Q are defined as parameters, where the rate parameters (α, β, γ, δ, ε, η) and the parameters for the equilibrium nucleotide frequencies π_i for $i \in \{A, C, G, T\}$ are defined. The off-diagonal components of the matrix Q quantify the flow of a nucleotide exchange by another nucleotide. The diagonal elements in Q are defined such that a row in the matrix sum to zero and represent the total rate of an exchange from a nucleotide i to any other nucleotide j.

The number of free parameters of a substitution model depend on the defined symmetry assumptions and the scaling of the parameters in the substitution model. For example in the GTR model the number of free parameters are defined in the following way: The sum of the nucleotide frequencies is one,

$$\sum_{i}^{A,C,G,T} \pi_i = 1 \tag{3.8}$$

thus, 3 free parameters are sufficient to describe the nucleotide frequencies. Assuming a reversible process (equation 3.6) and scaling the rate matrix Q to one (equation 3.3), the substitution rates can be described by 5 free rate parameters. In total, the GTR model has therefore 8 free parameters.

Within the GTR model (8 free parameters) a variety of reversible submodels can be defined, where the number of parameters are reduced by introducing additional restrictions. In the following a few of these submodels are introduced. The TN93 model (Tamura and Nei, 1993) describes a parameter for the ratio between transitions and transversions (κ) and another parameter the ratio between purine and pyrimidine transitions γ. The TN93 model has 5 free parameters with 2 free rate parameters and 3 parameters for the nucleotide frequencies. The HKY85 model (Hasegawa *et al.*, 1985) describes only the parameter for the ratio of transition and transversion rate κ. The HKY85 model has 4 free parameters, 1 free rate parameter and 3 free parameters for

the nucleotide frequencies. The F81 describes one parameter for the substitution rate and remains with 3 free parameters for the nucleotide frequencies. By assuming uniform nucleotide frequencies (π_i=0.25) and a parameter for the ratio between purine and pyrimidine substitutions describes a K80 model (Kimura, 1980) that has only 1 free parameter. The simplest model of DNA evolution is the JC model (Jukes and Cantor, 1969), where the rate of change from one nucleotide i to another nucleotide j is the same for all substitution rates and the equilibrium nucleotide frequencies are uniform (π_i=0.25). The JC model has no free parameters.

3.3 Non-reversible substitution models

The most general Markov model is shown in Figure 3.4, where the rates are defined by the product of the rate of a substitution from one nucleotide i to the nucleotide j and the nucleotide frequency π_j (Figure 3.4). The generalization to describe the substitution

$$\begin{array}{c} \\ A \\ G \\ C \\ T \end{array} \begin{array}{c} \begin{array}{cccc} A & G & C & T \end{array} \\ \begin{pmatrix} -(a\pi_C + b\pi_G + c\pi_T) & a\pi_C & b\pi_G & c\pi_T \\ g\pi_A & -(g\pi_A + d\pi_G + e\pi_T) & d\pi_G & e\pi_T \\ h\pi_A & i\pi_C & -(h\pi_A + i\pi_C + f\pi_T) & f\pi_T \\ j\pi_A & k\pi_C & l\pi_G & -(j\pi_A + k\pi_C + l\pi_G) \end{pmatrix} \end{array}$$

Figure 3.4: The most general instantaneous rate matrix Q. The diagonal elements are defined such that the rows sum up to zero. The rate parameters $a, b, c, d, e, f, g, h, i, j, k, l$ define the relative rates of the substitution from one nucleotide to any other nucleotide. The parameters $\pi_A, \pi_C, \pi_G, \pi_T$ define the nucleotide frequencies.

process leads to a Markov model that does not assume reversibility. The non-reversible substitution describes the instantaneous rate matrix Q as following

$$Q = \begin{pmatrix} - & \alpha & \beta & \gamma \\ \delta & - & \varepsilon & \eta \\ \theta & \vartheta & - & \iota \\ \kappa & \lambda & \mu & - \end{pmatrix} \tag{3.9}$$

The so called unrestricted model (Yang, 1994b) has 12 parameters (Greek letters), one for each substitution type. Note, in the unrestricted model the nucleotide frequencies are

a function of the parameters. The reason to this constraint is that there might not exist an equilibrium nucleotide frequency for the substitution model (the largest eigenvalue of Q is not 0). In the unrestricted model the actual base frequencies of the sequences are used as the equilibrium nucleotide frequencies. The total number of substitutions are standardized to one, the model has in total 11 free parameters.

A variety of additional constraints can be defined to simplify the unrestricted model. In general, substitutions can not be distinguished on which strand they occur. A substitution that occurred on one strand will result in the complementary substitution on the other strand. In Sueoka (1995) a strand symmetric model was introduced, where the substitution rates between complementary substitutions get the same parameter assigned.

$$Q = \begin{array}{c} \\ A \\ G \\ C \\ T \end{array} \begin{array}{c} \begin{array}{cccc} A & G & C & T \end{array} \\ \begin{pmatrix} - & \alpha & \beta & \gamma \\ \lambda & - & \delta & \varepsilon \\ \beta & \gamma & - & \alpha \\ \delta & \varepsilon & \lambda & - \end{pmatrix} \end{array} \tag{3.10}$$

In the matrix Q, for example, $A \rightarrow G$ is strand complementary to $T \rightarrow C$ and hence are assigned to the same parameter α. The model describes parameters for 6 complementary substitution pairs and has 5 free parameters.

3.4 The Maximum likelihood

The substitution models are used to compute the distances and for the estimation of the substitution process among the sequences observed in an alignment that are represented by a phylogenetic tree (Figure 3.5). The substitution model describes the process along the branches that most likely generated the observed sequences. In general, the parameters of a specified substitution model Q are estimated to compute a likelihood for the model and a given tree. Let T denote a phylogenetic tree and M a substitution model for a sequence alignment D. The likelihood of the data given a substitution model is computed as follows. Suppose D_s be a site pattern or column in the alignment (Figure 3.1). For this site pattern the product of the transition probabilities in $P(t)$ for

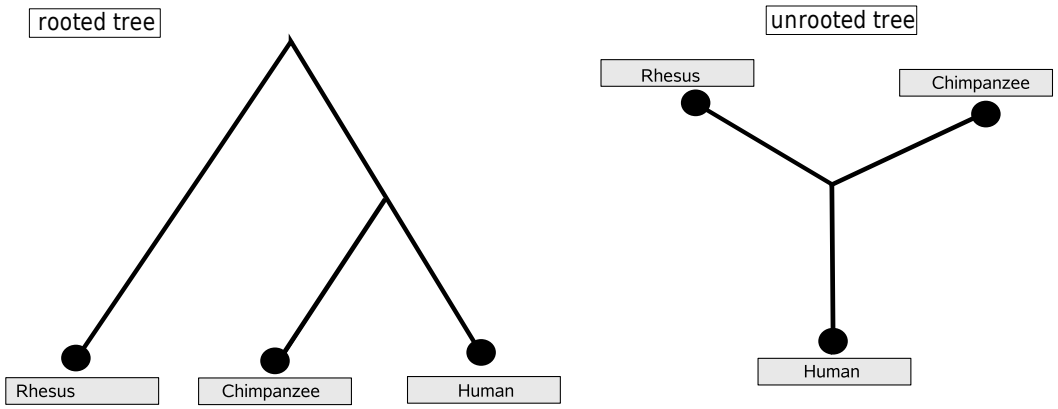

Figure 3.5: A rooted and an unrooted 3 species tree. The most recent common ancestor is represented by the internal nodes, where the external nodes represent the observed contemporary species. The branches in the tree represent the time estimated from a substitution model. Both trees are computationally equivalent.

given nucleotide states at the internal nodes over all branches t in the tree is calculated. The likelihood for the site pattern is defined by the sum of the products for all possible nucleotide states at the internal nodes. The likelihood to observe D_s is denoted by:

$$P(D_s|T, M) \tag{3.11}$$

The likelihood function $L(T, M)$ computes the total likelihood over all sites in an alignment by the sum of the log likelihoods over all sites:

$$logL(T, M) = \sum_{s=1}^{m} logP(D_s|T, M) \tag{3.12}$$

The log scale is used to avoid arithmetic underflow, because the probabilities of the site patterns are usually close to zero. The parameters of the substitution model are separately estimated by maximizing the likelihood function L. In general, iterative global optimization procedures are used for this purpose (Swofford *et al.*, 1996). The likelihood method allows to estimate the parameters for a given model to describe the substitution process leading to the observed sequences in an alignment. A method to infer the most appropriate substitution model or number of parameters for a given alignment is described in the following section.

3.4.1 The Likelihood-Ratio-Test

A substitution model with several parameters such as the GTR model or the unrestricted model described in the previous sections can be simplified when further symmetries are assumed between the parameters. When the number of parameters are reduced within a substitution model, the simplified model is called nested within the more complex model. Usually, the more complex substitution model provides a better fit to the data (higher likelihood) than the model with fewer parameters. However, the more complex model will also have a larger variance in the estimation that might lead to an overfit of the data.

The standard method to compare the likelihood between two nested substitution models to select the most appropriate is a Likelihood-Ratio-Test (LRT) (Felsenstein, 2004). The statistic of the test is described by:

$$\Delta = 2(log_e L_1 - log_e L_0) \tag{3.13}$$

The log likelihood of the parameter rich model is denoted by L_1 and the null model with fewer parameters by L_0. In this particular case the Δ statistic follows approximately a χ^2 distribution with the degree of freedom according to the differing numbers of free parameters between the null and alternative model.

Chapter 4

The influence of transcription on the substitution process

In this chapter the role of strand-specific substitution patterns in transcribed genomic regions are described. The extent of the $A \rightarrow G$ has been suggested to be specifically increased over the $T \rightarrow C$ in transcribed genomic regions and was explained to result from transcription-coupled-repair. A genome-wide study is conducted for the estimation of the strand-specific substitution process from the human-chimpanzee-rhesus genome alignment. Using a Likelihood-Ratio-Test, it is shown that the unrestricted nonreversible substitution model gives a significantly better fit to the data from a transcribed alignment fraction than a simpler model in which $A \rightarrow G$ and $T \rightarrow C$ are assigned to the same rate parameter. Furthermore, the extent of the differences between the substitution patterns in transcribed and non-transcribed genomic regions are estimated and compared.

In the course of his work, Erwin Chargaff has established several rules describing the relative frequencies of the four nucleotides A, G, C, and T in DNA sequences. His first parity rule states that A occurs with the same frequency as T, and G occurs with the same frequency as C in all DNA molecules. This rule contributed substantially to the understanding that native DNA occurs as a double helix where two antiparallel DNA strands are paired via H-bond formation between the complementary bases A and T, and G and C, respectively. While the general applicability of the first parity rule is undisputed, Chargaffs second rule of intrastrand parity is not. According to this rule, the complementary bases should occur with the same frequency also along a single DNA strand. However, this intrastrand parity rule is only approximately followed on a genome-wide level, and substantial deviations are observed on a local level (Touchon and

Rocha, 2008). This raises the question how the relative frequency of the four nucleotides along a DNA sequence is locally modulated. The base composition of contemporary DNA sequences is determined by the substitution process, which changes DNA sequences over time (c.f., Chapter 3). Thus, one needs to hypothesize that genomic regions with different base compositions differ also in their substitution processes. In the past years several biological factors have been proposed to influence the substitution process on region specific scale and, thus the base composition of DNA sequences: mutation bias (e.g., Wolfe *et al.*, 1989), natural selection (e.g., Eyre-Walker and Hurst, 2001), biased gene conversion (BGC,e.g., Duret and Arndt, 2008). Common to all these factors is that they affect both DNA strands to the same extent.

More recently, the focus has been extended to strand-specific processes that affect the substitution process of the two DNA strands to a different extent (Touchon and Rocha, 2008). In the literature a variety of terms are used to distinguish between the two DNA strands. In this chapter the two DNA strands are distinguished by the terms leading and lagging strand when the process of DNA replication is referred. For the process of DNA transcription the non-coding strand is defined as the template for the RNA Polymerase to copy the mRNA strand and the coding strand is defined as the opposite strand. As a unifying principle it is suggested that single stranded DNA is more vulnerable to nucleotide changes than either double stranded DNA or single stranded DNA protected by large protein complexes. For example, it has been shown in prokaryotes that deviations from the intrastrand parity rule can be attributed to processes related to DNA replication. The lagging strand, which remains temporarily single-stranded during replication, is distinguished from the leading strand by having compositional skews of G > C, and, although less prominent, of T > A (Lobry, 1996). This would correspond to $T \rightarrow C$ and to a lesser extend $A \rightarrow G$ transitions occurring more frequently on the lagging than on the leading strand. The correlation of this compositional skew and replication process is so marked, that origins of replication could be reliably predicted by analyzing compositional skews in bacterial genomes (Lobry, 1996). In eukaryotes a similar but less pronounced influence of replication on compositional skews has been observed (Huvet *et al.*, 2007). Transcription is the second biological process that leaves one DNA strand transiently single stranded and has been associated to compositional skews. After separation of the template and the coding strands by the transcription machinery, only the template strand is protected by the protein complex of the RNA

polymerase. In both bacteria and eukaryotes it has been shown that this difference between the two strands results in a different mutation pattern. In bacteria $C \rightarrow T$ transitions have been found to occur more frequently on the coding strand than on the transcribed strand (Francino and Ochman, 2001). In mammals, it was postulated that the rate of the $A \leftrightarrow G$ transition is higher on the coding than on the transcribed strand (Green, 2003; Mugal *et al.*, 2009). As a result a different compositional skew is abound for the transcribed than for the non-transcribed fraction of the genome. One biological model that is used to explain these rate differences between the complementary strands is provided by the process of transcription coupled repair (TCR; Figure 4.1). According to this model, an $A \rightarrow G$ mutation occurs more frequently on the coding strand that results in G:T mismatches along the genomic transcribed fraction of a gene. In vivo and in vitro assays have shown that the $MutS\alpha$ repair enzyme binds efficiently to such G:T mismatches (Jiricny *et al.*, 1988; Lamers *et al.*, 2000). It was therefore postulated that the binding of $MutS\alpha$ to such a bulky mismatch is able to stall the transcription machinery and induce a specific repair mechanism.

In this chapter a study is conducted to describe strand-specific substitution patterns in the human genome that is estimated from a transcribed and a non-transcribed alignment fraction. Bielawski and Gold (2002) analyzed replication associated strand asymmetry between the leading and lagging strand in mitochondrial DNA sequences. For this purpose they developed a Likelihood-Ratio-Test (c.f. chapter 3) to infer, whether a more complex substitution model gives a significant better fit to the data than a simpler strand symmetric model. In the strand symmetric model, a single rate parameter is assigned for each pair of complementary substitution rates (Sueoka, 1995, see chapter 3, substitution model defined in 3.10). However, the more complex non strand symmetric model with one additional parameter allows to distinguish between complementary substitution rates. Bielawski and Gold (2002) used three more complex substitution models

Figure 4.1 ***(following page)*:** Transcription-coupled-repair in mammalian genomes as proposed by Green (2003). **a)** During transcription the complementary DNA strands are transiently single stranded. While the transcribed strand (non-coding strand) is protected by the transcription machinery the coding strand is more exposed to DNA damage. **b)** MutSα recognizes and binds efficiently G:T mismatch pairs **c)** A DNA repair machinery is activated at RNA polymerase (RNAP) stalled lesions. **d)** Preferential repair of non-coding strand that favors the incorporation of G that leads to an increased fixation of $A \rightarrow G$ mutations on the coding strand.

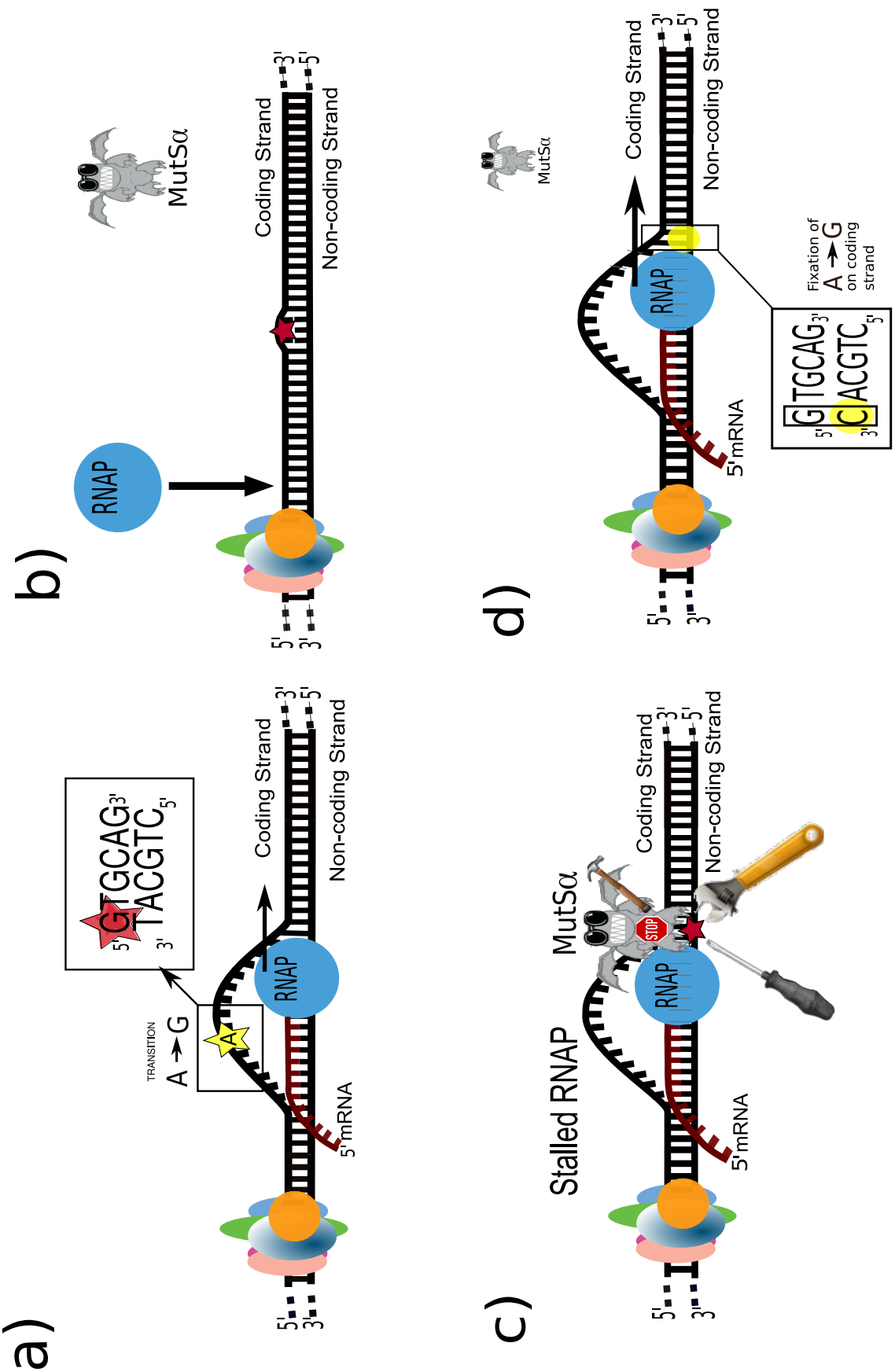
a)
b)
c)
d)
RNAP
MutSα
Coding Strand
Non-coding Strand
5'mRNA
TRANSITION
A→G
GTGCAG
CACGTC
Stalled RNAP
STOP
Fixation of
A→G
on coding
strand

that assigned individual rate parameters for $G \rightarrow A \neq C \rightarrow T$, $A \rightarrow G \neq T \rightarrow C$ and $C \rightarrow A \neq G \rightarrow T$, respectively.

A genome-wide analysis using the Likelihood-Ratio-Test of Bielawski and Gold (2002) for the analysis of the strand asymmetry of substitutions associated to transcription has not been performed to date. The method allows to answer the question whether a more complex non strand symmetric substitution model would be more appropriate to describe the substitution patterns in the corresponding transcribed genomic regions from the human-chimpanzee-rhesus genome alignment. In the following a similar Likelihood-Ratio-Test will be described to test for the strand symmetry between pairs of substitution rates estimated from sampled alignments corresponding to human transcribed and non-transcribed genomic regions. The direction of a particular strand-specific substitution rate is quantified as ratio to the corresponding strand complementary substitution rate. Finally, the difference of substitution rates between transcribed and non-transcribed alignment fraction are discussed.

4.1 Testing the strand symmetry in transcribed genomic regions

4.1.1 The transcribed and non-transcribed alignment fraction

The transcribed genomic regions from the human genome were selected from genomic transcript coordinates corresponding to genes that are also expressed in the germline. A set of non-transcribed genomic regions were defined by the intergenic left and right flanking regions of genomic transcripts, where the flanking region was not in the direct neighborhood of another gene. The alignments corresponding to the defined genomic regions were extracted from the human-chimpanzee-rhesus genome alignment (see chapter 2, Table 2.1). In the following, the alignment set corresponding to the transcribed regions will be termed *transcribed alignment fraction* and the alignment set corresponding to the non-transcribed genomic regions will be termed *non-transcribed alignment fraction*. Additional subsets from the transcribed alignment fraction corresponded to exon, intron, interspersed repeats and a subset where CpG related transitions were excluded.

The datasets were sampled from the concatenated alignments fractions corresponding

to a particular dataset. The alignment set of the transcribed fraction and the alignment set of the non-transcribed fraction were each concatenated (see section 2.4). The transcribed alignment fraction comprised a total of 634 Mb and the non-transcribed alignment fraction a total of 295 Mb excluding all columns with gap characters, ambiguous or masked nucleotides. From both datasets 1000 bootstrap alignments, each consisting of 100 Kb in size were sampled.

4.1.2 Likelihood-Ratio-Test using reversible models

Two *reversible* null models with 4 rate parameters are defined assuming strand symmetry of transversion rates M_0^1 ($A \leftrightarrow C{=}T \leftrightarrow G$) and the strand symmetry of transition rates M_0^2 ($A \leftrightarrow C{=}T \leftrightarrow G$). The alternative model is defined by the general reversible model (GTR) with 5 free rate parameters (Figure 4.2).

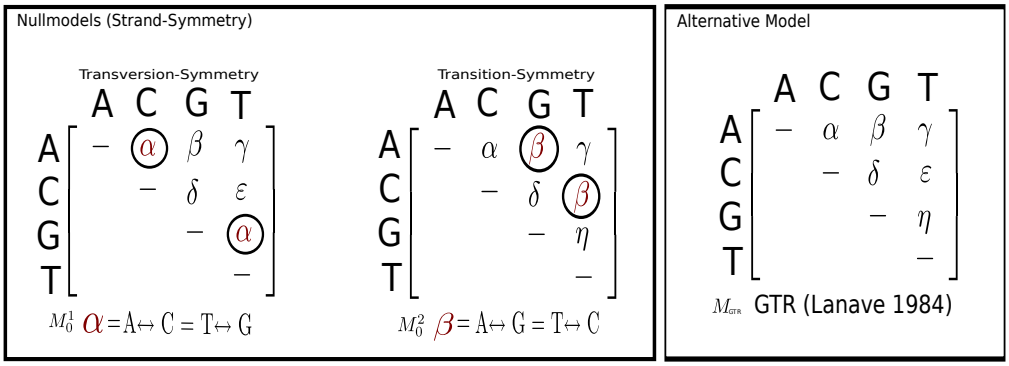

Figure 4.2: Reversible substitution models used for the Likelihood-Ratio-Test. The null models have 4 free rate parameters, each, and the alternative GTR model has 5 free rate parameter.

The log likelihood of the alternative model M_{GTR} and the strand symmetric models $M_0^{1,2}$ were estimated using *paml* (Yang, 2007). The substitution models $M_0^{1,2}$ differ by having one parameter less than the alternative model M_{GTR}. The statistic for the Likelihood-Ratio-Test follows therefore approximately a χ^2 distribution with one degree of freedom. A confidence limit of 5% was chosen for the tests.

The fraction of Likelihood-Ratio-Tests rejecting the null hypothesis of a strand symmetry between a pair of substitution rates was computed and compared between the sampled alignments corresponding to human transcribed and non-transcribed genomic

regions. The null hypothesis for strand symmetry was rejected, when >95% of the performed tests for a particular dataset rejected the simpler strand symmetric substitution model. The strand symmetry assumption of transition rates was rejected in the transcribed fraction and could not be rejected in the non-transcribed fraction (Figure 4.3). In contrast, for transversion rates the strand symmetry assumption could not be rejected in both the transcribed and non-transcribed fraction.

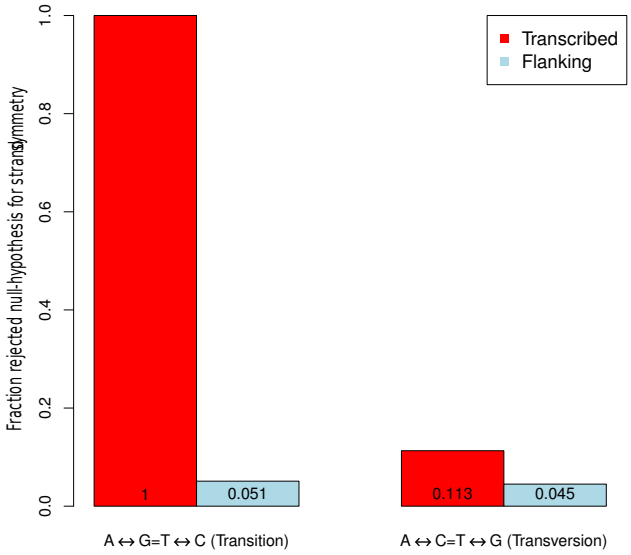

Figure 4.3: Testing for strand symmetry of substitution rates using reversible substitution models. The null hypothesis for the strand symmetry between transitions ($\alpha = A \leftrightarrow G = T \leftrightarrow C$) and between transversions ($\beta = A \leftrightarrow C = T \leftrightarrow G$) was tested in the transcribed alignment fraction and non-transcribed alignment fraction. The fraction of tests that reject M_0 in the LRT are shown. In total, 1000 sampled alignments of the transcribed fraction and 1000 sampled alignments of the non-transcribed fraction (Flanking) were used for the tests. The strand-symmetry for a particular dataset was rejected when at least 95% of the corresponding alignments rejected the null-hypothesis. In the transcribed fraction the transition strand symmetry assumption was rejected in all tested alignments, whereas the transversion strand symmetry assumption was rejected in 11% of the tested alignments. The non-transcribed fraction the strand symmetry assumption for transitions and transversions was rejected in $\sim$ 5% of the performed tests.

4.1.3 Likelihood-Ratio-Test using non-reversible substitution models

When using *reversible* models it is not possible to infer, whether the rejection of the strand symmetry assumption between the transitions $A \rightarrow G$ and $T \rightarrow C$, $G \rightarrow A$ and $C \rightarrow T$ or both contributed to the preference for the GTR model. Therefore, a second analysis was performed using an unrestricted non-reversible substitution model.

In total, 10 strand symmetric models were defined for the strand-symmetry of each of the six complementary substitution rate pairs, and for the 4 remaining substitution rates that are assumed reversible in the GTR model (Figure 4.4). The alternative model was the unrestricted model (GTR) with 11 free rate parameters (Figure 4.4). The log likelihoods of the substitution models were estimated using *paml* (Yang, 2007). The individual substitution models M_0 differ by having one parameter less than the alternative model M_A. The statistic for the Likelihood-Ratio-Test follows therefore approximately a χ^2 distribution with one degree of freedom. Again, a confidence limit of 5% was chosen for the tests. The fraction of Likelihood-Ratio-Tests rejecting the null hypothesis of strand symmetry was computed and compared between the sampled bootstrap alignments corresponding to the transcribed and non-transcribed regions in the human genome. In addition, the transcribed fraction was divided in subsets corresponding to exons and introns, a subset where CpG related substitutions were excluded, and the fraction corresponding to the 4 categories of interspersed repeats. The null hypothesis for strand symmetry was rejected, when >95% of the performed tests for a particular subset rejected the simpler strand symmetric substitution model. The strand symmetry for the $A \rightarrow G$ and $T \rightarrow C$ transitions was rejected in all subsets, except for the non-transcribed and exon alignment fraction. In contrast, the strand symmetry for the complementary pair $G \rightarrow A$ and $C \rightarrow T$ was not rejected in any subset (Figure 4.1). The other performed LRTs for symmetry did not discriminate between the transcribed and non-transcribed alignment fraction.

Figure 4.4 *(following page)*: Non-reversible substitution models used for the LRT. A Likelihood-Ratio-Test is used to estimate whether a null model that assumes strand symmetry between rates corresponding to complementary substitutions or assume reversibility between substitution rates describes the data better than an unrestricted model. The null models have 10 free parameters and the alternative unrestricted model has 11 free parameters.

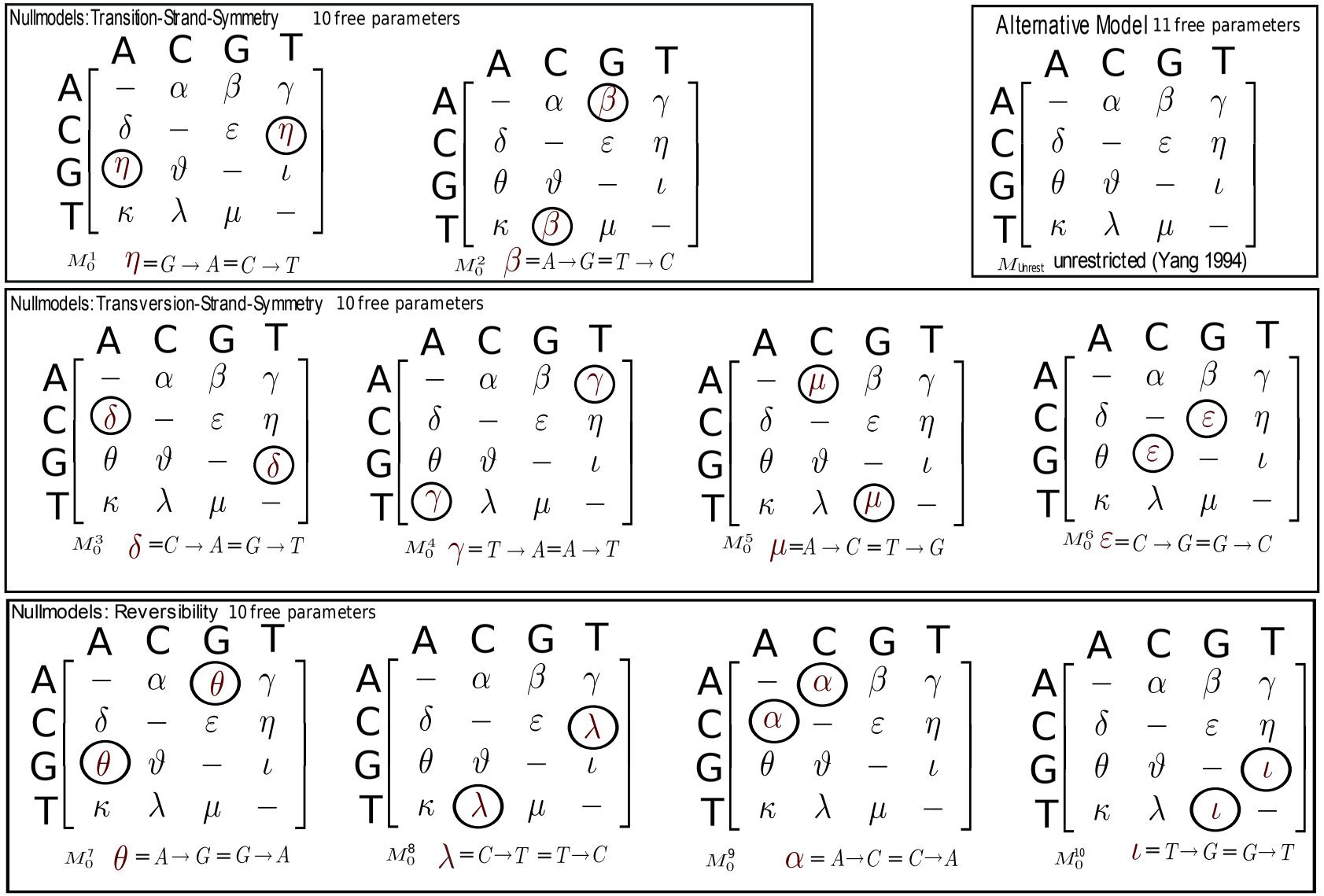
Nullmodels: Transition-Strand-Symmetry 10 free parameters
A C G T
A − α β γ
C δ − ε η
G θ ϑ − ι
T κ λ μ −
M_0^1 $\eta = G \to A = C \to T$
M_0^2 $\beta = A \to G = T \to C$
Alternative Model 11 free parameters
M_{Unrest} unrestricted (Yang 1994)
Nullmodels: Transversion-Strand-Symmetry 10 free parameters
M_0^3 $\delta = C \to A = G \to T$
M_0^4 $\gamma = T \to A = A \to T$
M_0^5 $\mu = A \to C = T \to G$
M_0^6 $\varepsilon = C \to G = G \to C$
Nullmodels: Reversibility 10 free parameters
M_0^7 $\theta = A \to G = G \to A$
M_0^8 $\lambda = C \to T = T \to C$
M_0^9 $\alpha = A \to C = C \to A$
M_0^{10} $\iota = T \to G = G \to T$

		Transcribed	Flanking	Intron	Exon	non-CpG	LINE	SINE	LTR	DNA
	transition sym.									
M_0^1:η	$G \to A = C \to T$	0.604	0.050	0.644	0.936	0.682	0.814	0.513	0.760	0.932
M_0^2:β	$A \to G = T \to C$	**1.000**	0.103	**1.000**	0.932	**1.000**	**1.000**	**0.991**	**0.998**	**1.000**
	transversion sym.									
M_0^3:δ	$C \to A = G \to T$	0.284	0.123	0.313	0.555	0.238	0.298	0.488	0.209	0.345
M_0^4:γ	$A \to T = T \to A$	0.187	0.086	0.193	**0.956**	0.110	0.207	0.196	0.111	0.187
M_0^5:μ	$A \to C = T \to G$	0.073	0.088	0.102	0.724	0.061	0.160	0.362	0.091	0.184
M_0^6:ε	$C \to G = G \to C$	0.217	0.109	0.238	**0.958**	0.072	0.207	0.172	0.192	0.297
	reversible sym.									
M_0^7:θ	$A \to G = G \to A$	**1.000**	**1.000**	**1.000**	0.910	**1.000**	**1.000**	0.934	**1.000**	**1.000**
M_0^8:λ	$C \to T = T \to C$	**1.000**	**1.000**	**1.000**	0.919	**1.000**	**1.000**	**0.994**	**1.000**	**1.000**
M_0^9:α	$A \to C = C \to A$	0.034	0.735	0.052	0.802	0.059	0.226	0.677	0.045	0.154
M_0^{10}:ι	$T \to G = G \to T$	0.191	0.711	0.292	0.783	0.129	0.746	0.159	0.155	0.519

Table 4.1: Testing for strand symmetry of substitution rates using non-reversible substitution models. The null hypothesis for the strand-symmetry of rates between strand complementary substitutions and for reversibility assumption of substitutions was tested in the transcribed and non-transcribed alignment fraction. A variety of additional datasets have been extracted from the transcribed dataset such as an intron and exon subset, a subset where CpG related substitutions were excluded and a subset corresponding to the 4 categories of interspersed repeats (LINE, SINE, LTR and DNA transposons). The fraction of tests rejecting the strand symmetric model between complementary substitution rates and for reversibility of substitution rates are shown. In total, the null-hypothesis was tested in 1000 alignments 100 Kb in length that were sampled from the individual datasets. The strand symmetry for a dataset was rejected when at least 95% of the corresponding alignments rejected the null-hypothesis (datasets exceeding 95% shown in bold).

4.1.4 The direction of the strand-specific substitution rates

A more detailed view on the substitution strand symmetry is obtained by comparing the ratios of complementary substitution rates estimated from the transcribed and non-transcribed alignment fractions (Figure 4.5). The substitution rate parameters were estimated from the unrestricted non-reversible substitution model using paml (Yang, 1994a). In the transcribed fraction the ratio between complementary transitions $A \rightarrow G$ and $T \rightarrow C$ was in average 1.26. The ratio between other strand complementary substitution rates showed only an average ratio of 1.1. An exception are the transversions $A \rightarrow C$ and $T \rightarrow G$ that showed strand symmetry in the transcribed and non-transcribed dataset. In the non-transcribed alignment fraction all performed comparisons showed a strand symmetry.

The transition rates $G \rightarrow A$ and $C \rightarrow T$ have the highest rates followed by the $A \rightarrow G$ and $T \rightarrow C$ transitions. Transversion rates were about 4 fold lower than transition rates. The estimated substitution rates were then compared between the transcribed and non-transcribed fraction. Two transition rates ($G \rightarrow A$, $A \rightarrow G$) and three transversion rates ($C \rightarrow G$, $A \rightarrow C$, $T \rightarrow G$) are significantly increased in the transcribed fraction (t-test, $p \leq 0.05$). The remaining 7 substitution rates showed a significant decreased rate in the transcribed fraction (t-test, $p \leq 0.05$). The distributions of the rates for the individual substitution types are shown in Figure 4.6 A. To judge the extent of the substitution rate differences between the transcribed and non-transcribed fraction the difference of the mean substitution rates estimated from both alignment fractions are shown (Figure 4.6 B). Although a significant difference was observed between all substitution rates of the transcribed and non-transcribed alignment fraction, a large difference is more meaningful than a small or a slight change. The $A \rightarrow G$ transition is remarkably increased in the transcribed fraction, whereas other substitution rates are

Figure 4.5 ***(following page)*:** Ratio between strand complementary substitution rates. The individual distributions and mean of the substitution rate ratios between strand complementary substitution rates that were estimated from 1000 bootstrap sampled alignments in the transcribed and non-transcribed fraction using an unrestricted non-reversible substitution model are shown. In the transcribed fraction the ratio of the transitions $A \rightarrow G$ and $T \rightarrow C$ was in average 1.26 and largest in comparison to the other ratios with an average of 1.1 in the transcribed fraction. The transversions $A \rightarrow C$ and $T \rightarrow G$ showed an average ratio of 1 in the transcribed fraction. All ratios from strand complementary substitution rates estimated from the non-transcribed fraction had also an average ratio of 1.

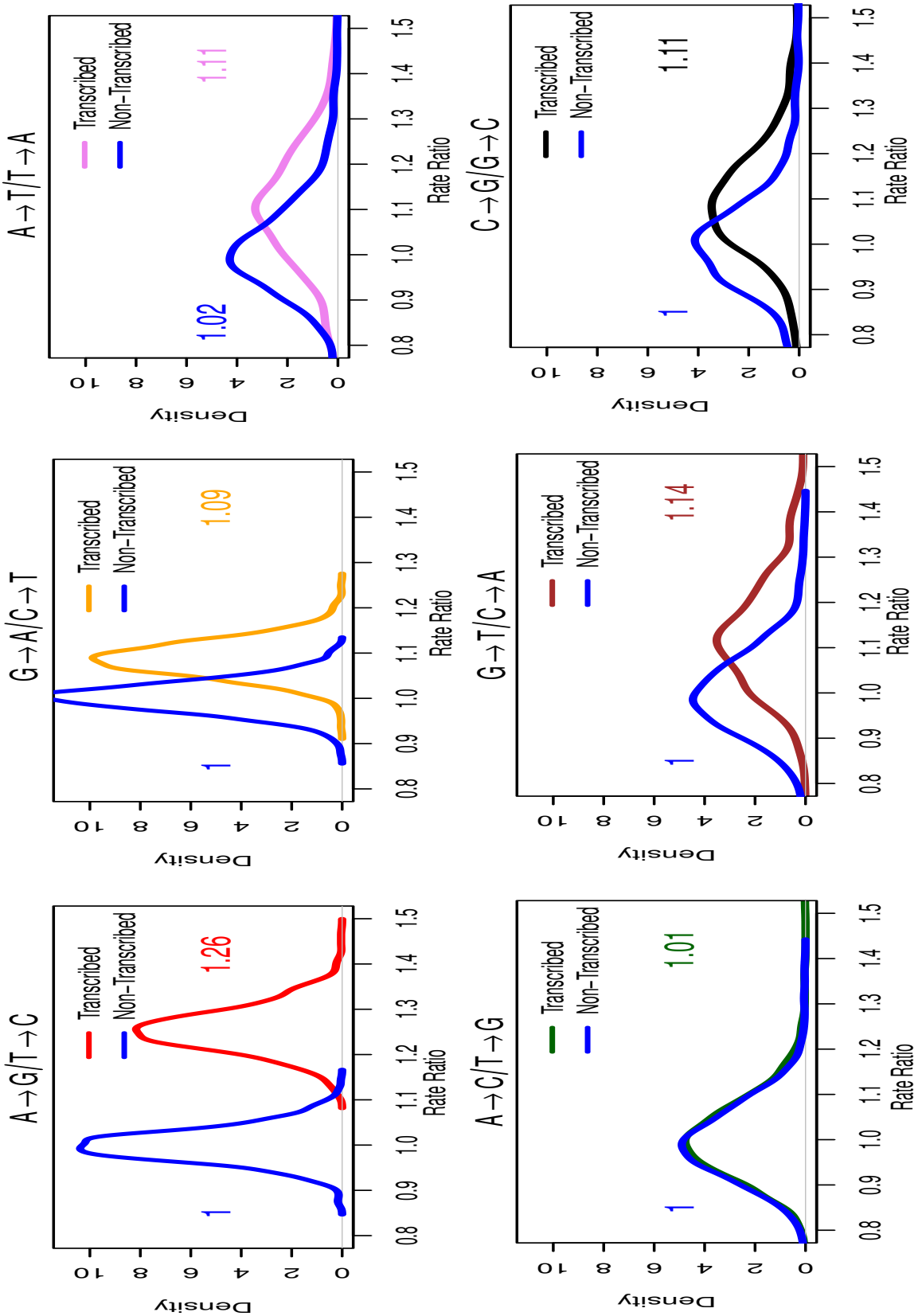
A→G/T→C
Transcribed
Non−Transcribed
1.26
1
Density
Rate Ratio
G→A/C→T
Transcribed
Non−Transcribed
1.09
1
Density
Rate Ratio
A→T/T→A
Transcribed
Non−Transcribed
1.11
1.02
Density
Rate Ratio
A→C/T→G
Transcribed
Non−Transcribed
1.01
1
Density
Rate Ratio
G→T/C→A
Transcribed
Non−Transcribed
1.14
1
Density
Rate Ratio
C→G/G→C
Transcribed
Non−Transcribed
1.11
1
Density
Rate Ratio

decreased or only slightly changed compared to the non-transcribed fraction.

4.2 Discussion

Transcription-coupled repair has been suggested to specifically increase the rate of A→G transitions relative to the rate of the complementary change, T→C (Green, 2003). Yet, a genome-wide statistical analysis of this proposed transition asymmetry in transcribed regions has not been confirmed. Here, I have separated the human genome into two fractions. The first part consists of genes for which evidence exist that they are transcribed in the human germ line. The second part, corresponding to the bona-fide non-transcribed fraction of the human genome, is comprised by genomic regions located outside of known genes.

A Likelihood-Ratio-Test (LRT) revealed that in the transcribed dataset a more complex non-reversible substitution model (11 parameters) gives a significantly better fit to the data than the simpler model in which the same rate was assigned to the complementary A → G and T → C transitions (10 parameters). Notably, the strand symmetric null models for the 5 remaining pairs of complementary substitution pairs could not be rejected. For the non-transcribed alignment fraction none of the strand symmetric models could be rejected. Thus, I provide evidence that an increased rate of A→G over T→C substitutions is specific to transcribed sequences in the human genome. It may therefore be indeed an effect of transcription-coupled repair.

To analyze the impact of other components of the transcribed fraction to the results

Figure 4.6 ***(following page)*****:** **A)** Distribution of substitution rates estimated from the transcribed and non-transcribed dataset. Shown are the substitution rates estimated using the unrestricted substitution model (Yang, 1994a) from 1000 alignments sampled from the transcribed (red) and non-transcribed (blue) dataset. The distribution of the $A \rightarrow G$ transition rates shows the most prominent increase in the transcribed dataset compared to the non-transcribed dataset. Strand complementary substitution rates are placed next to each other in the diagram. The median of transitions are about 4-fold higher than the median of transversions. The $C \rightarrow T$ and $G \rightarrow A$ transition rates have the highest median rate followed by the $A \rightarrow G$ and $T \rightarrow C$ transition rates. **B)** Differences between the average substitution rates estimated from 1000 sampled alignments of the transcribed and non-transcribed dataset. Whereas the average $A \rightarrow G$ rate is prominently increased in the transcribed dataset the average of the other substitution rates are decreased or only slightly changed.

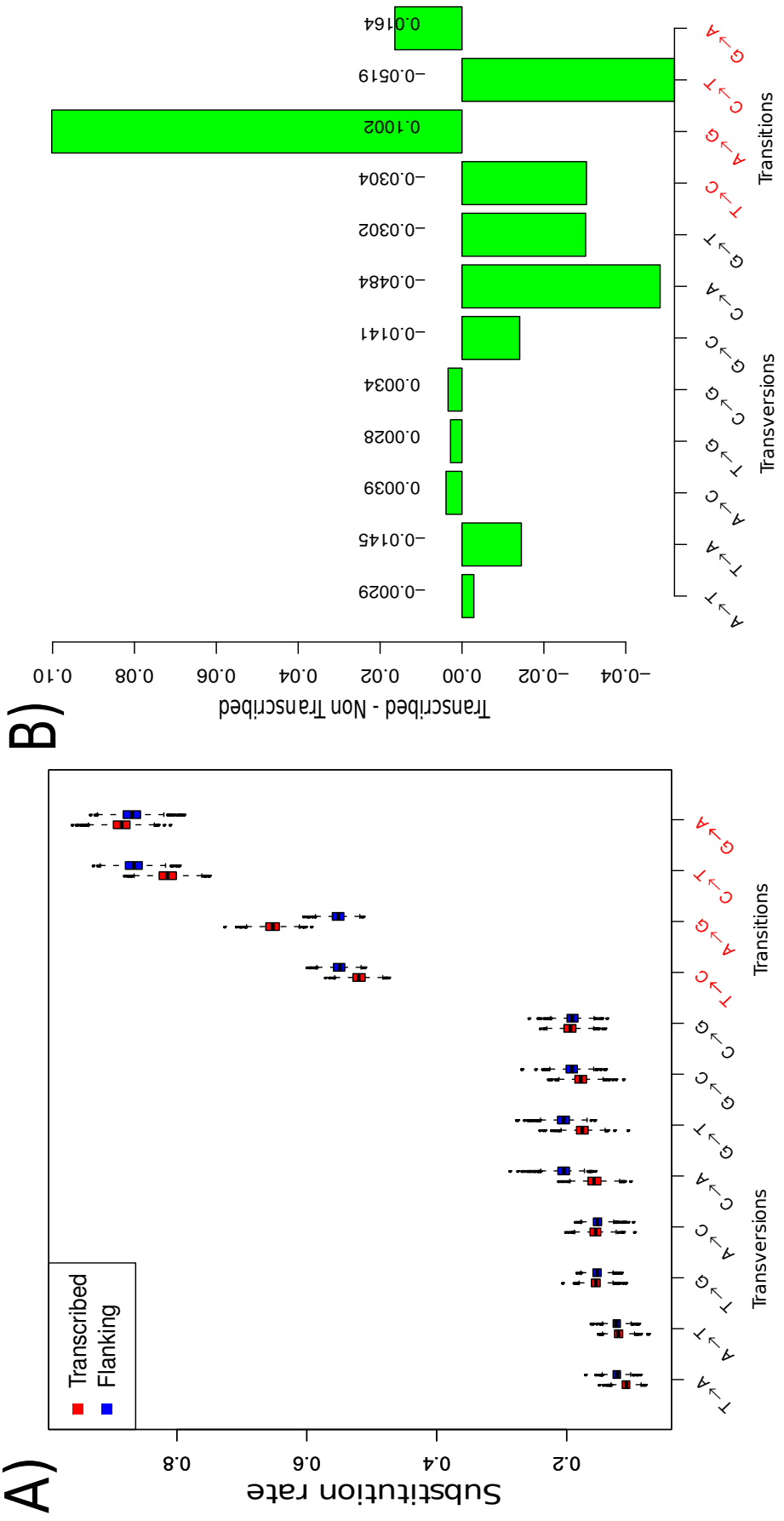
A)
Substitution rate
0.2
0.4
0.6
0.8
Transcribed
Flanking
Transversions
Transitions
T↖A
A↖T
A↖G
T↖C
A↖C
G↖T
G↖C
C↖G
T↖G
C↖A
C↖T
G↖A
B)
Transcribed - Non Transcribed
−0.04
−0.02
0.00
0.02
0.04
0.06
0.08
0.10
−0.0029
−0.0145
0.0039
0.0028
0.0034
−0.0141
−0.0484
−0.0302
−0.0304
0.1002
−0.0519
0.0164
Transversions
Transitions
A↖T
T↖A
C↖A
G↖C
G↖T
C↖G
C↖T
G↖A
T↖C
A↖G
T↖G
A↖C

obtained from the LRTs, the analysis was additionally performed in the protein-coding exons, in introns, a fraction where substitutions related CpG dinucleotides were excluded, and four fractions corresponding to interspersed repeats. Except for the exon fraction all other alignment fractions corresponding to the transcribed fraction rejected the simpler model for $A \rightarrow G = T \rightarrow C$. However, notably for the exon fraction is, that almost all symmetries introduced into the substitution models lead to LRT results that are at the border of significance (c.f. Table 4.1). This may be attributed to the particular mode of evolution in protein coding exons. The information is encoded in base triplets making the assumption of the neighbor independent substitution process inherent in the models used in this analysis inappropriate. In addition, the substitution rates are highly decreased in exonic sequences due to selective constraints. However, exons make up only for a small part of the transcribed fraction and have no influence on the results for the entire transcribed fraction. To examine a putative impact of CpG related transitions to the observed rejection of the strand symmetry an additional dataset was examined, where CpG related substitutions were excluded. However, as for the entire transcribed alignment fraction the simpler model $A \rightarrow G = T \rightarrow C$ was rejected. This indicates that an increased $A \rightarrow G$ rate is not an effect of CpG-related substitutions.

The substitution model parameters were estimated from sampled alignments of the concatenated alignment fractions for the different datasets, where the estimates represent a global average. It is therefore not expected that results change for other gene subsets that define the transcribed alignment fraction. The study shows that the observed increase of the $A \rightarrow G$ substitution rate in the transcribed fraction of the human genome has a significant impact to distinguish the substitution model between the transcribed and non-transcribed alignment fraction.

Chapter 5

Species-Specific evolving regions in the human and chimpanzee genomes

In the previous chapter it was shown that the substitution rates $A \rightarrow G \neq T \rightarrow C$ in transcribed genomic regions. This can be explained by transcription-coupled-repair (Green, 2003). The extent of the $A \rightarrow G$ signature for a gene could be therefore used as an indicator for the transcription activity in the genome of a particular species. Thus, genes that are differentially expressed in humans and chimpanzees are subject to different extents of transcription coupled repair, and thus should differ in their rates and patterns of DNA sequence evolution. In this chapter, the homogeneity of the substitution model between human and chimpanzee is tested to identify transcribed genomic regions with species-specific substitution patterns.

A substitution model provides a stochastic framework to model the substitution process between DNA sequences in an alignment. As introduced in chapter 3, a markov process is used for this purpose that assumes homogeneity, stationarity and reversibility. The reversibility of the process assumes that a substitution and the corresponding reverse substitution are not distinguished. When the homogeneity of the substitution model is assumed the substitution patterns are the same and independent from time for all branches in the phylogenetic tree. In such a homogeneous substitution model an equilibrium nucleotide composition exists, and is the same for all taxa considered, to which the sequences evolve and approximate in time infinity. The stationarity of the substitution model assumes that the sequences have reached already the equilibrium nucleotide composition which will then remain unchanged during the process. However,

these assumptions are commonly applied simplifications to model the substitution process and are not always valid when biological sequence data are analyzed. Species that do not evolve alike evolve towards a different equilibrium nucleotide composition and can therefore vary extensively in the genomes GC content. For example the genome of the protozoan parasite *Plasmodium falciparum* has a very low GC content of $\sim$ 20% (Gardner *et al.*, 2002) in comparison to *Plasmodium vivax* that has a GC content of $\sim$ 45% (Carlton *et al.*, 2001). However, when the homogeneity assumption is not valid a more complex substitution model may be more appropriate to describe the evolutionary process. Such a more complex "non-homogeneous substitution model" describes the evolutionary process individually for each branch in the tree (e.g., Barry and Hartigan, 1987).

Different strategies are introduced for statistical comparisons of the substitution patterns between species. A simple approach was introduced by the disparity index (Kumar and Gadagkar, 2001) that measures the observed compositional differences between a pair of sequences to infer whether the homogeneity of the substitution patterns do not differ more than expected from the divergence from the sequences. However, for comparisons between sequences that have the same nucleotide composition such as, e.g., human and chimpanzee, such a test is not appropriate. Therefore, a more sensitive method that estimates the substitution process between the sequences in an alignment is required. A parametric bootstrap approach to test the homogeneity assumption of the substitution model in a phylogenetic tree has been described by the Model-Homogeneity-Test (MHT) in Weiss and von Haeseler (2003). In the MHT, the statistic Δ measures the deviations between the substitution models that are estimated from sequence pairs in an multiple sequence alignment. From all pairwise substitution rate matrices a covariance matrix is computed and decomposed. The test statistic is then defined by the sum of eigenvalues of the decomposed covariance matrix. It is necessary to determine whether the differences between the pairwise estimated substitution models, captured in Δ are significant or whether they arise due to the stochastic nature of the substitution process and the finite amount of data. Even if sequences evolve according to the same substitution model, their substitution patterns can vary by chance such that the estimated pairwise substitution models differ from each other. The Model-Homogeneity-Test uses a simulation procedure to infer the significance of Δ to reject the homogeneity of the substitution model. For this purpose, a model for the null-hypothesis that the substitution process

is homogeneous over the entire tree is required. To arrive at such a model, the average of the pairwise substitution rate matrices is computed and used as a null-model. The variation of Δ that is expected by chance is inferred from sequence alignments that are generated under the homogeneous null-model. The procedure generates 1000 simulated alignments to compute the distribution of Δ_{sim}. The error probability when rejecting the homogeneity of the substitution model in the tree is then assumed from the fraction of Δ_{sim} values $\geq \Delta_{obs}$.

The Model-Homogeneity-Test has been designed to test the homogeneity of the substitution model for an entire phylogenetic tree. For a comparison of the substitution processes between individual branches more complex non-homogeneous substitution models are required. A non-homogeneous model allows to distinguish the substitution process between individual species. An extension to the MHT for testing the homogeneity of the substitution model between individual branches in a tree, called the Single-Branch-Test (SBT), was developed by Gunter Weiss and Arndt von Haeseler (unpublished). The substitution rate matrices are estimated for each branch in the tree from pairwise sequence comparisons in an alignment (Baake, 1998). The statistic is defined as a contrast between a set of two or more branches, where the variations between the models are measured as squared distance between the corresponding substitution rate matrices. The null-distribution of the defined contrast is again inferred by parametric bootstrap, where sequence alignments are simulated under the homogeneity assumption. The Single-Branch-Test is described in detail in the next section.

5.1 Estimation of branch-specific substitution models

The transition probability matrix $P(t)$ describes the substitution process of a lineage from the ancestral state to the observed present-day sequence. As the transition probabilities are not directly observable from sequence data, it is shown in the following how to estimate $P(t)$ from pairwise sequence comparisons. In a pairwise sequence comparison the time units t leading to the sequence X_1 and X_2 from the ancestral sequence X_0 is unknown: Let $h_{(i,j)}^{(r,s)}$ denote the frequency of having nucleotides i and j $(i, j \in \{A, C, G, T\})$ in sequences r and s, respectively. These probabilities are gathered in the so-called divergence matrix $H^{(r,s)}$.

The definition of Q allows to estimate the evolutionary distance and the substitution

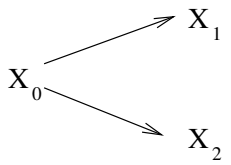

model from the enumerated substitutions in a pair of sequences when a reversible process is assumed (Baake, 1998).

Assuming stationarity and reversibility of the substitution process the divergence matrix can be expressed as

$$H^{(r,s)} = diag(\pi_A, \pi_C, \pi_G, \pi_T) \cdot P^{(r,s)}. \tag{5.1}$$

The transition probability matrix for the path from sequence x to y is then given by

$$P^{(r,s)} = diag(\frac{1}{\pi_A}, \frac{1}{\pi_C}, \frac{1}{\pi_G}, \frac{1}{\pi_T}) \cdot H^{(r,s)}. \tag{5.2}$$

From the pairwise leaf-to-leaf transition matrices branch specific transition matrices can be estimated (Baake, 1998) by the following: Let i, j, k denote leaves in an unrooted three taxon tree and m the internal node (Figure 5.1). The return-trip transition matrix $M^{(i,m)}$ for an external branch connecting leaf i and node m can be expressed as:

$$\begin{aligned} M^{(i,m)} &= P^{(i,m)} \cdot P^{(m,i)} \\ &= P^{(i,j)} \cdot (P^{(k,j)})^{-1} \cdot P^{(k,i)}. \end{aligned} \tag{5.3}$$

The equation shown in 5.3 requires only leaf-to-leaf transition matrices. Thus, the return-trip matrices $M^{(i,m)}$ can be expressed in terms of divergence matrices (Eq. 5.3). The transition probability matrix $M^{(i,m)}$ is defined as exponential of the instantaneous rate matrix $Q^{(i,m)}$:

$$M^{(i,m)} = exp(Q^{(i,m)}(t)) \tag{5.4}$$

Assume $M^{(i,m)}$ has a spectral decomposition (Bailey *et al.*, 1990):

$$M^{(i,m)} = U \cdot diag(e^{\lambda_1 t_{i,m}}, e^{\lambda_2 t_{i,m}}, e^{\lambda_3 t_{i,m}}, e^{\lambda_4 t_{i,m}}) \cdot U^{-1} \tag{5.5}$$

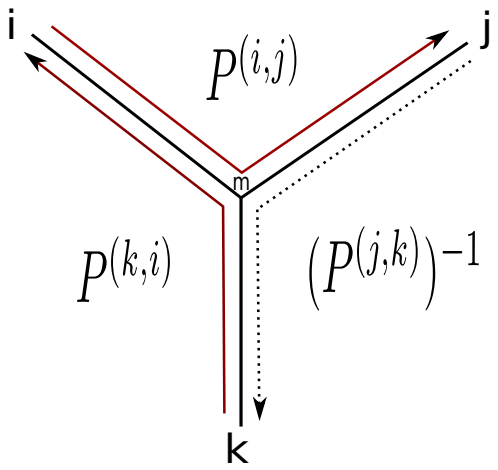

Figure 5.1: Return-trip transition matrices reconstructed from pairwise leaf-to-leaf transition matrices (Baake, 1998)

The matrix $M^{(i,m)}$ is decomposed to the left eigenvectors in U, the eigenvalues defined in λ and right eigenvectors. The instantaneous rate matrix $Q^{(i,m)}$ is computed from the logarithm of the eigenvalues, where $e^{\lambda_j t_{i,m}}$ is replaced by $\lambda_j t_{i,m}$.

$$Q^{(i,m)} = U \cdot diag(\lambda_1 t_{i,m}, \lambda_2 t_{i,m}, \lambda_3 t_{i,m}, \lambda_4 t_{i,m}) \cdot U^{-1} \tag{5.6}$$

For a given alignment the substitution rate matrix Q is estimated for each branch in the unrooted tree of human, chimpanzee and rhesus. The test for the homogeneity of the substitution patterns are performed by a contrast of the human and chimpanzee branch. The variations between the substitution models are quantified by a statistic that measures the squared distance δ of the corresponding substitution rate matrices:

$$\delta = \sum_{i=1}^{12} (q_i^{(human)} - q_i^{(chimp)})^2. \tag{5.7}$$

The vectors $q^{(human)}$ and $q^{(chimp)}$ describe the off-diagonal elements of the individual rate matrices Q of the human and chimpanzee branch in the tree. For the null-hypothesis that the substitution process is homogeneous over the entire tree an average substitution rate matrix is computed from the substitution rate matrices of the branches and used as null-model. The null model q_{null} is defined by averaging the substitution rates in the

vectors q^i from all branches i in the three taxon tree:

$$q_{null} = \frac{1}{n} \sum_{i=1}^{n} q^{(i)} \tag{5.8}$$

The probability to reject the homogeneity assumption over the defined branches is estimated from the fraction of δ_{sim} values $\geq \delta_{\text{obs}}$. An overview of the procedure is shown in Figure 5.2.

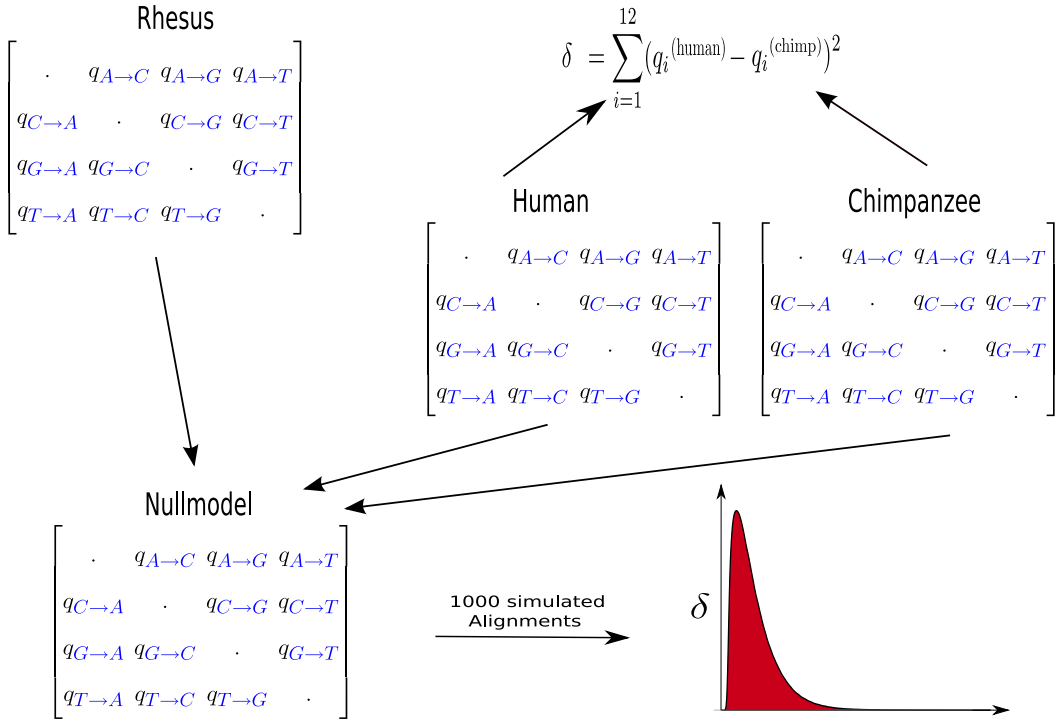

Figure 5.2: Testing model homogeneity between human and chimpanzee. The substitution rate matrices are estimated for the branches in the human, chimpanzee and rhesus tree. The difference between the human and chimpanzee substitution matrices are inferred by a squared distance. The homogeneous model for the tree that is used for the simulation procedure is the average substitution rate matrix of all branches. Sequence alignments are simulated under the homogeneous model to obtain the null-distribution of δ. The critical value of δ to reject the homogeneity assumption between the human and chimpanzee substitution model is determined from the simulated null-distribution.

5.2 Testing the homogeneity assumption of the substitution model between humans and chimpanzees

A sliding window approach was used to screen the human genome for regions that evolve in a species-specific manner. The individual alignment window datasets that were used for the study are described in detail in chapter 2 (Table 2.1). The SBT was applied to each alignment window to identify genomic regions for which the human substitution model differs significantly from the chimpanzee substitution model. To assess the influence of the window length on the outcome of the test, different window sizes of 125, 250, 500, and 1000 Kb were used. In addition, the transcribed fraction of the 125 Kb windows as well as the transcribed fraction of individual genes was analyzed separately. The confidence limit for the SBT was set to $p \leq 0.05$. An alignment window for which the homogeneity assumption between human and chimpanzee substitution process was rejected is referred to as significant alignment window in the following. The results of the analysis are summarized in table 5.1.

The impact of the alignment length on the power to detect a significant difference between the models was verified by comparing the fraction of significant tests of the alignments between the different alignment window sizes. The fraction of significant alignment windows is slightly increased in the bigger window sizes with 5.69% tests in the 125 Kb to 8.1% tests of the 1000 Kb alignment windows (Table 5.1). This indicates that the power of the test increases with the sample size.

The signal to detect a difference between the human and chimpanzee substitution models is expected to be weak due to the low number of substitutional sequence differences between both species. As only a small fraction of significant alignment windows were detected (c.f. Table 5.1), the distribution of the p-values obtained from the genome-wide analysis are expected to follow almost an uniform distribution. The power of the SBT to detect a difference between the human and chimpanzee substitution model is examined by a probability-probability plot. The probability-probability plot allows to compare the cumulative p-value distribution to a cumulative uniform distribution (Figure 5.3). For the different datasets only a small deviation to an uniform distribution is observed that slightly increases for bigger window sizes.

Dataset	Total windows tested	Significant	Fraction (significant)
1000 Kb	2176	177	8.13%
500 Kb	4321	287	6.64%
250 Kb	8608	544	6.32%
125 Kb	17138	974	5.68%
TRF_{125Kb}	12596	717	5.69%
$TRF_{Transcript}$	7292	412	5.65%

Table 5.1: Results of the SBT between human and chimpanzee. Overview of the results obtained for the alignments of the 125 Kb to 1000 Kb alignment window (*Dataset*) and the transcribed fraction of the 125 Kb windows (TRF_{125Kb}) and the transcribed fraction of individual genes ($TRF_{Transcript}$). Shown is the total number of alignment windows as well as the number and the percentage of significant alignment windows.

When multiple tests are performed at a significance level of 5% one accepts to falsely reject the null hypothesis of model homogeneity in 5% of all performed tests. In my analysis, about 5% of the performed tests reject the null hypothesis. Hence, it is necessary to show that the substitution models do not differ solely by chance due to the multiple tests that have been performed. A detailed analysis of the substitution patterns is conducted to describe the differences between the human and chimpanzee model in the significant alignment windows.

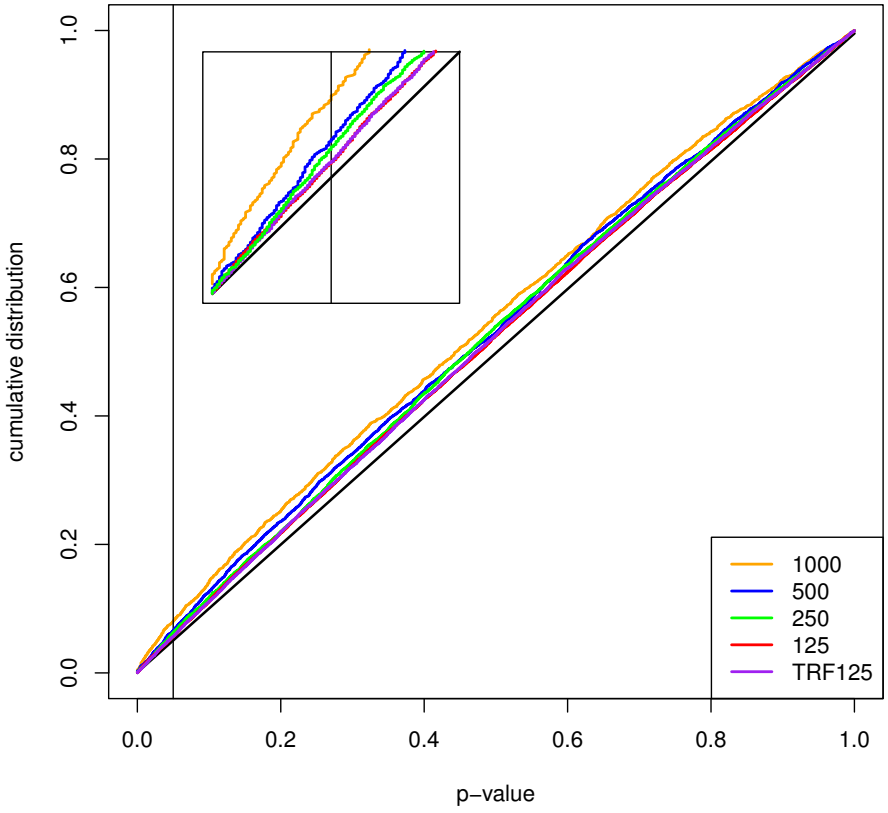

Figure 5.3: Probability-Probability plot of the SBT nominal p-values. The plot shows the percentages of tests falling at or below a given p-value from the SBT in 125 KB to 1000 KB alignment windows, and the transcribed fraction datasets. The diagonal (black) illustrates a distribution of samples from a uniform distribution. The vertical line shows the 5% confidence limit. Only a small deviation of the p-value distributions to a uniform distribution is observed.

5.2.1 Normalization of δ estimated from different alignment windows

The number of analyzable ungapped alignment positions and the amount of divergence between the sequences differ among the alignment windows. With an increasing size of an alignment or increasing sequence divergence the distance measure of δ decreases due to the higher accuracy and precision of the estimates. How close the estimated δ is to the true unknown value is dependent on the accuracy and the variation of δ around the true value, i.e., on the precision of the estimate δ. For the comparison of the δ statistic estimated among different alignment windows a normalization procedure is therefore required that is discussed in detail in chapter 6. The estimated δ is then scaled to a sample size of 50 000 analyzable alignment columns and a pairwise sequence divergence of 1 %. For each alignment window the branch length of the unrooted three species tree is inferred using the neighbor-joining algorithm (Saitou and Nei, 1987).

The scaling factor for the estimates δ relative to a branch length of 0.005 expected substitutions per site for the human and chimpanzee branch as was determined from a calibration curve (chapter 6, Figure 6.6). For a variety of branch lengths, the mean of δ was computed from 1000 simulated alignments of 50 Kb in length, generated with the same substitution model for all branches in the tree. The model was defined by a random substitution rate matrix explained in detail in chapter 6. δ was measured between two branches with branch lengths between 0.001 and 0.2 expected substitutions per site. The calibration curve is defined by an interpolation function F that describes δ as function of the branch length. The function allows to determine the expected δ for any given branch length b. The scaling factor for δ estimate is then determined by the ratio of $F_{0.005}$ and F_b, where b denotes branch length estimated for human and chimpanzee from the given alignment window. The normalization of δ considering the alignment size and branch length is computed by:

$$\delta_{norm} = \delta \cdot F_{0.005}/F_b \cdot L_s/L_{50Kb} \tag{5.9}$$

L_s denotes the number of analyzable alignment columns of an alignment window and L_{50Kb} denotes the reference alignment size of 50 Kb. The effect of the normalization procedure is shown in Figure 5.4.

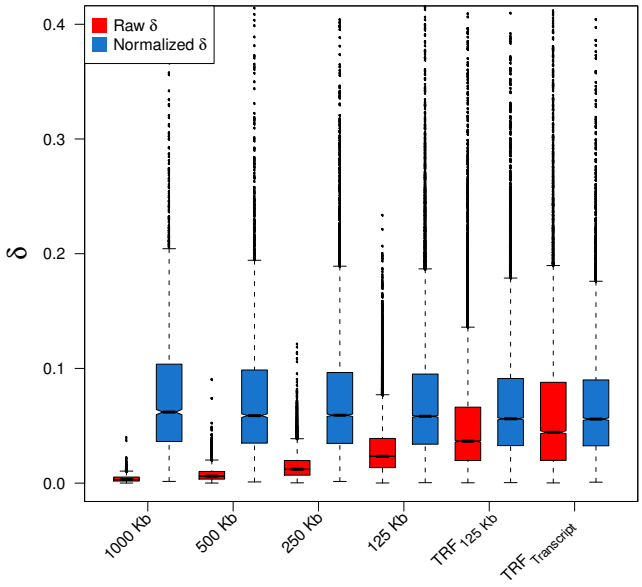

Figure 5.4: The distribution of δ obtained from the alignment datasets of 1000 Kb, 500 Kb, 250 Kb, 125 Kb windows, the transcribed fraction of the 125 Kb windows (TRF 125) and the transcribed fraction of individual genes (Ensembl) are shown before (red) and after normalization (blue). δ is normalized relative to a pairwise sequence divergence of 1% between human and chimpanzee and an alignment size of 50 Kb.

5.2.2 Overview of the significant alignment windows

In the following, it was investigated whether the fractions of significant alignment windows or the distributions of δ differ among the chromosomes. The enrichment of significant alignment windows for each chromosome was inferred using the Fisher exact test (Table 5.3). The number of significant alignment windows are enriched on chromosome X (42/491, 8.5%), chromosome Y (6/31, 19.35%) and chromosome 6 (52/712, 7.3%). Multiple testing was considered by estimating the false discovery rate (FDR, Benjamini and Y. (1995)). The FDR denotes the expected fraction of false positive tests among the significant alignment windows. When multiple tests are considered chromosome X and Y remain significant for a FDR < 0.1. The distribution of δ estimated from the transcribed fraction of the 125 Kb alignment windows were compared between the chromosomes by an one factor ANOVA analysis. This shows that the distributions of δ are significantly different between the chromosomes (ANOVA, p$\leq$2.2e-16). Figure 5.5

shows the corresponding distributions of δ for each chromosome. Note, chromosome Y has a remarkably increased distribution of δ compared to the other chromosomes. The ANOVA analysis remains significant when chromosome Y is excluded.

So far, I have searched for alignment windows which had a significant difference between the substitution models of human and chimpanzee. Intuitively, an alignment with a large δ suggests that the differences between the human and chimpanzee substitution models also have a biological significance. Subsequently I selected those windows for further analysis that show the strongest difference among all tested alignment windows. For further analysis the alignment windows with a a significant p-value and with a δ in the 5% largest δ values were selected (Figure 5.5). The selected alignment windows comprised a total of $\sim 4.5\%$ for the different datasets (Table 5.2).

Dataset	Total	$p \leq 0.05; \delta > \delta_{95\%}$	Percentage Selected
1000 Kb	2176	107	4.92 %
500 Kb	4321	205	4.74 %
250 Kb	8608	395	4.59 %
125 Kb	17138	771	4.5 %
TRF_{125Kb}	12596	565	4.49 %
$TRF_{Transcript}$	7292	328	4.5 %

Table 5.2: Significant alignment windows with $\delta > \delta_{95\%}$ from all tests after normalization. Alignment windows were selected with strongest difference between the estimated human and chimpanzee substitution model.

5.2.3 Characterization of the substitution patterns in significant alignment windows

In the next step, the aim was to identify which type of substitution contributes significantly to the rejection of the substitution model homogeneity assumption between human and chimpanzee. The δ statistic allows only to measure the overall differences between the human and chimpanzee models by the squared distance between the corresponding rate matrices. Therefore, the Single-Branch-Test was extended by defining a statistic to measure the differences between each component of the human and chimpanzee substitution model.

The individual substitution rates were tested whether they differ significantly between

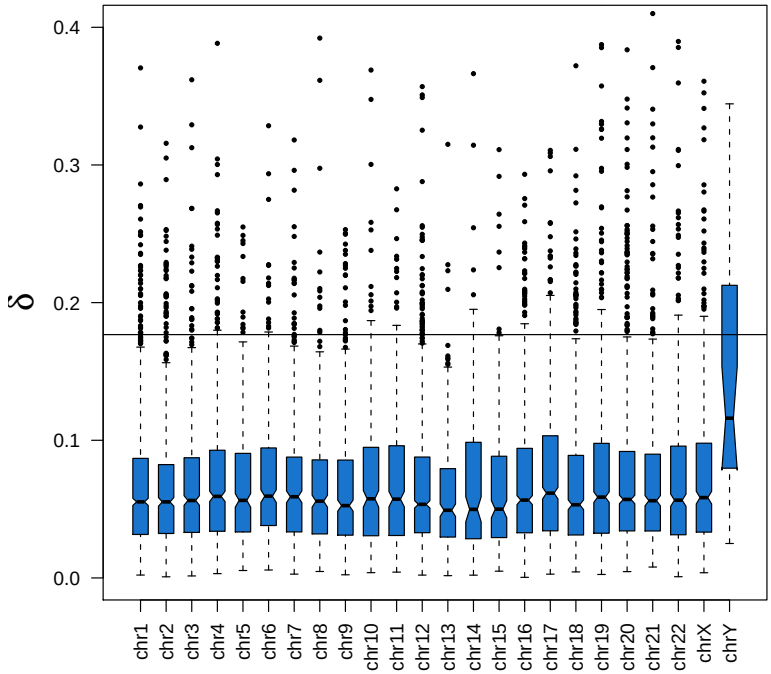

Figure 5.5: Human and chimpanzee model differences for the 24 human chromosomes. The plot shows the distributions of δ estimated from the transcribed fraction of the 125 Kb alignment windows (TRF_{125Kb}). The horizontal line denotes the genome-wide 95% quantile of the δ distribution estimated from all alignment windows. Significant alignment windows with a δ above the horizontal line and a p-value $\leq$0.05 are selected for further analysis.

the human and chimpanzee model for all 125 Kb alignment windows in the transcribed fraction of the human genome (TRF_{125Kb}). The statistic is defined as a squared difference for each of the 12 substitution rates i between $q^{(human)}$ and $q^{(chimpanzee)}$.

$$\delta_i = (q_i^{(human)} - q_i^{(chimpanzee)})^2 \tag{5.10}$$

The null-distribution of each δ_i for each substitution type is inferred from the 1000 simulated alignments that were generated under a homogeneous model.

The number of how often the rate equality for each substitution type was rejected between the human and chimpanzee model was counted and compared between the set of significant alignment windows ($SBT_p \leq 0.05; \delta > \delta_{95\%}$) and the non-significant alignment windows of the TRF_{125Kb} alignment dataset (Figure 5.6). As the human and chimpanzee substitution model underlying this analysis are reversible the counts of tests that rejected equality for the individual substitution types are averaged for the six reversible substitution rate pairs.

The observed model differences between the human and chimpanzee substitution models are mainly driven by a difference between the transition rates. The significant alignment windows rejected the substitution rate equality between the human and chimpanzee model for the transitions $A \leftrightarrow G$ in >50%, for the transitions $T \leftrightarrow C$ in >50% and for each of the transversions ($A \leftrightarrow C$, $T \leftrightarrow G$, $G \leftrightarrow C$, $T \leftrightarrow A$) in <20 %. In the non-significant alignment windows, only less than $\leq 5\%$ rejected the substitution rate equality for the different substitution types.

Chromosome	Percentage (%)	Significant	Expected	Total	P-value	FDR
1	5.05	58	65.35	1148	0.8533	0.9986
2	4.27	44	58.63	1030	0.9859	0.9986
3	4.57	40	49.86	876	0.9450	0.9986
4	6.96	46	37.63	661	0.0899	0.4315
5	6.04	40	37.68	662	0.3693	0.8057
6	**7.30**	**52**	**40.53**	**712**	**0.0374**	**0.2992**
7	6.21	54	49.52	870	0.2691	0.8057
8	5.98	33	31.42	552	0.4103	0.8206
9	7.32	38	29.54	519	0.0657	0.3942
10	5.23	33	35.92	631	0.7216	0.9986
11	4.20	25	33.87	595	0.9601	0.9986
12	6.11	37	34.50	606	0.3516	0.8057
13	4.26	14	18.73	329	0.9007	0.9986
14	5.39	20	21.12	371	0.6332	0.9986
15	6.33	25	22.48	395	0.3195	0.8057
16	4.23	16	21.52	378	0.9175	0.9986
17	6.44	29	25.62	450	0.2690	0.8057
18	4.98	14	16.00	281	0.7350	0.9986
19	5.64	19	19.18	337	0.5517	0.9458
20	2.33	7	17.08	300	0.9986	0.9986
21	8.05	12	8.48	149	0.1421	0.5684
22	5.86	13	12.64	222	0.4992	0.9216
X	**8.55**	**42**	**27.95**	**491**	**0.0053**	**0.0864**
Y	**19.35**	**6**	**1.76**	**31**	**0.0072**	**0.0864**

Table 5.3: Enrichment analysis of significant tests for the 24 human chromosomes
For each *chromosome* the *percentage* and number of *significant* alignment windows, the number of *expected* significant alignment windows and the *total* number of alignment windows are shown. The enrichment of significant alignment windows on a chromosome was estimated by a one-sided Fisher Exact Test (*p-value*). Chromosome 6, X and Y show an enrichment for significant alignment windows (confidence limit for nominal p-value $p \leq 0.05$). To account for multiple testing, a p-value correction was performed using the FDR. The FDR estimates the expected false discovery rate and is < 0.1 for the X and Y chromosome.

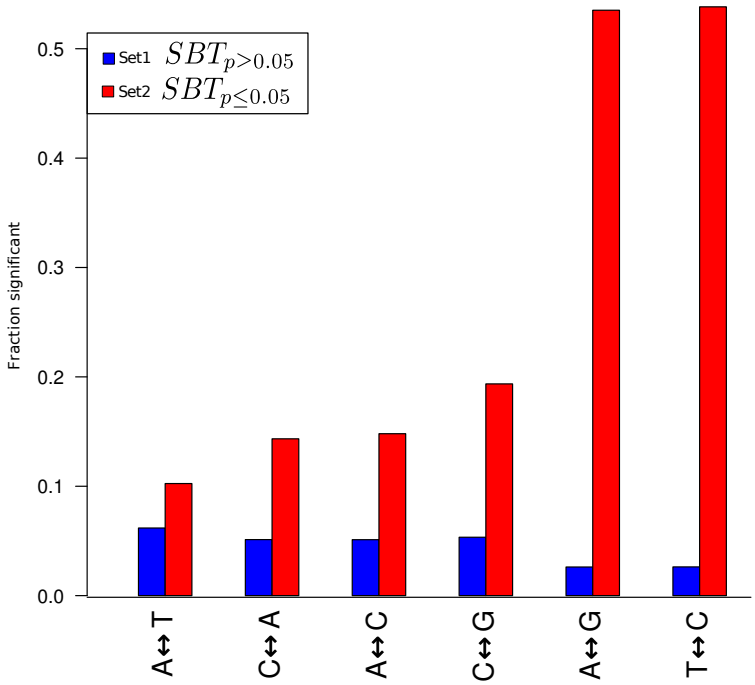

Figure 5.6: Substitution rates with a significant difference between the human and chimpanzee models. The Single-Branch-Test was extended to identify which type of substitution contributed significantly to the rejection of the substitution model homogeneity assumption between human and chimpanzee detected. The analysis was performed using the TRF_{125Kb} dataset. Shown are the fractions of rejected equality between the human and chimpanzee models for the individual substitution types. The results for the set of significant alignment windows is shown in red. The results for the set of non-significant alignment windows are shown in blue. Transition rates ($A \leftrightarrow G$ or $T \leftrightarrow C$) showed in $> 50\%$ and each of the transversion rates showed in $< 20\%$ a significant difference between the human and chimpanzee model. In non-significant alignment windows $\leq 5\%$ rejected rate equality for all the individual substitution types between the human and chimpanzee model.

5.2.4 Species-specific transition patterns in the human and chimpanzee genomes

In the following the distributions of the substitution rate differences between the corresponding human and chimpanzee substitution models are analyzed in more detail. The analysis is again performed on the TRF_{125Kb} dataset. As the underlying substitution models are reversible, the differences between the 12 off-diagonal substitution rates in the vector of $q^{(human)}$ and $q^{(chimpanzee)}$ were averaged for the six reversible substitution rate pairs.

In the significant alignment windows, the distributions of substitution rate differences are bimodal for the transition rates and unimodal for the transversion rates (Figure 5.7). This indicates that there is a strong tendency for a significant window to have a high transition rate in humans and a low transition rate in chimpanzees and vice versa. For the transversion rates no such trend is observed. The non-significant alignment windows show no remarkable difference of the transition rates and transversion rates between the human and chimpanzee model.

The observed differences in significant alignment windows are supposed to be driven by different extents of transcription-coupled repair. In significant alignment windows a difference of the extent of the strand-specific $A \rightarrow G$ increase in either the human or the chimpanzee substitution model is therefore expected. The strand-specific $A \leftrightarrow G$ increase is quantified as the $A \leftrightarrow G \ /T \leftrightarrow C$ ratio and is compared between the human and chimpanzee substitution model that was estimated from the transcribed fraction 125 Kb alignment windows. Moreover, the ratios between the human and chimpanzee substitution models in significant and non-significant alignment windows were compared. Indeed, the extent of the $A \leftrightarrow G \ /T \leftrightarrow C$ ratios are remarkably different between the human and chimpanzee model in the significant alignment windows (Figure 5.8). The $A \leftrightarrow G \ /T \leftrightarrow C$ ratios between both species show a bimodal distribution with two peaks at a ratio of $\sim$1.4 and $\sim$1 in either human or chimpanzee. This indicates that there is a strong tendency for a significant window to have an increased $A \leftrightarrow G \ /T \leftrightarrow C$ ratio in humans and a decreased $A \leftrightarrow G \ T \leftrightarrow C$ ratio in chimpanzees and vice versa. In the non-significant alignment windows the $A \leftrightarrow G \ /T \leftrightarrow C$ ratios between both species are unimodal and show no remarkable difference (Figure 5.8).

5.3 Discussion

Human and chimpanzee DNA sequences are believed to evolve according to the same substitution model. Exceptions to this assumption have been described (Ebersberger and Meyer, 2005, e.g.,), but a genome-wide analysis of this aspect has not been performed. It was aimed to identify regions in the transcribed fraction of the human and chimpanzee genomes that evolve species-specific. To this end, the human, chimpanzee and rhesus branch specific substitution matrices (Baake, 1998) were estimated for 12,596 non-overlapping windows 125 Kb in size, representing the transcribed part in the human-chimpanzee-rhesus genome alignment. For each window a squared distance δ was computed between the two substitution rate matrices, Q_{human} and $Q_{chimpanzee}$. A parametric bootstrap approach was used to simulate the null-distribution of δ under the homogeneity assumption, i.e., when the substitution model is the same on all branches. If the value of δ fell outside of the 95% quantile of the null-distribution, the homogeneity assumption was rejected for the corresponding window. In total, 717 windows were found evolving in a species-specific manner. A closer look on the individual types of substitutions in these windows revealed, that mainly differences in the transition rates were responsible for rejecting the substitution model homogeneity for both species. Notably, the extent of the strand-specific $A \leftrightarrow G$ over $T \leftrightarrow C$ transition bias is markedly different between human and chimpanzee in the significant regions. The strand-specific increase of A→G over T→C substitutions on the transcribed strand is interpreted as signature of transcription coupled repair (Green, 2003). The results suggest that species-specific differences in the germline gene expression of the corresponding genes account for the different modes of evolution.

A major problem of the conducted analysis is the choice of an appropriate window size. On one hand a fine-scaled analysis on the gene level with small window sizes is desired. And on the other hand a sufficient sample size for accurate estimates of the substitution model is required to overcome numerical problems of zero entries in the divergence matrix. Based on a simulation study, I assessed the minimal window size to

Figure 5.7 ***(following page)*:** Substitution rate differences between human and chimpanzee in significant and non-significant alignment windows The rate differences of transitions (red) between the human and chimpanzee models show a bimodal distribution only in significant alignment windows.

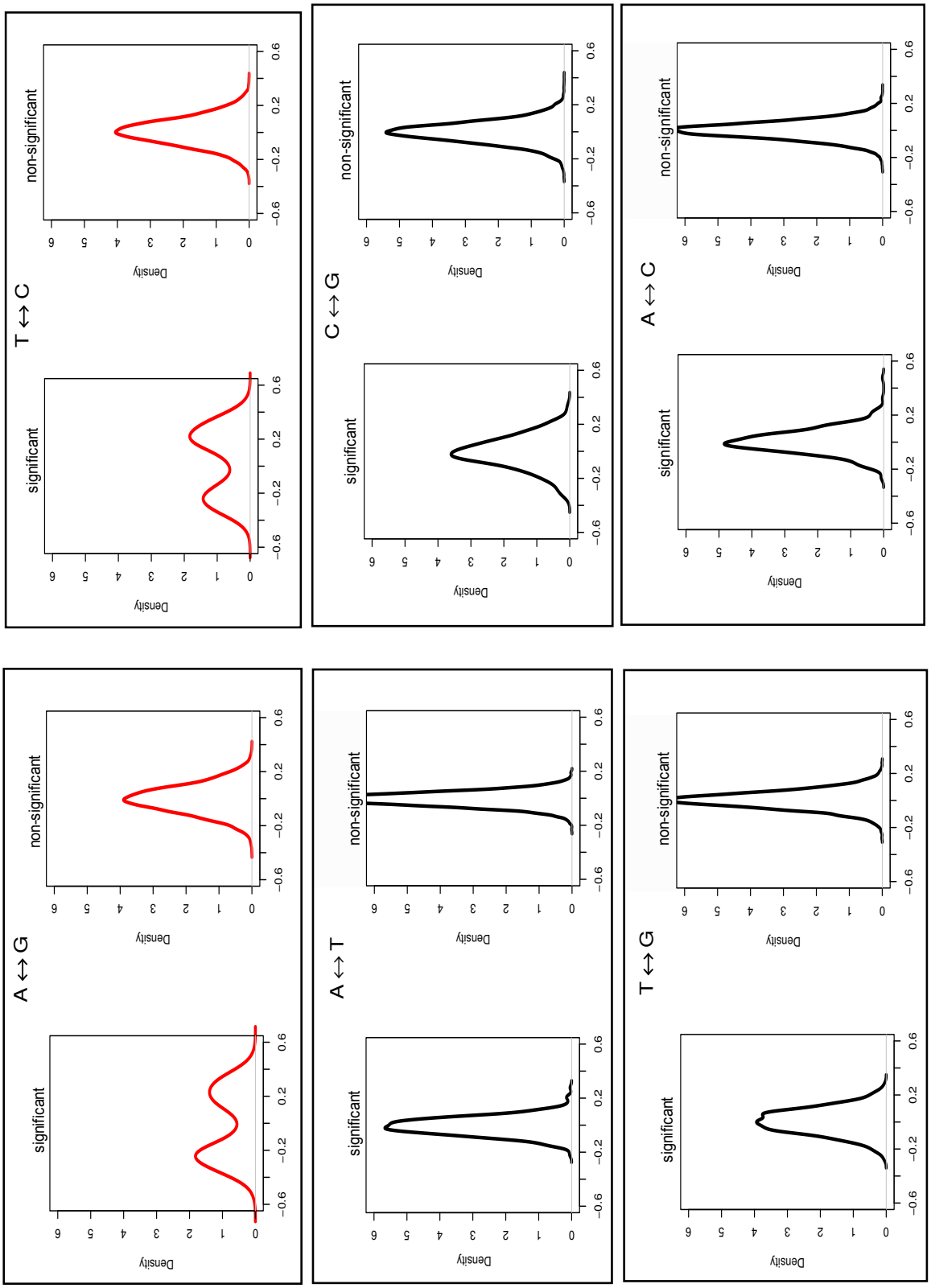
A ↔ G
significant
non-significant
A ↔ T
significant
non-significant
T ↔ G
significant
non-significant
T ↔ C
significant
non-significant
C ↔ G
significant
non-significant
A ↔ C
significant
non-significant
Density
0
1
2
3
4
5
6
−0.6
−0.2
0.2
0.6

be at least 15 Kb for human, chimpanzee and rhesus alignments (see section 6.2). The cut-off for the minimal size for the TRF_{125Kb} dataset was 23 Kb, and hence sufficient to prevent numerical problems. A higher resolution of the model differences is expected with an increasing number of observed substitutions. The fraction of significant tests should therefore increase with the size of the alignment and with the divergence of the sequences from the corresponding branches that are tested. As expected the fraction of significant tests increases slightly from the smaller (125 Kb, 5%) to the bigger (1000 Kb, 8%) sized alignment windows.

The distribution of the estimated p-values appeared almost uniformly distributed and the fraction of observed significant alignment windows was only marginally larger than 5%, which would be expected significant just by chance at the chosen significance level. This finding is not too surprising. The close evolutionary relationship between the two species suggest that the majority of genomic regions may simply evolve alike. Indeed, several studies showed that a general homogeneity of the substitution process between the human and chimpanzee was suggested (Webster *et al.*, 2003; Ebersberger *et al.*, 2002). Therefore, only a low fraction of differently evolving genomic regions was expected. Their detection is then further more hindered by the limited amount of divergence between human and chimpanzee sequences making the detection of significant differences between the species-specific substitution models hard. To show that it is not likely that the identified candidate regions did not come out as significant solely due to multiple testing, the different substitution patterns between human and chimpanzee were analyzed.

For this analysis, the set of alignment windows was selected, where the homogeneity of the human and chimpanzee substitution model was rejected ($p \leq 0.05$) and that additionally resulted in a δ that exceeded the 95% quantile estimated for all alignment windows. The rationale for selecting only alignments with a large δ was to focus on

Figure 5.8 ***(following page)*:** $A \leftrightarrow G$ /$T \leftrightarrow C$ rate ratio of human and chimpanzee in significant and non-significant alignment windows The distributions of the transition ratio $A \leftrightarrow G$ /$T \leftrightarrow C$ estimated from the human (x-axis) and chimpanzee (y-axis) substitution model from significant alignment windows are compared in a density and a contour plot. In *significant* alignment windows a bimodal distribution is observed, where a mean 1.5 fold $A \leftrightarrow G$ /$T \leftrightarrow C$ transition ratio in human corresponds to a mean 1 fold $A \leftrightarrow G$ /$T \leftrightarrow C$ transition ratio in chimpanzee and vice versa. In non-significant alignment windows a mean of 1.25 fold $A \leftrightarrow G$ /$T \leftrightarrow C$ ratio is observed in both species.

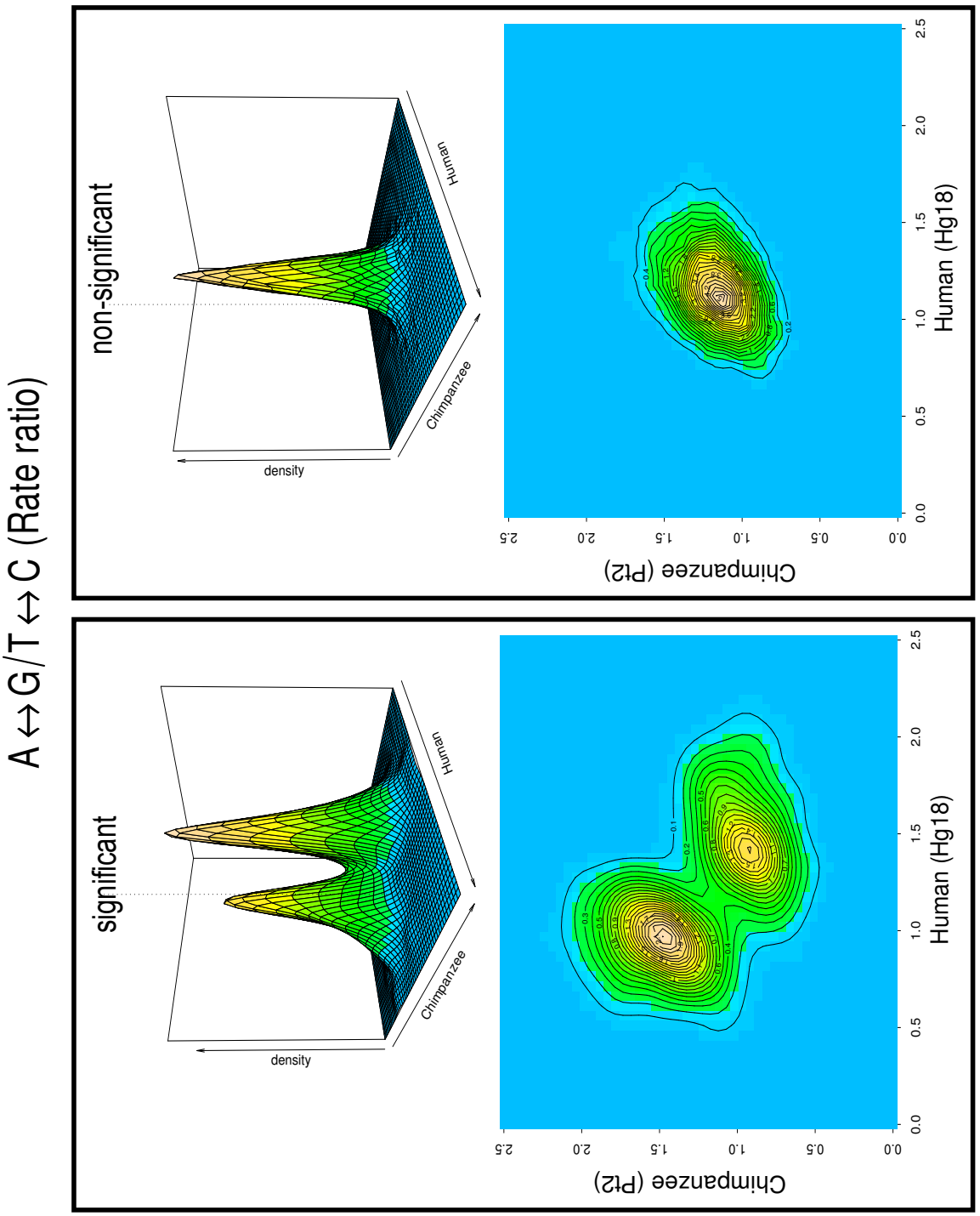
A ↔ G/T ↔ C (Rate ratio)
non-significant
density
Human
Chimpanzee
Chimpanzee (Pt2)
Human (Hg18)
0.0
0.5
1.0
1.5
2.0
2.5
significant
density
Human
Chimpanzee
Chimpanzee (Pt2)
Human (Hg18)

such windows, where the difference between human and chimpanzee substitution models is substantial, and may also be biologically significant. A total of 565 from the 717 significant alignment windows were used for further analysis ($TRF_{125Kb,p\leq 0.05,\delta>95\%}$).

The δ statistic agglomerates the difference between the human and chimpanzee substitution model as a single value distance measure. It was verified whether the δ statistic captures the sought-after differences of strand-specific substitution patterns by identifying which substitution rates contributed most to the distance measure δ. A statistic for each substitution rate was defined, where the null-distribution was estimated from simulated alignments that were evolved under the homogeneity assumption for each alignment window. In significant alignment windows it was observed that either the $A \leftrightarrow G$ or the $T \leftrightarrow C$ transition were significant, whereas the difference of other substitution rates (i.e. transversions) between the human and chimpanzee models were less pronounced. Therefore, it can be presumed that the δ statistic is mostly influenced by the differences of transition rates between human and chimpanzee.

Interestingly, the difference of the individual transition rates compared between the human and chimpanzee model in significant alignment windows showed a bimodal distribution. This suggested an increased $A \leftrightarrow G$ or $T \leftrightarrow C$ in either human or chimpanzee, which results from a strand-specific increase of $A \leftrightarrow G$ over $T \leftrightarrow C$ in only one species. The comparison of the $A \leftrightarrow G$ over $T \leftrightarrow C$ ratio between the human and chimpanzee models confirmed this presumption in the significant alignment windows. A ~ 1.4 fold increased $A \leftrightarrow G$ over $T \leftrightarrow C$ rate in one species is opposed to a ratio of ~ 1 fold in the respective other species.

In summary, our analysis shows that the significant alignment windows are consistent in their pattern of difference between humans and chimpanzees. There is argues strongly against multiple testing artifacts during their selection. Rather it implies that this difference in this mode of evolution between the two species is biologically meaningful. Interestingly, the differences between the substitution models in human and chimpanzee are in agreement with the hypothesis that the corresponding regions experience differing extents of transcription-coupled repair reflecting a differential expression of the corresponding genes in the germline.

Chapter 6

Simulation and evaluation studies

The Single-Branch-Test introduced in chapter 5 was used to detect significant differences between the substitution model of human and chimpanzee. In this chapter the Single-Branch-Test is evaluated to detect a change in the substitution model between two branches in an unrooted 3 species tree. Further, the influence of the alignment size and the branch lengths in the tree on the test statistic δ is evaluated.

6.1 Evaluation of the Single-Branch-Test

In this section, the statistical power of the Single-Branch-Test (SBT) to detect a change in the substitution model is inferred from a simulation procedure. The simulation is performed by testing the homogeneity of the substitution model between two branches in a 3 species tree. Two sets of alignments are generated, one using the same model Q for all branches in the tree and a second, where the substitution model Q is changed to Q^* in one branch (Figure 6.1).

The differences between the substitution models are more likely being detected when the number of observed substitutions is higher. This can be achieved by enlarging either the alignment size or the branch length. For the simulation study the alignment size was kept fixed to a size of 25 Kb and the length of the branches was varied. The homogeneity of the substitution model was tested between the two branches b and c that have the same branch length ranging from 0.001 to 0.1 substitutions per site, where the length of the outgroup branch a is doubled (Figure 6.1). A set of 1,000 alignments with a size of 25 Kb were generated according to an unrooted 3 species tree. In the following a significant

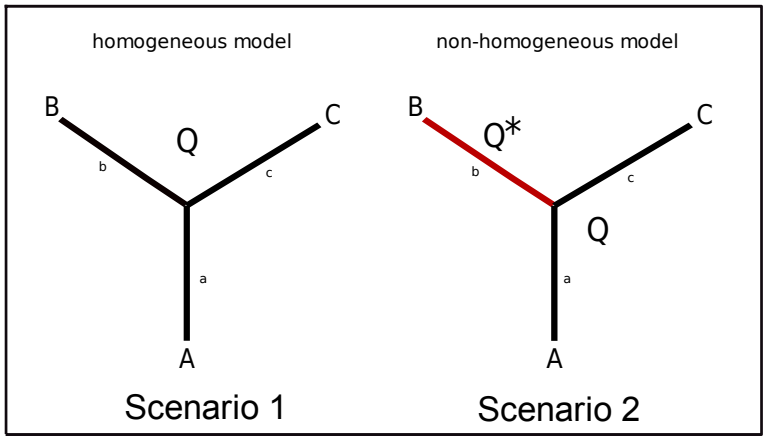

Figure 6.1: Homogeneous and non-homogeneous substitution process within a phylogenetic tree. Sequence evolution was modeled along a three taxon tree under two different scenarios. In scenario 1 sequences evolve with the same model on all branches in the tree. In scenario 2 sequence evolution along the branch b (red) was modeled with a modified substitution model Q^*.

test denotes a test performed for an alignment, where the homogeneity assumption of the substitution model between the two branches was rejected.

In total, 3 datasets were generated using the same model Q on all branches with uniform nucleotide frequencies $\pi_0 = (0.25, 0.25, 0.25, 0.25)$. For the first dataset all rate parameters were equal with $r_0 = (1, 1, 1, 1, 1, 1)$. To reduce the effect of the random sampling error the number of alignments was increased for the second dataset to 10,000 alignments generated with $r_0 = (1, 1, 1, 1, 1, 1)$. For the third dataset the rate parameters were randomly generated (r_r). The random rate parameters r_r were generated by the following procedure: The off diagonal elements of the matrix are sampled from a uniform distribution {0,1}, and the diagonal elements were then chosen such that the rows sum up to 1. The resulting random rate matrix R was normalized by dividing all entries by the sum of the diagonal (trace). The rate parameters in r_r are defined from the six rates in the upper triangle of the random rate matrix R.

To arrive at a modified substitution model, Q^*, the nucleotide frequencies were altered to $\pi_1 = (0.15, 0.25, 0.25, 0.35)$, and $\pi_2 = (0.15, 0.2, 0.3, 0.35)$. More severely altered models Q^* were generated by changing the rate parameters to $r_1 = (1, 1, 1, 1, 2, 1)$ and $r_1 = (1, 1, 1, 1, 4, 1)$. For each of the four Q^* models one dataset was created. Additionally, an alignment set was generated, where individual randomly generated rate

parameters r_r were assigned in Q_r and Q_r^*.

For the simulation study the sequence simulation program TRIGEN that is based on the Single-Branch-Test code was developed. The program allows to specify individual substitution models and branch lengths for each branch in an unrooted 3 taxon tree.

The power of the Single-Branch-Test to detect a difference in the substitution model between two branches was assessed by the fraction of significant tests for a set of alignments. For the alignments that were generated using the same substitution model for all branches in the tree the homogeneity of the substitution model was falsely rejected in a percentage of 3.2 % to 5.7 %. The slight variations around the percentage of 5% expected by chance due to multiple testing are explained by the random sampling error. The random sampling error is reduced when the dataset is extended from 1,000 to 10,000 alignments. The percentages for the different branch lengths showed less variations and converge closer to 5% (Table 6.1).

Relative to the observed percentage of 5% tests that are expected significant by chance, the percentage of significant tests increases notably with increasing branch lengths when the substitution model is changed in one branch. When moderate differences are introduced between Q and Q^* by changing the nucleotide frequency parameters the fraction of significant tests increases for branch lengths >0.005 expected substitutions per site. For more rigorous differences between Q and Q^*, where one rate parameter was two- and fourfold increased or random rate parameters were assigned in Q and Q^*, an increase was also observed for the smallest branch length of 0.002 and 0.001 expected substitutions per site (Table 6.1). However, with increasing branch length it is more likely to detect a difference between the substitution models due to more accurate estimates.

6.2 Minimal window size

For the accurate estimation of the substitution model an appropriate choice of the alignment size is required. When the sequence divergence is low or the alignment size is too small not all substitution types are observed in a pairwise sequence comparison. The missing observations lead to zero entries in the divergence matrix H (c.f., equation 5.1) that can cause wrong estimates of the rates in Q. In the following an example for a divergence matrix with zero entries inferred from an alignment between sequence B and

		0.001	0.002	0.005	0.01	0.02	0.05	0.1
	homogeneous							
1	Q_{r_0,π_0}	0.032	0.043	0.046	0.040	0.044	0.041	0.032
2	$Q^{10,000}_{r_0,\pi_0}$	0.0380	0.0460	0.0493	0.0483	0.0529	0.0516	0.0540
3	Q_{r_r,π_0}	0.044	0.042	0.057	0.045	0.043	0.040	0.048
	non-homogeneous							
4	$Q_{r_0,\pi_0}, Q^*_{r_0,\pi_1}$	0.048	0.057	0.127	0.223	0.439	0.813	0.955
5	$Q_{r_0,\pi_0}, Q^*_{r_0,\pi_2}$	0.051	0.080	0.145	0.291	0.561	0.893	0.986
6	$Q_{r_0,\pi_0}, Q^*_{r_1,\pi_0}$	0.085	0.179	0.432	0.720	0.946	0.998	1.000
7	$Q_{r_0,\pi_0}, Q^*_{r_2,\pi_0}$	0.403	0.766	0.991	1.000	1.000	1.000	1.000
8	$Q_{r_r,\pi_0}, Q^*_{r_r,\pi_0}$	0.456	0.729	0.931	0.983	0.991	0.999	1.000

Table 6.1: Evaluation study for the Single-Branch-Test. The homogeneity of the substitution model between two branches was tested for 8 alignment sets that were generated using a homogeneous model Q (1-3) for all branches and a non-homogeneous model, where a different model Q^* was assigned to one branch (4-8). Shown are the fractions of test results obtained for each dataset consisting of 1000 alignments with a size of 25 Kb. For the simulation using a homogeneous model a dataset with 10,000 alignments with a size of 25 Kb was considered as well (2). The homogeneous substitution model (1-3) was generated with uniform nucleotide frequencies, where the rate parameters were defined in r_0, from a randomly generated rate parameters r_r. Moderate changes in the substitution model are implied by altering the nucleotide frequency parameters (4,5) and more rigorous changes by altering the rate parameters (6,7,8) between Q and Q^*. The parameters that were used to generate the datasets are the nucleotide frequencies: $\pi_0 = (0.25, 0.25, 0.25, 0.25)$, $\pi_1 = (0.15, 0.25, 0.25, 0.35)$, $\pi_2 = (0.15, 0.2, 0.3, 0.35)$, the rate parameters: $r_0 = (1, 1, 1, 1, 1, 1)$, $r_1 = (1, 1, 1, 1, 2, 1)$, $r_2 = (1, 1, 1, 1, 4, 1)$ and randomly generated rate parameters r_r.

C is shown:

$$H^{(B,C)} = \begin{array}{c} \\ A \\ C \\ G \\ T \end{array} \begin{array}{c} \begin{array}{cccc} A & C & G & T \end{array} \\ \begin{pmatrix} 0.260500 & 0.000000 & 0.000500 & 0.000250 \\ 0.000000 & 0.246000 & 0.000750 & 0.000000 \\ 0.000500 & 0.000750 & 0.245000 & 0.000000 \\ 0.000250 & 0.000000 & 0.000000 & 0.245500 \end{pmatrix} \end{array}$$

To overcome the problem of zero entries in the divergence matrix a large alignment size or a higher sequence divergence between the sequences is required. In the following a simulation study is described to infer the minimal alignment size that is required to obtain accurate estimates of Q. For different branch lengths of 0.001, 0.002, 0.005, 0.01, 0.02, 0.05 and 0.1 expected substitutions per site, a set of 1000 alignments are generated

ranging from 100 bp to 30000 bp. For the simulation, a GTR model with uniform nucleotide frequencies was used, where the rate parameters were randomly generated as described in section 6.1.

The zero entries that occur in the divergence matrix H between a chosen pair of sequences are counted for each alignment and then averaged and rounded to integers for each alignment set. As expected, the number of zero entries decreases with increasing branch lengths or alignment size. For example, for a branch length of 0.005 expected substitutions per site an alignment size of at least 15 Kb is sufficient to avoid zero entries in the divergence matrix (Figure 6.2). For smaller branch lengths such as 0.002 expected substitutions per site larger alignments with a size of at least 30 Kb should be considered.

6.3 Evaluation of the test statistic δ

The statistic for the Single-Branch-Test is defined by the squared distance δ between the substitution rate vectors q of two branches i and j (equation 5.7). In this chapter the accuracy and precision (Taylor, 1996) of δ to measure the distance between two substitution models is evaluated with respect to the influence of the alignment size and the branch lengths. The accuracy defines how close δ is to the unknown true value and the precision describes the scatter of the estimates of δ (Figure 6.3). When the homogeneity of the substitution model is assumed, δ should reflect the random variations of the substitution process between the branches of a tree that converge near zero with an increasing accuracy and precision of the estimates. In this section the distributions of δ were simulated for different alignment sizes, substitution models and branch lengths.

For the evaluation, δ was estimated from simulated alignments for an unrooted 3 taxon tree. Two sets of alignments were generated, one using a homogeneous model for all branches in the tree, and a second using a non-homogeneous model, where the substitution model was changed for one branch. The rate parameters of the substitution models were randomly generated as described in section 6.1. The alignments were generated using the TRIGEN program (c.f. section 6.1).

The impact of the alignment size and the branch length on the measurement of δ was inferred by the following. For the evaluation study, δ is computed for two branches

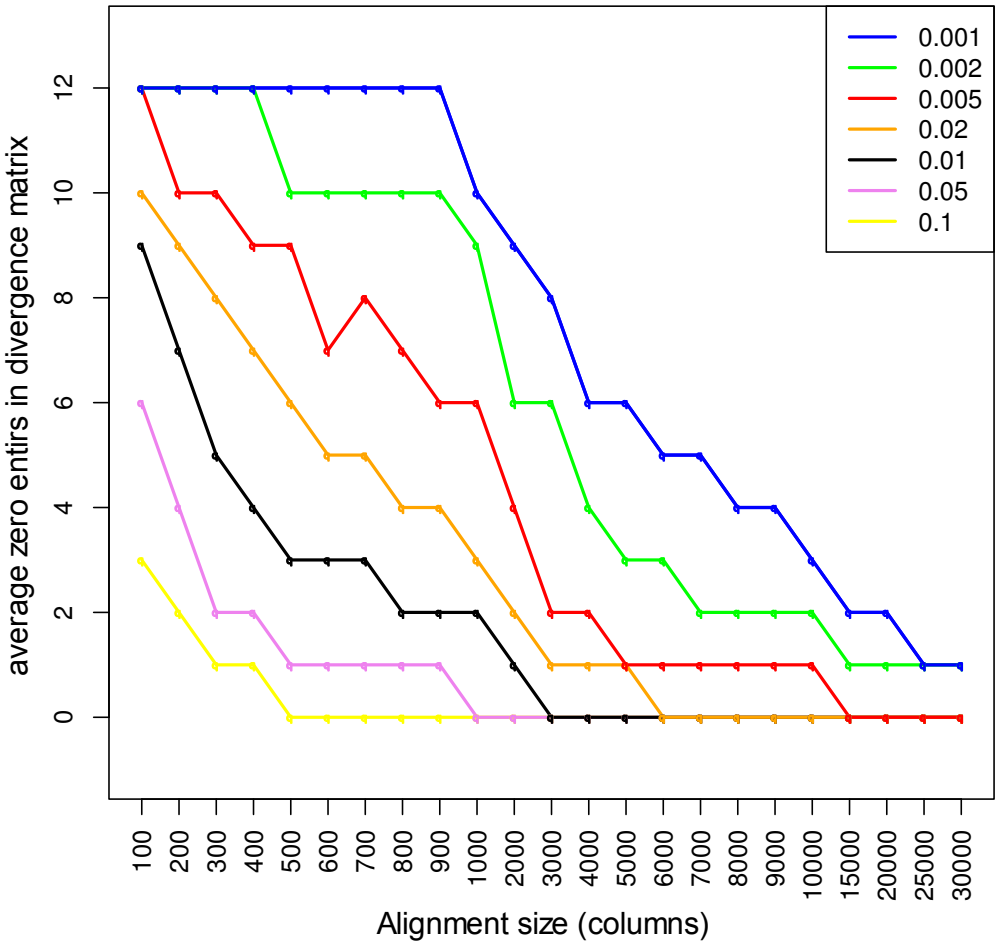

Figure 6.2: Number of expected zero entries in a divergence matrix. 1000 alignments each were generated for varying alignment sizes (100 to 30000 alignment columns) and branch lengths (0.001 to 0.1 expected substitutions per site). The average number of zero entries in the divergence matrices is shown for the different alignment sizes and branch lengths.

b and c in a 3 taxon tree from simulated sequence alignments (Figure 6.4 B). In the first part, the branch lengths of the tree were kept constant and the alignment size was varied from 5 Kb to 1 Mb (Figure 6.4 D.1). In the second part, the alignment size was kept constant and the length of the branches in the tree were varied between 0.001 and 0.2 substitutions per site (Figure 6.4 D.2). The third part, the alignment size and the lengths of the branches b and c were kept constant and the length of branch a (outgroup) was varied between 0.005 to 0.25 substitutions per site (Figure 6.4 D.3).

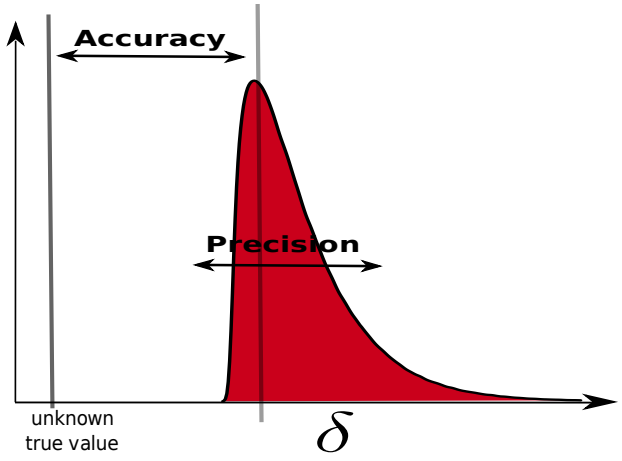

Figure 6.3: The accuracy describes how close the estimate δ is to the unknown true value and the precision describes the scatter of δ.

6.3.1 Effects of the alignment length on the estimate of δ

The accuracy of δ is expected to improve with increasing alignment size as more substitutions can be considered to describe the substitution process. In a simulation procedure δ was estimated from simulated alignments of different lengths for a tree with constant branch lengths. The lengths of the branches b and c were set to 0.005 expected substitutions per site and the length of branch a was set to 0.01 expected substitutions per site. The alignment size was varied in 5 Kb steps from 5 Kb to 100 Kb and further to 125 Kb, 250 Kb, 500 Kb and 1 Mb (24 intervals in total).

The statistic δ is used to measure the variations between the substitution models of

Figure 6.4 ***(following page)*****:** Evaluation of δ. For the simulation procedure sequence alignments were generated using a homogeneous (Simulation 1) and non-homogeneous (Simulation 2) substitution model. For Simulation 2, the substitution model for the branch b differs from the other branches a and c in the tree. The values of the rate parameters were randomly generated. The statistic δ was estimated for the branches b and c from the simulated alignments. To measure the impact of the alignment size and branch length on the estimate of δ the following settings were used: 1) The lengths of all branches were kept constant and the sizes of the alignments were varied from 5 Kb to 1 Mb. 2) The alignment size was kept constant and the lengths of the branches in the tree were varied from 0.001 to 0.2 expected substitutions per site. 3) The alignment size and the length of branches b and c were kept constant and the length of branch a was varied from 0.001 to 0.2 expected substitutions per site.

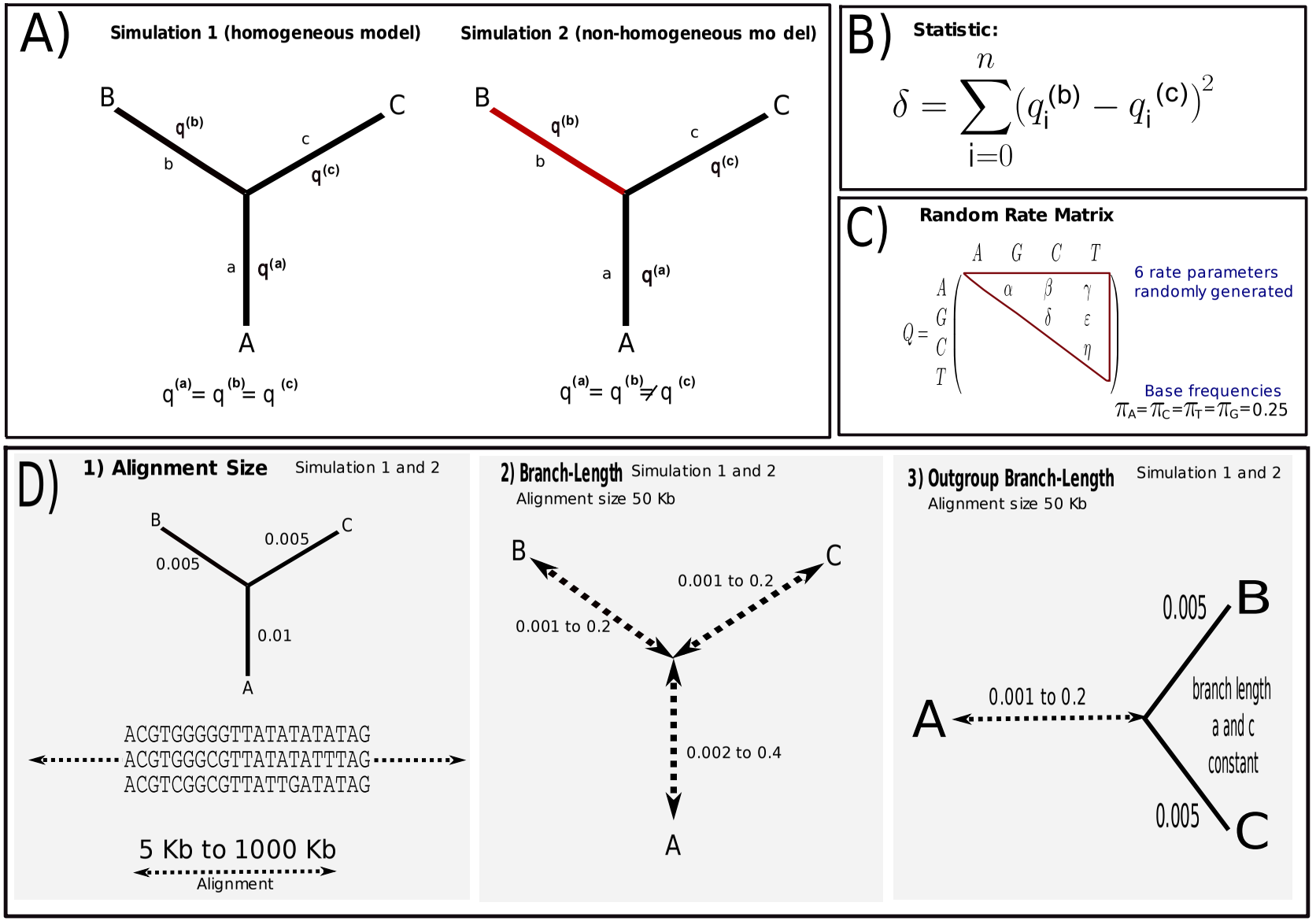
A)
Simulation 1 (homogeneous model)
Simulation 2 (non-homogeneous mo del)
B
C
A
q(b)
q(c)
q(a)
a
b
c
q(a)= q(b)= q(c)
q(a)= q(b)≠ q(c)
B)
Statistic:
$\delta = \sum_{i=0}^{n} (q_i^{(b)} - q_i^{(c)})^2$
C)
Random Rate Matrix
A G C T
α β γ
δ ε
η
6 rate parameters randomly generated
Base frequencies
$\pi_A=\pi_C=\pi_T=\pi_G=0.25$
D)
1) Alignment Size
Simulation 1 and 2
0.005
0.005
0.01
ACGTGGGGGTTATATATATAG
ACGTGGGCGTTATATATTTAG
ACGTCGGCGTTATTGATATAG
5 Kb to 1000 Kb
Alignment
2) Branch-Length
Simulation 1 and 2
Alignment size 50 Kb
0.001 to 0.2
0.001 to 0.2
0.002 to 0.4
3) Outgroup Branch-Length
Simulation 1 and 2
Alignment size 50 Kb
0.005
0.001 to 0.2
branch length a and c constant
0.005

branch b and c. In simulation 1 a homogeneous model was used for all branches in the tree. In simulation 2 a non-homogeneous model was used. For the non-homogeneous model, the substitution model was modified for branch b (Figure 6.4). The effect on the estimate of δ caused by the varying alignment lengths is remarkable, especially for length <20Kb (Figure 6.5) . As expected, δ is substantially increased when the substitution model is changed on one branch. For alignment length $\geq$ 20 Kb, the distributions of the δ estimate are by and large similar. Only for the short alignments (5-15Kb) the δ distribution is slightly shifted towards larger values. In summary, this indicates that for alignments $\geq$ 20 Kb length, the alignment length has only very little influence on the δ estimate.

6.3.2 Branch length effects

The accuracy of δ is expected to improve with increasing branch lengths as more substitutions can be considered to describe the process. In total, 21 unrooted three taxon trees were generated, where the individual trees varied in their branch lengths. The branch lengths were chosen from the interval between 0.001 to 0.2 expected substitutions per site for the branches b and c. The branch length of branch a was set two twice the branch length of branch b and c. The alignment size was fixed to 50 Kb. In simulation 1 again 1000 alignments were generated for each individual tree using a homogeneous substitution model for the three branches. In simulation 2 the different substitution model was chosen for branch b compared to branch a and c.

An influence on the estimate of δ for branches b and c caused by the varying branch length is observed for short branches of < 0.01 expected substitutions per site. Again, as expected δ between b and c is highly increased when the substitution model is changed in branch b. For the short branches < 0.01 a slight shift of δ towards larger values is observed in comparison to longer branches. The branch length has therefore not a strong influence on the estimate of δ when the substitution model differs between the branches (Figure 6.6).

6.3.3 Effects of the outgroup divergence on the estimate of δ

The accuracy of δ measured between the branches b and c is evaluated for a putative influence of the length of the outgroup branch a. For the simulation the length of the

branches b and c were fixed to 0.005 expected substitutions per site and the outgroup branch a was increased from 0.001 to 0.2 expected substitutions per site. In total, 21 trees were considered. For each tree, 1000 alignments were generated with uniform nucleotide frequencies, using a homogeneous model and a non-homogeneous substitution model (Figure 6.7). The outgroup branch length does not affect the δ measurement for the branches b and c. A slight increase of δ was observed only for very large outgroup branch lengths with more than 0.1 expected substitutions per site.

6.4 Normalization of δ

For the analysis of real sequence data stemming from different regions of a genome, both the divergence between sequences and the number of analyzable alignment columns can vary. In the previous section I have shown that both alignment length and extent of sequence divergence have an influence on the δ estimate. In the following a normalization procedure for δ is developed that considers the size of the alignment and the length of the branches for the estimates.

The bias on δ caused by the alignment size can be modeled by a linear factor. The factor is described as ratio of the number of alignment columns L_{size} to an arbitrarily chosen reference size of 50 Kb (L_{50Kb}). The normalized δ is obtained from the normalization function F_{N1} by:

$$F_{N1}(\delta) = \delta * L_{size}/L_{50Kb} \tag{6.1}$$

Figure 6.4 shows the result of the normalization on δ estimates for different alignment sizes.

The influence on δ caused by different branch length is modeled by a calibration curve that was estimated from simulated alignment sets. For a fixed alignment size of 50 Kb, 1000 alignments were generated for varying branch length, using a homogeneous model for all branches in the tree (Figure 6.4 a). For each branch length the average of δ was estimated from 1000 simulated alignments. The calibration Function F_{cal} was defined from the linear interpolation between the averages of δ estimated for each branch length as function to the branch length. The distributions of δ were normalized to a fixed

reference branch length of $bl_{0.01}$ by the following:

$$F_{N2}(\delta) = \delta * F_{cal}(bl_{0.01})/F_{cal}(bl) \tag{6.2}$$

The branch length bl of the branches b and c was estimated from the alignments using the Neighbor-Joining method (Saitou and Nei, 1987). Figure 6.4 b shows the result of the normalization procedure. The normalized δ is now independent from the branch length.

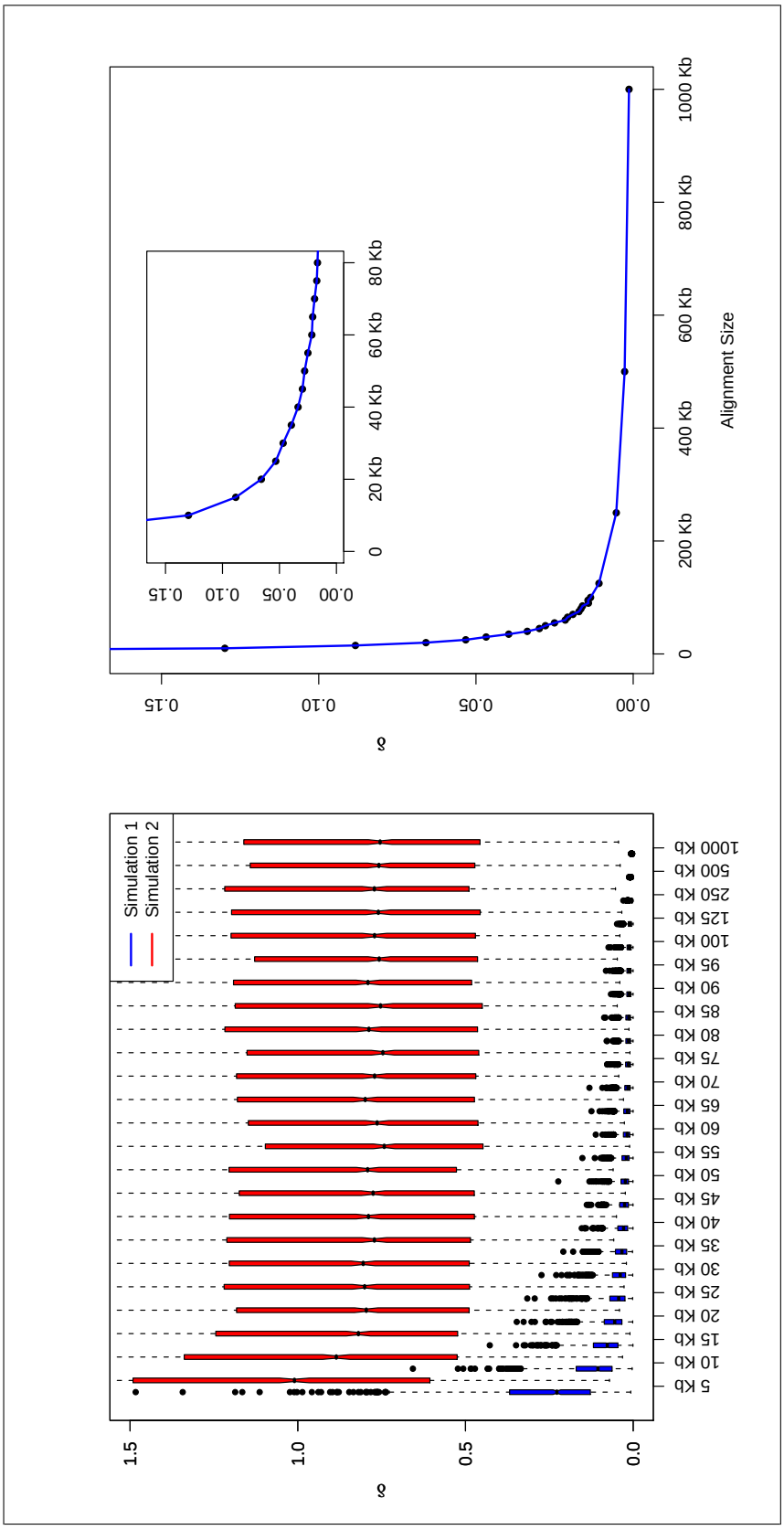

Figure 6.5: Influence of the alignment size on δ. The left plot shows the distribution of δ estimates for different alignment sizes when a homogeneous model (blue, simulation 1), and a non-homogeneous model (red, simulation 2) was used. In total, 1000 alignments 50 Kb in size were generated for each alignment size. The linear interpolation (blue) between the averages of δ estimated for the different alignment sizes describe the calibration function of δ as function to the alignment sizes.

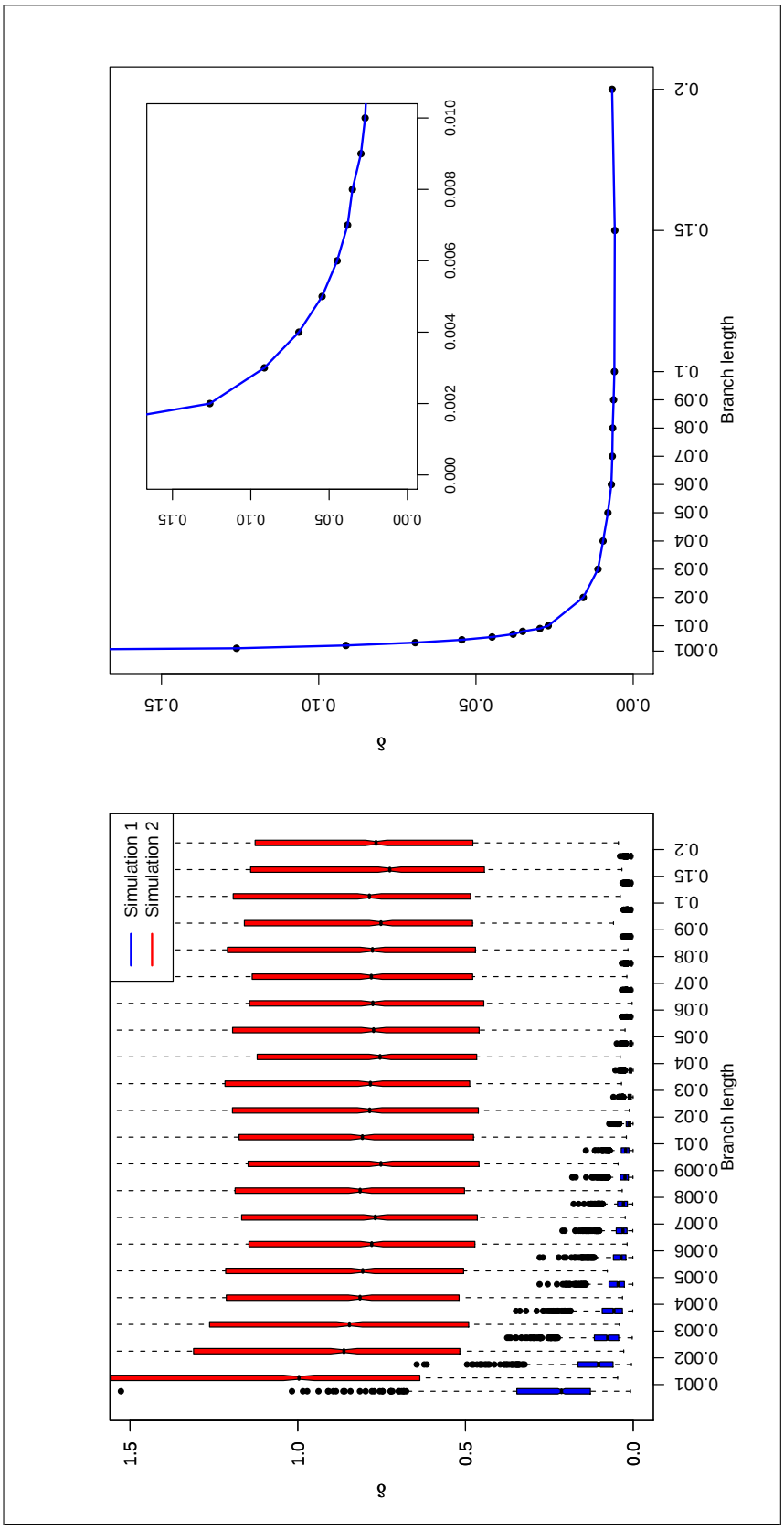

Figure 6.6: Influence of the branch length on δ. The left plot shows the distribution of δ estimates for different branch length when a homogeneous model (blue, simulation 1), and a non-homogeneous model (red, simulation 2) was used. In total, 1000 alignments 50 Kb in size were generated for each branch length. The average of δ for different alignment sizes are shown in the right plot.

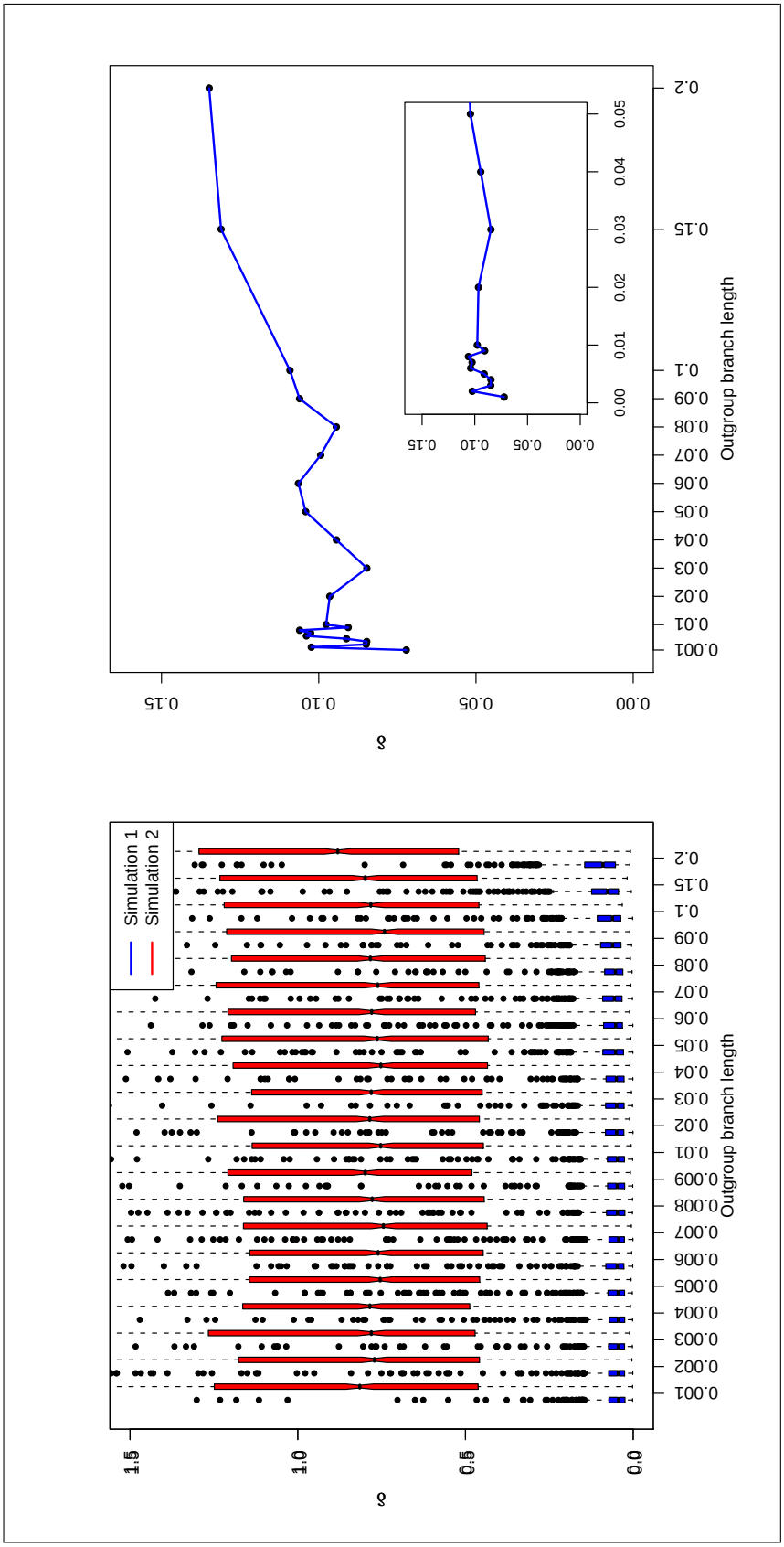

Figure 6.7: Influence of the branch length of branch a on δ that was estimated between branch b and c. The left plot shows the distribution of δ estimates for different branch length of branch a when a homogeneous model (blue, simulation 1), and a non-homogeneous model (red, simulation 2) was used. The branch length of b and c was 0.005 and kept constant. In total, 1000 alignments 50 Kb in size were generated for each branch length. The average of δ for different alignment sizes are shown in the right plot.

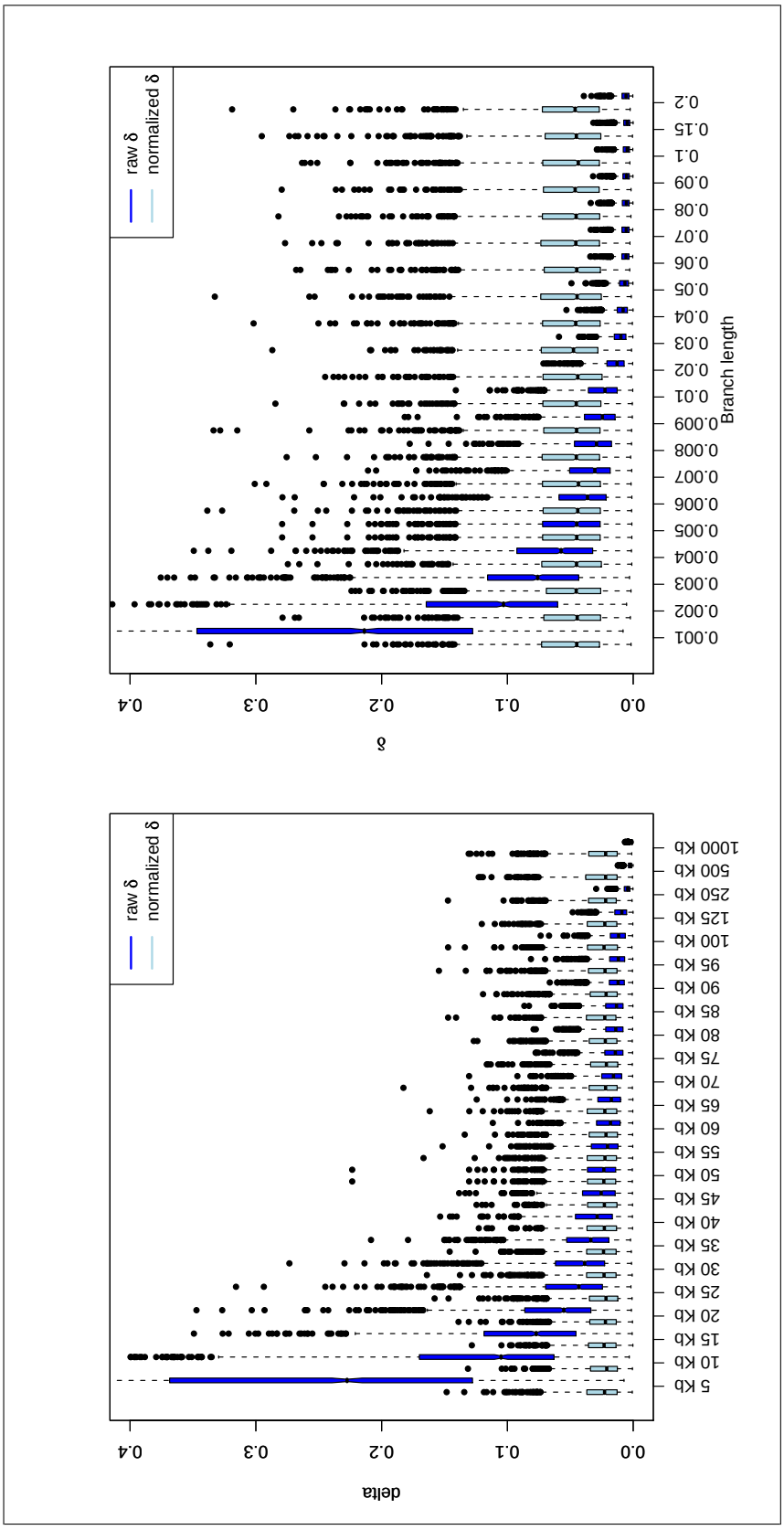

Figure 6.8: Effect of the δ normalization. The left plot shows the effect of the normalization of δ with respect to varying alignment sizes. The right plot shows the effect of the normalization of δ with respect to varying branch lengths. δ is adjusted to a branch length of 0.005 (left) and an alignment size of 50 Kb (right).

6.5 How to decrease the computing time of the Single-Branch-Test

The Single-Branch-Test uses a parametric bootstrap approach to estimate the null distribution of δ from 1,000 simulated alignments that were generated according to a homogeneous model for all branches in the tree. The speed-up of the procedure can be realized by two general approaches. The first is a simple stopping rule, where the simulation procedure runs until a fixed number of simulated test statistics had exceeded the observed one from the data, i.e., exceeded the chosen confidence limit. The second strategy is to estimate the p-values directly from a standard null distribution of δ corresponding to a fixed alignment size and branch length. For δ no standard null distribution was assumed as the estimates of the branches in the tree are expected to be highly correlated. Therefore the distribution of δ given the null-hypothesis is true are determined by a parametric bootstrap approach. However, the simulation study conducted in the previous section showed that the correlations between two branches are mainly dependent on the branch length and the alignment size. For a normalized δ value, the null distribution corresponding to fixed alignment size and branch length can be considered (c.f. section 6.4). When the paramaters of a chosen standard distribution are fitted to a null distribution of δ corresponding to a fixed alignment size and branch length, the probability to reject the homogeneity of the substitution model between two branches can then be directly estimated from the cumulative distribution function of the standard distribution.

6.5.1 Estimating the p-values of the Single-Branch-Test from a Gamma distribution

The Gamma distribution model has a shape and a scaling parameter for a distribution of positive continuous values and is therefore appropriate to model the null distribution of δ. The parameters of the Gamma distribution were fitted to the null distribution of δ corresponding to a fixed branch length and alignment size. The Gamma distribution has a scale parameter k and a shape parameter λ. The density function is described by:

$$f(x) = \frac{\lambda^k x^{k-1} e^{-\lambda x}}{\Gamma(k)}, x > 0 \tag{6.3}$$

As the null distribution of δ is estimated only once, the number of samples was increased from 1,000 to 10,000 samples to further reduce the effects of random sampling errors. The null distribution of δ was estimated from 10,000 alignments that were generated according to a homogeneous model for all branches in the tree with branch lengths of 0.005 (expected substitutions per site) and an alignment size of 50 Kb. The parameters of the Gamma distribution were estimated using the *fitdistr()* function in R from the MASS package (Venables and Ripley, 2002). The null distribution of δ was then compared to 10,000 randomly sampled values of the Gamma distribution according to the estimated scale parameter k=2.44 and shape parameter λ=43.41. The Gamma distribution shows a good fit to the null distribution of δ (Figure 6.9). With the estimated parameters of the Gamma null distribution the probability that the given null-hypothesis is true can be directly estimated from the Gamma cumulative distribution function.

To show, whether the parametric approach can be applied on real data the p-values of the Single-Branch-Test estimated for the TRF_{125KB} dataset obtained from the parametric bootstrap approach were compared to p-values that were estimated from the Gamma distribution with the given parameters. For each alignment window in the TRF_{125KB} dataset the p-value corresponding to the normalized δ value was estimated from the Gamma cumulative distribution function. In Figure 6.10, the p-values estimated from the parametric bootstrap null distribution and from the gamma null distribution of δ show as expected a high correlation with $R^2 = 0.94$. The estimation of the p-values from a standard distribution extensively accelerate the computation time of the Single-Branch-Test as the simulation procedure to obtain the null distribution of δ between two branches is not required.

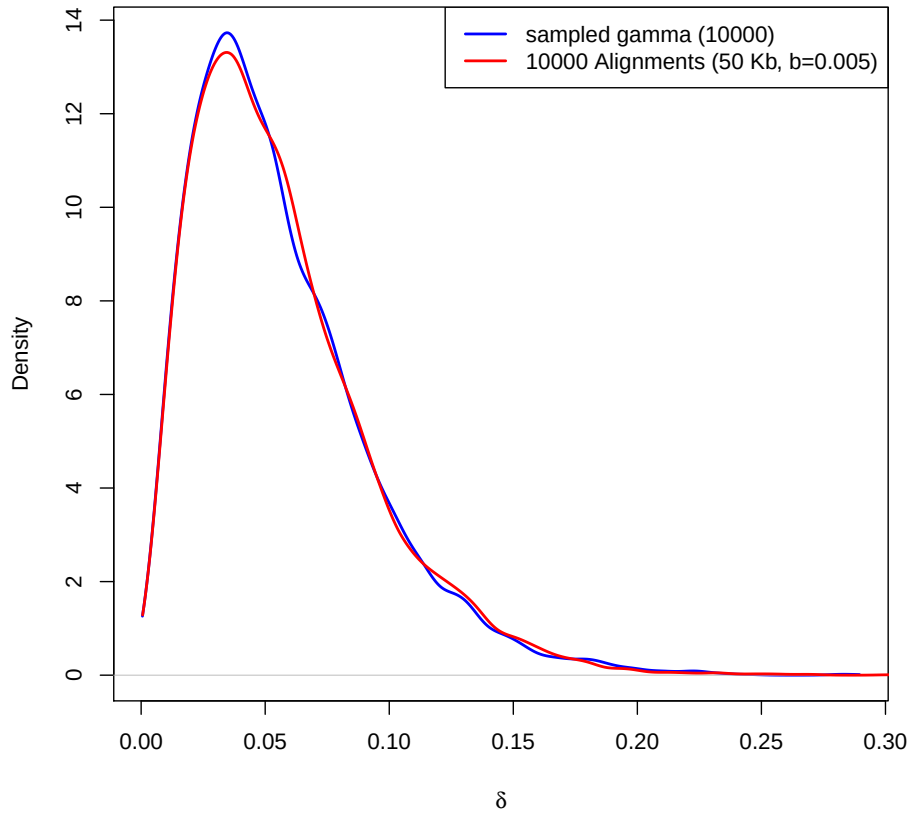

Figure 6.9: Fitting the parameters of a Gamma distribution to the null distribution of δ. δ was estimated from 10,000 simulated alignments generated using a homogeneous model for all branches in a 3 taxon tree with an alignment size of 50 Kb. The Gamma distribution is randomly sampled for 10,000 values from a Gamma distribution with the scale parameter k=2.44 and shape parameter λ=43.41.

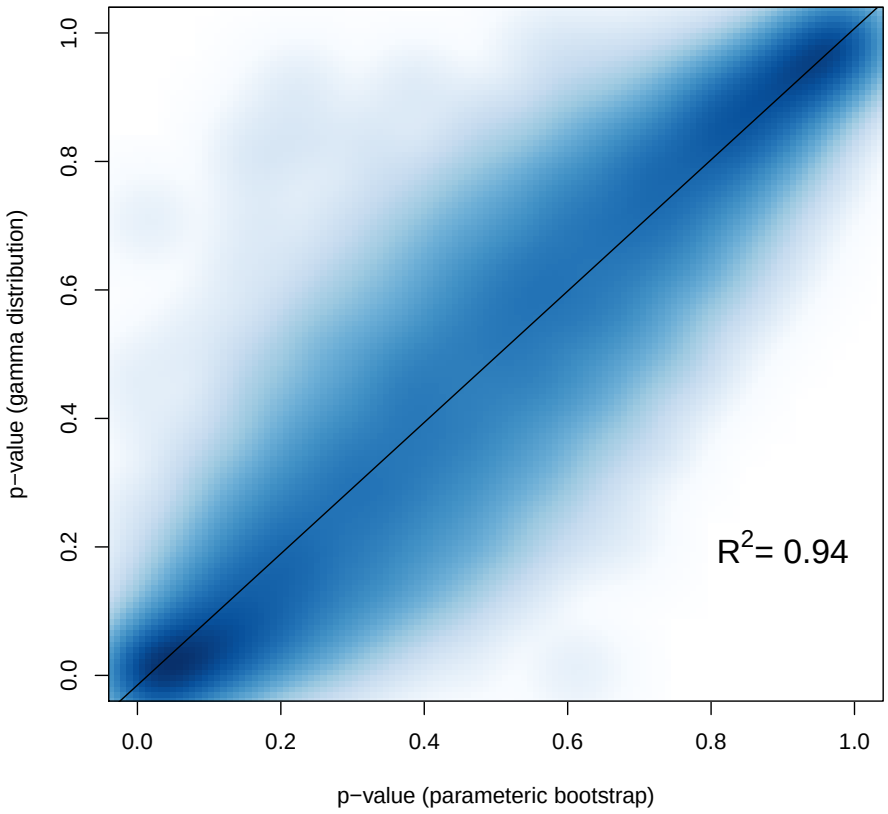

Figure 6.10: Comparing p-values of the TRF_{125Kb} dataset estimated from the parametric bootstrap approach and from the gamma distribution function.

6.6 Discussion

In this chapter the sensitivity and reliability of the Single-Branch-Test to detect a change in the substitution model was evaluated. Moreover, the minimal size of the alignment that is required for accurate estimates was inferred, and the influence of the alignment size and branch length on the test statistic δ was assessed.

In the first part, the homogeneity of the substitution model between two branches was tested for simulated alignments using the Single-Branch-Test. A set of alignments were generated using different branch lengths under a homogeneous and a non-homogeneous substitution model for the branches. In the non-homogeneous substitution model, the substitution model differed only between the two branches that were tested in the Single-Branch-test. The probability to reject falsely the homogeneity assumption between two branches was in agreement with the expected 5% tests that are expected significant by chance due to multiple testing (Table 6.1).

The differences of the substitution model between the branches could be better resolved by larger alignment sizes and when branch lengths are increased. This is since more substitutions were available, a better inference of the underlying substitution model is facilitated. The more precise the parameters are estimated the smaller can the model distance be to be still significant. The fraction of significant tests therefore increases with the size of the alignments or the branch length. The fraction of significant tests increased substantially when branch-specific substitution models were used. More pronounced model differences were more often detected than only subtle differences as e.g. differences in the equilibrium frequency. In summary, the results show that the Single-Branch-Test is reliable and sensitive enough to detect a difference in the substitution model between two branches. In chapter 5, a study was conducted to test the homogeneity of the substitution model between the human and chimpanzee branch. The branch length between human and chimpanzee corresponds in average to a branch length of 0.005 expected substitutions per site. For this branch length the Single-Branch-Test is expected to detect only datasets with strong differences between the substitution models as only the simulated datasets with the strongest substitution model differences a percentage of 99.1% correctly rejected the nullhypothesis (dataset 7, Table 6.1).

In the second part, a simulation was conducted to infer the minimal size of the alignment that is required to obtain accurate estimates of the substitution model. Zero entries

in a divergence matrix are a problem for the estimation of the substitution model when the alignment size is limited and the sequence divergence is low. Such zero entries can cause numerical problems for the estimation of the substitution rates in Q, and hence need to be avoided.

For the estimation of Q between human and chimpanzee, the simulation suggests that for a branch length of 0.005 an alignment size of 15 Kb is sufficient to avoid the occurrence of zero entries in the divergence matrix. Note, that for the simulated datasets randomly generated rate matrices were used that have putatively larger variations between the rates within a model than in a model that was estimated from real data. The approximate cut-off of a minimal alignment size 15 Kb for a branch length > 0.005 is therefore sufficient for real or simulated data.

The statistic δ is used in the Single-Branch-Test to measure the distance between the substitution models of two branches. In the third part of this chapter, a simulation study was presented that assessed the impact of varying alignment sizes and branch lengths and outgroup branch length to the measure of δ. The increase of both the alignment size and the branch length decreases the measured distance of δ between two branches due to a higher accuracy and precision of the estimates. On the other hand, the outgroup branch length proved to have little impact on δ that is measured between the other two branches. Therefore it can be presumed that the branch-specific substitution models can be accurately estimated independent of the choice of the outgroup.

A normalization procedure was developed to account for influences on the accuracy of δ caused by different alignment sizes and branch lengths. The branch length effect on δ was modeled by fitting a curve to the mean values of δ obtained from simulated datasets for differing alignment sizes and branch lengths. I could show that after the normalization the measure of δ was independent of the alignment size and branch length. For the study conducted in chapter 5 the alignment windows that rejected the homogeneity of the model between the human and chimpanzee branch with the largest distance δ were selected among all alignment windows. The variations of the alignment length and branch lengths among the alignment windows can lead to a bias for selecting shorter alignment windows or alignment windows with a low sequence divergence when the normalization would not be considered.

The parametric bootstrap approach of the Single-Branch-Test is time intensive for a genome-wide analysis that uses large alignment sizes. For each alignment the null

distribution of δ is determined from a simulated dataset of 1,000 alignments that are simulated with a homogeneous model. One way, to reduce the computation time is to reduce the number of simulations. To estimate whether a test rejects the null hypothesis it suffices to run the simulation until the observed δ exceeds δ_{null} in 5% of the simulations. However, for a test that rejects the null-hypothesis significantly the computation time would not be reduced as only less than 5% of the simulated δ values are larger than the observed δ.

A more effective alternative is to model the null-distribution of δ by a known standard distribution. The shape and rate parameters of a Gamma distribution were estimated for a null distribution of δ from an alignment dataset with fixed alignment size and branch length (e.g. 50 Kb and a branch length of 0.005). The p-values corresponding to the normalized δ values of the TRF_{125Kb} dataset were recomputed from a Gamma cumulative distribution function according to the estimated shape and rate parameters. The comparison of the p-values estimated from the bootstrap approach to the p-values estimated from the Gamma distribution are as expected highly correlated. This approach would allow to substantially reduce the computing time especially for large-scale datasets with large alignment sizes as the simulation procedure would not be required in the Single-Branch-Test. Such a speed-up would be desirable, compared to the bootstrap method, which is currently used.

Chapter 7

Functional analysis of candidate genes

This chapter describes a Gene Ontology enrichment analysis to characterize the biological role of the set of candidate genes that were identified from the significant alignment windows described in chapter 5.

In chapter5 a set of alignment windows were identified, for which human and chimpanzee showed a significantly different extent of the strand-specific $A \leftrightarrow G$ rate. The difference of the strand-specific $A \leftrightarrow G$ rate between the two species over the other can be interpreted as a signal that the expression of the corresponding genes has changed either in humans or chimpanzees. These genes may therefore play a role in processes leading to phenotypic differences between humans and chimpanzees.

A biological meaningful interpretation of the results obtained from a genome-wide screen is essential to draw conclusions about the underlying affected processes in the cell. Among the most popular and most widely used are Gene Ontology (Ashburner *et al.*, 2000), Panther (Thomas *et al.*, 2003) and the molecular signature database (Subramanian *et al.*, 2005). The molecular signature database (Subramanian *et al.*, 2005) provides curated collections of genes that are derived from experiments in which chemical and genetic approaches are applied to pertubate gene expression, canonical pathways and several pathway databases such as KEGG (Kanehisa and Goto, 2000), BioCarta (http://www.biocarta.com). The pathway databases provide manually curated pathway maps that are based on well studied protein-protein interactions.

The Gene Ontology (Ashburner *et al.*, 2000),provides a structured and defined vocab-

ulary describing the role of genes and gene products in eukaryotic cells. Terms from this vocabulary are assigned to genes to reflect functional information about this gene provided by a variety of sources, e.g. from experimental analysis (e.g.,direct assay) from an experimental analysis (e.g. a direct assay), from author statements in the literature or computational analysis (e.g., inferred from sequence similarity). The assignments in the Gene Ontology are manually revised by a curator and complemented by automatic assignments that are inferred from computational analyses that are not manually revised. Gene products are described in the Gene Ontology (GO) by a terminology that is divided in three domains: 1) Biological Process, 2) Molecular Function and 3) Cellular Component. Gene Ontology terms are organized as nodes in a directed acyclic graph. A directed acyclic graph is a graph with no directed cycles, i.e., a path that starts in any node n_i does not lead back to the same node n_i.

A catalogue of statistical approaches can be applied to obtain the relevant biological terms that describe the characteristics of a list of genes. Although, there is no unified strategy most methods compare a list of candidate genes derived from a genome-wide screen or experiment to a set of reference genes and test for an enrichment of associated ontology terms. The reference gene list is usually defined by all genes available in the organism's genome or by the list of genes that were considered in the analysis. The most common approach is to infer an over- or under-representation of ontology terms in the candidate gene set. The statistical methods to test for an enrichment commonly applied are the hyper-geometric test (Robinson *et al.*, 2002, one sided Fisher exact test), Fisher exact test (Zeeberg *et al.*, 2003; Beissbarth and Speed, 2004), χ^2 test (Khatri *et al.*, 2002) and a binomial test (Maere *et al.*, 2005).

7.1 Gene Ontology enrichment analysis

The Gene Ontology annotation for all human genes in Ensembl was retrieved from hsapiens gene Ensembl (build 53) using the "biomaRt" (Durinck *et al.*, 2005) package from Bioconductor (Gentleman *et al.*, 2004). The pipeline for the gene ontology enrichment analysis was implemented using the "topGO" R package (Alexa *et al.*, 2006) and the GOstat R package (Beissbarth and Speed, 2004) from Bioconductor in R version R-2.8.1. The significance level of the enrichment for a gene ontology term was determined by a hyper-geometric test (one sided Fisher Exact Test).

7.1.1 Selected candidate and reference genes

An overview of the number of genes overlapping within the genomic coordinates of the 125 Kb alignment windows in the transcribed fraction of the human genome is shown in Table 7.1. An alignment window overlaps in average with 2.79 individual genes. For significant alignment windows the candidate gene set comprised a total of 1,420 genes. The reference gene set comprises a total of 25,236 genes.

	Alignment windows	Genes (avg %)	Genes (total)
TRF_{125Kb}	12,596	2.79	26,656
$p \leq 0.05$	717	2.83	1,956
Candidate $_{p \leq 0.05, \delta > q_{95\%}}$	565		1,420
Reference			25,236

Table 7.1: Gene content within the TRF_{125Kb} dataset. The numbers of significant and non-significant alignment *windows*, the *average* and *total* number of genes overlapping with the alignment windows are shown. The candidate genes were defined by the genes that overlap with the 565 significant alignment windows having the strongest substitution model differences between human and chimpanzee measured by δ. The remaining genes were used as reference.

7.1.2 Significantly enriched Gene Ontology terms

From all 26,656 Ensembl genes covered by the alignment windows only 50% were annotated with a gene ontology term. For the enrichment analysis only terms assigned to ≥ 3 candidate genes were considered for the analysis. The enrichment analysis was performed separately for the three classes Biological Process (BP); 917 terms, Molecular Function (MF); 386 terms and Cellular Component (CC); 198 terms (Table 7.2). The p-value distributions resulting from the gene ontology enrichment analysis are shown in a PP-Plot (Figure 7.1). The deviation from the uniform distribution is more prominent for the Biological Process and Molecular Function and less pronounced for Cellular Component terms. Gene Ontology terms with a nominal p-value ≤ 0.05 in the enrichment analysis are selected as significantly enriched in the candidate gene set. For the GO class Biological Process a total of 153 significant terms, for the Molecular Function 60 significant terms, and for Cellular Component 16 significant terms were inferred (Table 7.2).

	Biological Process	*Molecular Function*	*Cellular Component*
Terms (p≤0.05)	153	60	16
Terms (tested)	917	386	198
Candidates	750 (52.8%)	797 (58.1%)	825 (58.1%)
Annotated Reference	12,978 (48.7%)	13,983 (52.5%)	14,234 (53.4%)

Table 7.2: Overview of the results from the Gene Ontology enrichment analysis. Shown are the number of significant terms (*Terms (p≤0.05)*), the total number of tested *terms*, number of annotated *candidates*, the number of *annotated reference* genes and the total number of candidate genes (*Candidates (total)*) for the three GO domains separately. In total, 908/1420 (63.9%) candidate genes were annotated with least one term of the three GO domains. Overall, 15,780/26,656 (59.2%) genes were annotated with at least one term of the three GO domains.

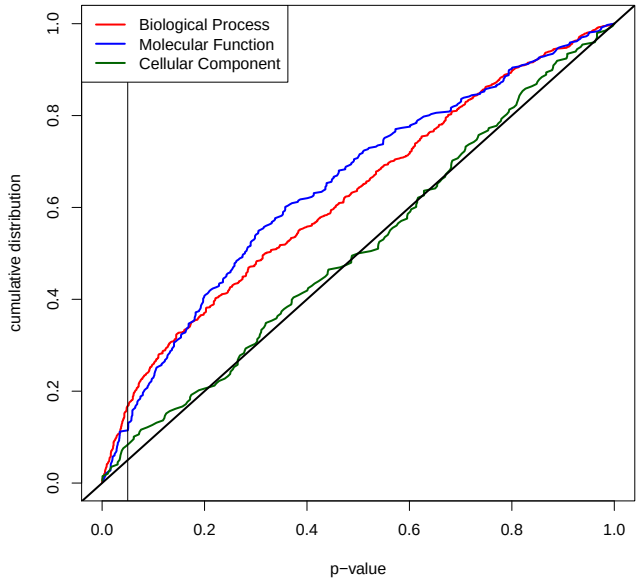

Figure 7.1: Probability-probability plot of the nominal p-values inferred from the enrichment analysis in the three gene ontology domains (Biological Process, Molecular Function, Cellular Component).The black diagonal line represents a cumulative uniform distribution. Terms were selected with a p-value ≤ 0.05 (vertical line) for further analysis.

7.1.3 Graphic representation of enriched Gene Ontology terms

The tabular output of a gene ontology enrichment analysis includes redundant information for related terms (e.g. parent to child relations) and is often difficult to interpret. This is the more the case when the number of significantly enriched terms is high. The

most intuitive approach to facilitate the interpretation of the results is a visual graph representation of all significantly enriched terms.

The significant terms for the three GO domains (Table 7.2) were arranged in a sub-ontology that was generated by the following procedure. A gene ontology graph object was built containing the set of significant terms using the GOgraph function of the GOstat R package (Beissbarth and Speed, 2004). To reduce the size of the resulting graph, a procedure was implemented that iteratively deletes non significant parental term nodes from the graph. In this iterative procedure the corresponding significant child terms of a deleted node are connected to the parental nodes of the deleted node. The resulting GO graphs for Molecular Function and Cellular Component sub-ontology were plotted using the Rgraphviz (Carey *et al.*, 2005) R package and then edited manually. The graph for the Biological Process sub-ontology was imported to the Cytoscape graph visualization tool (Shannon *et al.*, 2003) to perform the graph layout and manual editing. The GO terms were subsequently organized into a map of functional groups based on their shared roles in biological processes.

The Biological Process graph has in total 153 nodes corresponding to the significantly enriched GO terms (Figure 7.2). The significant enriched terms are related to embryonic developmental processes, anatomical structure morphogenesis, and organ development, such as gut, brain, spinal cord, limb, skelet and neurogenesis, gliogenesis and axonogenesis. Further, terms for cell morphogenesis, cell migration, learning and pain are overrepresented. Significant terms for signal transduction are enriched for a variety of receptor signaling pathways, e.g., Wnt receptor, epidermal growth factor receptor and glutamate signaling pathway. Further, terms are enriched for the regulation of replication, transcription, protein translation and chromatin and histone modification.

For the Molecular Function sub-ontology 60 terms were significantly enriched that are shown in Figure 7.3. Terms for a variety of receptor activities are seen more often than expected by chance, such as the β-adrenergic receptor activity, androgen receptor activity, opioid receptor activity, vascular endothelial growth factor receptor activity, C-C chemokine receptor activity and interleukin-1 receptor activity and prostaglandin E receptor activity. An enrichment was also observed for binding of cytokine, GTP, cAMP and GTPase and for transmembrane transporter activity that involves a variety of ion transporter, symporter and antiporter activity for sulfate, sodium, hydrogen, amino-acids and sugar. Further, terms related to the regulation of transcription involve

transcription factor activity, transcription factor repressor activity, ribonucleases and histone deacetylase activity are enriched.

The analysis of the Cellular Component sub-ontology revealed an enrichment for 16 terms that are shown in Figure 7.4. Here, terms representing the keratin filament, secretory granule, histone deacetylase complex, the cAMP-dependent protein kinase complex, and the post- and pre-synaptic membrane and synapse are enriched.

7.2 Enrichment analysis for curated gene sets

This section gives an overview of the candidate genes by constructing a map of the genes and their association to pathways and experimental gene set collections from the Molecular Signature database (Subramanian *et al.*, 2005). The Molecular Signature database is divided in 5 collections for positional gene sets (C1), curated gene sets (C2), motif gene sets (C3), computational gene sets (C4) and gene ontology gene sets (C5). To identify overrepresented gene sets an enrichment analysis was conducted for the curated gene sets that are termed in the following as C2 gene sets. The candidate and reference genes used for the enrichment analysis are defined in Table 7.1. The gene

Figure 7.2 *(following page)*: Map of the GO Biological Process (BP) enrichment analysis. Shown is a graph of 153 significantly enriched terms. The boxes show the GO identifier, the expected number of genes (EXP) and, in brackets, the number of significant and annotated genes assigned to the term. The box-color reflects the p-value (P) that range from red ($p \leq 0.001$) to yellow ($p \leq 0.05$). The edges denote parent to child relations among the GO terms. Terms were grouped into 5 main categories i) developmental processes in embryogenesis, ii) signal transduction, iii) regulation of biological processes, iv) chromatin/histone modification and v) biosynthetic processes. The GO terms related to developmental processes cover organ development such as brain, gut, muscle, spinal cord, limb, skelet, epidermis, anatomical structure development and embryonic morphogenesis. Further, terms for neurogenesis, glial cell differentiation, axonogenesis, learning, cell migration and cell morphogenesis are enriched. The second category shows an enrichment for a variety of signal transduction processes, such as Wnt receptor, glutamate, epidermal growth factor receptor signaling pathway, protein Kinase C, arf protein, second-messenger mediated signaling and Intra-S-DNA damage checkpoint. The third category is comprised by terms involved in regulatory biological processes. Among them are regulations of replication, transcription, protein translation. The fourth group describes terms for translational protein modification (e.g., methylation, alkylation) and histone deacetylation. The fifth group describes biosynthetic processes for GTP, CTP and UTP. For a tablular format of the results see Table A.1.

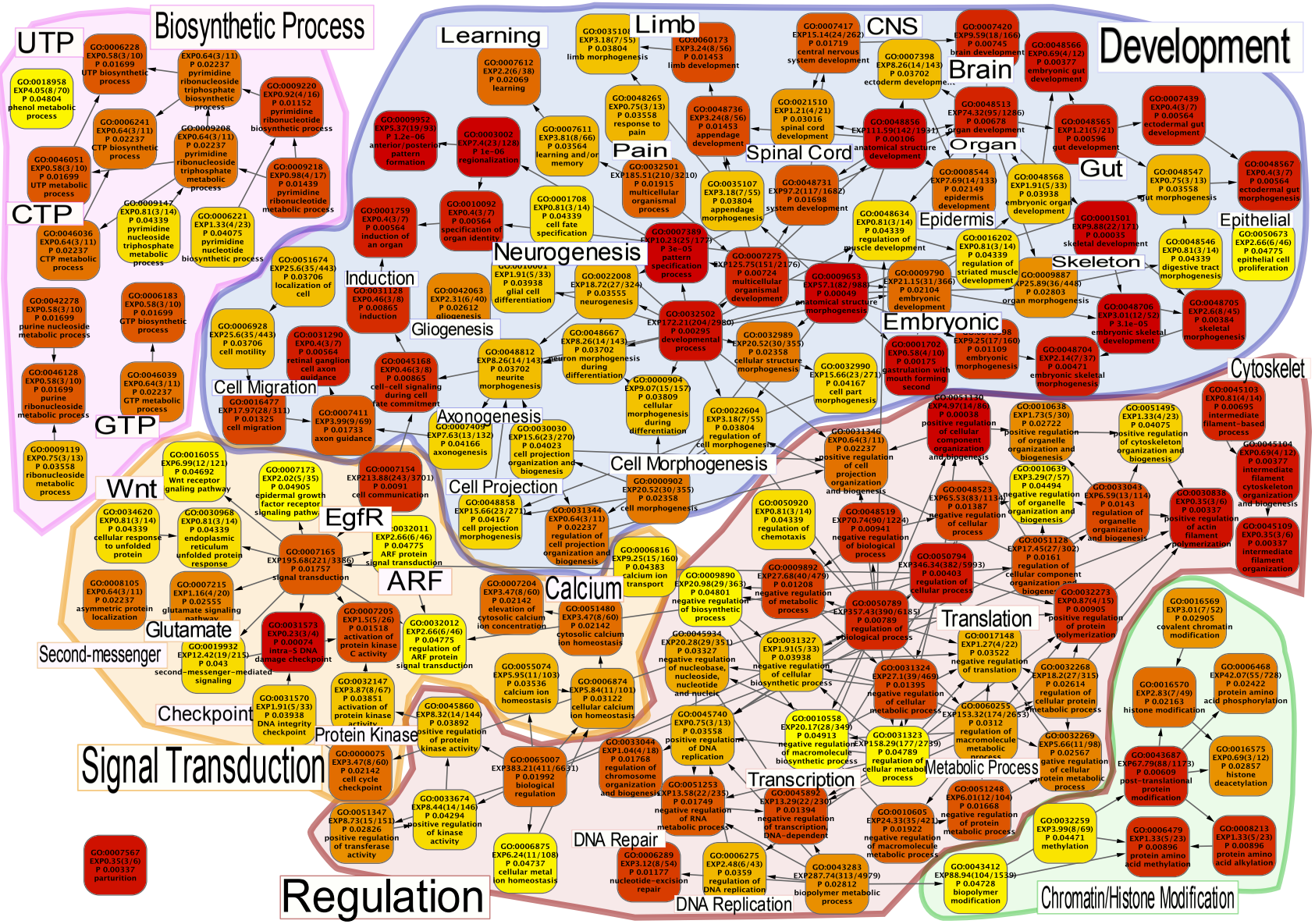
Biosynthetic Process
UTP
GO:0006228 EXP0.58(3/10) P 0.01699 UTP biosynthetic process
GO:0018958 EXP4.05(8/70) P 0.04804 phenol metabolic process
GO:0006241 EXP0.64(3/11) P 0.02237 CTP biosynthetic process
GO:0046051 EXP0.58(3/10) P 0.01699 UTP metabolic process
GO:0009147 EXP0.81(3/14) P 0.04339 pyrimidine nucleoside triphosphate metabolic process
GO:0006221 EXP1.33(4/23) P 0.04075 pyrimidine nucleotide biosynthetic process
GO:0009220 EXP0.92(4/16) P 0.01152 pyrimidine ribonucleotide biosynthetic process
GO:0009218 EXP0.98(4/17) P 0.01439 pyrimidine ribonucleotide metabolic process
GO:0009208 EXP0.64(3/11) P 0.02237 pyrimidine ribonucleoside triphosphate metabolic process
GO:0009206 EXP0.64(3/11) P 0.02237 pyrimidine ribonucleoside triphosphate biosynthetic process
CTP
GO:0046036 EXP0.64(3/11) P 0.02237 CTP metabolic process
GTP
GO:0042278 EXP0.58(3/10) P 0.01699 purine nucleoside metabolic process
GO:0006183 EXP0.58(3/10) P 0.01699 GTP biosynthetic process
GO:0046128 EXP0.58(3/10) P 0.01699 purine ribonucleoside metabolic process
GO:0046039 EXP0.64(3/11) P 0.02237 GTP metabolic process
GO:0009119 EXP0.75(3/13) P 0.03558 ribonucleoside metabolic process
Development
Limb
GO:0035108 EXP3.18(7/55) P 0.03804 limb morphogenesis
GO:0060173 EXP3.24(8/56) P 0.01453 limb development
CNS
GO:0007417 EXP15.14(24/262) P 0.01719 central nervous system development
GO:0007398 EXP8.26(14/143) P 0.03702 ectoderm developme...
Brain
GO:0007420 EXP9.59(18/166) P 0.00745 brain development
GO:0048566 EXP0.69(4/12) P 0.00377 embryonic gut development
GO:0048513 EXP74.32(95/1286) P 0.00678 organ development
GO:0048565 EXP1.21(5/21) P 0.00596 gut development
Organ
Gut
GO:0007439 EXP0.4(3/7) P 0.00564 ectodermal gut development
GO:0048547 EXP0.75(3/13) P 0.03558 gut morphogenesis
GO:0048567 EXP0.4(3/7) P 0.00564 ectodermal gut morphogenesis
Learning
GO:0007612 EXP2.2(6/38) P 0.02069 learning
Pain
GO:0007611 EXP3.81(8/66) P 0.03564 learning and/or memory
GO:0048265 EXP0.75(3/13) P 0.03558 response to pain
GO:0048736 EXP3.24(8/56) P 0.01453 appendage development
Spinal Cord
GO:0021510 EXP1.21(4/21) P 0.03016 spinal cord development
GO:0048731 EXP97.2(117/1682) P 0.01698 system development
GO:0048856 EXP111.59(142/1931) P 0.00106 anatomical structure development
GO:0009952 EXP5.37(19/93) P 1.2e-06 anterior/posterior pattern formation
GO:0003002 EXP7.4(23/128) P 1e-06 regionalization
GO:0032501 EXP185.51(210/3210) P 0.01915 multicellular organismal process
GO:0035107 EXP3.18(7/55) P 0.03804 appendage morphogenesis
GO:0007389 EXP10.23(25/177) P 3e-05 pattern specification process
GO:0007275 EXP125.75(151/2176) P 0.00724 multicellular organismal development
Neurogenesis
GO:0001759 EXP0.4(3/7) P 0.00564 induction of an organ
GO:0010092 EXP0.4(3/7) P 0.00564 specification of organ identity
GO:0001708 EXP0.81(3/14) P 0.04339 cell fate specification
Induction
GO:0031128 EXP0.46(3/8) P 0.00865 induction
GO:0042063 EXP2.31(6/40) P 0.02612 gliogenesis
GO:0010001 EXP1.91(5/33) P 0.03938 glial cell differentiation
GO:0022008 EXP18.72(27/324) P 0.03555 neurogenesis
Gliogenesis
GO:0048667 EXP8.26(14/143) P 0.03702 neuron morphogenesis during differentiation
GO:0032502 EXP172.21(204/2980) P 0.00295 developmental process
GO:0009653 EXP57.1(82/988) P 0.00049 anatomical structure morphogenesis
GO:0009790 EXP21.15(31/366) P 0.02104 embryonic development
Embryonic
GO:0032989 EXP20.52(30/355) P 0.02358 cellular structure morphogenesis
GO:0001702 EXP0.58(4/10) P 0.00175 gastrulation with mouth forming second
GO:0048704 EXP2.14(7/37) P 0.00471 embryonic skeletal morphogenesis
GO:0048706 EXP3.01(12/52) P 3.1e-05 embryonic skeletal development
GO:0048705 EXP2.6(8/45) P 0.00384 skeletal morphogenesis
Epidermis
GO:0048634 EXP0.81(3/14) P 0.04339 regulation of muscle development
GO:0016202 EXP0.81(3/14) P 0.04339 regulation of striated muscle development
GO:0048568 EXP1.91(5/33) P 0.03938 embryonic organ development
GO:0001501 EXP9.88(22/171) P 0.00035 skeletal development
Skeleton
GO:0009887 EXP25.89(36/448) P 0.02803 organ morphogenesis
Epithelial
GO:0048546 EXP0.81(3/14) P 0.04339 digestive tract morphogenesis
GO:0050673 EXP2.66(6/46) P 0.04775 epithelial cell proliferation
Cell Migration
GO:0016477 EXP17.97(28/311) P 0.01325 cell migration
GO:0007411 EXP3.99(9/69) P 0.01733 axon guidance
GO:0006928 EXP25.6(35/443) P 0.03706 cell motility
GO:0031290 EXP0.4(3/7) P 0.00564 retinal ganglion cell axon guidance
GO:0045168 EXP0.46(3/8) P 0.00865 cell-cell signaling during cell fate commitment
Axonogenesis
GO:0007409 EXP7.63(13/132) P 0.04166 axonogenesis
GO:0030030 EXP15.6(23/270) P 0.04023 cell projection organization and biogenesis
GO:0048812 EXP8.26(14/143) P 0.03702 neurite morphogenesis
Cell Morphogenesis
GO:0000902 EXP20.52(30/355) P 0.02358 cell morphogenesis
GO:0000904 EXP9.07(15/157) P 0.03809 cellular morphogenesis during differentiation
GO:0022604 EXP3.18(7/55) P 0.03804 regulation of cell morphogenesis
GO:0032990 EXP15.66(23/271) P 0.04167 cell part morphogenesis
Cell Projection
GO:0048858 EXP15.66(23/271) P 0.04167 cell projection morphogenesis
GO:0031344 EXP0.64(3/11) P 0.02237 regulation of cell projection organization and biogenesis
GO:0031346 EXP0.64(3/11) P 0.02237 positive regulation of cell projection organization and biogenesis
Cytoskelet
GO:0045103 EXP0.81(4/14) P 0.00695 intermediate filament-based process
GO:0045104 EXP0.69(4/12) P 0.00377 intermediate filament cytoskeleton organization and biogenesis
GO:0045109 EXP0.35(3/6) P 0.00337 intermediate filament organization
GO:0051130 EXP4.97(14/86) P 0.00038 positive regulation of cellular component organization and biogenesis
GO:0010638 EXP1.73(5/30) P 0.02722 positive regulation of organelle organization and biogenesis
GO:0051495 EXP1.33(4/23) P 0.04075 positive regulation of cytoskeleton organization and biogenesis
GO:0010639 EXP3.29(7/57) P 0.04494 negative regulation of organelle organization and biogenesis
GO:0033043 EXP6.59(13/114) P 0.0143 regulation of organelle organization and biogenesis
GO:0030838 EXP0.35(3/6) P 0.00337 positive regulation of actin filament polymerization
Wnt
GO:0016055 EXP6.99(12/121) P 0.04692 Wnt receptor signaling pathway
GO:0034620 EXP0.81(3/14) P 0.04339 cellular response to unfolded protein
GO:0030968 EXP0.81(3/14) P 0.04339 endoplasmic reticulum unfolded protein response
EgfR
GO:0007173 EXP2.02(5/35) P 0.04905 epidermal growth factor receptor signaling pathw...
GO:0007154 EXP213.88(243/3701) P 0.0091 cell communication
GO:0032011 EXP2.66(6/46) P 0.04775 ARF protein signal transduction
GO:0007165 EXP195.68(221/3386) P 0.01757 signal transduction
ARF
Calcium
GO:0006816 EXP9.25(15/160) P 0.04383 calcium ion transport
GO:0007204 EXP3.47(8/60) P 0.02142 elevation of cytosolic calcium ion concentration
GO:0051480 EXP3.47(8/60) P 0.02142 cytosolic calcium ion homeostasis
GO:0006874 EXP5.84(11/101) P 0.03122 cellular calcium ion homeostasis
GO:0055074 EXP5.95(11/103) P 0.03536 calcium ion homeostasis
Glutamate
Second-messenger
GO:0019932 EXP12.42(19/215) P 0.043 second-messenger-mediated signaling
GO:0007205 EXP1.5(5/26) P 0.01518 activation of protein kinase C activity
GO:0032012 EXP2.66(6/46) P 0.04775 regulation of ARF protein signal transduction
GO:0031573 EXP0.23(3/4) P 0.00074 intra-S DNA damage checkpoint
Checkpoint
GO:0031570 EXP1.91(5/33) P 0.03938 DNA integrity checkpoint
GO:0032147 EXP3.87(8/67) P 0.03851 activation of protein kinase activity
Protein Kinase
GO:0045860 EXP8.32(14/144) P 0.03892 positive regulation of protein kinase activity
Signal Transduction
GO:0000075 EXP3.47(8/60) P 0.02142 cell cycle checkpoint
GO:0051347 EXP8.73(15/151) P 0.02826 positive regulation of transferase activity
GO:0033674 EXP8.44(14/146) P 0.04294 positive regulation of kinase activity
GO:0065007 EXP383.21(411/6691) P 0.01992 biological regulation
GO:0033044 EXP1.04(4/18) P 0.01768 regulation of chromosome organization and biogenesis
GO:0007567 EXP0.35(3/6) P 0.00337 parturition
Regulation
GO:0006875 EXP6.24(11/108) P 0.04737 cellular metal ion homeostasis
DNA Repair
GO:0006289 EXP3.12(8/54) P 0.01177 nucleotide-excision repair
GO:0006275 EXP2.48(6/43) P 0.0359 regulation of DNA replication
GO:0043283 EXP287.74(313/4979) P 0.02812 biopolymer metabolic process
DNA Replication
Translation
GO:0050789 EXP357.43(390/6185) P 0.00789 regulation of biological process
GO:0017148 EXP1.27(4/22) P 0.03522 negative regulation of translation
GO:0031324 EXP27.1(39/469) P 0.01395 negative regulation of cellular metabolic process
GO:0031327 EXP1.91(5/33) P 0.03938 negative regulation of cellular biosynthetic process
GO:0045934 EXP20.28(29/351) P 0.03327 negative regulation of nucleobase, nucleoside, nucleotide and nucleic
GO:0009892 EXP27.68(40/479) P 0.01208 negative regulation of metabolic process
GO:0009890 EXP20.98(29/363) P 0.04801 negative regulation of biosynthetic process
GO:0050794 EXP346.34(382/5993) P 0.00403 regulation of cellular process
GO:0048519 EXP70.74(90/1224) P 0.00941 negative regulation of biological process
GO:0048523 EXP65.53(83/1134) P 0.01387 negative regulation of cellular process
GO:0050920 EXP0.81(3/14) P 0.04339 regulation of chemotaxis
GO:0051128 EXP17.45(27/302) P 0.0161 regulation of cellular component organization and biogenesis
GO:0032273 EXP0.87(4/15) P 0.00905 positive regulation of protein polymerization
Transcription
GO:0045740 EXP0.75(3/13) P 0.03558 positive regulation of DNA replication
GO:0010558 EXP20.17(28/349) P 0.04913 negative regulation of macromolecule biosynthetic process
GO:0031323 EXP158.29(177/2739) P 0.04789 regulation of cellular metabolic process
GO:0060255 EXP153.32(174/2653) P 0.0312 regulation of macromolecule metabolic process
GO:0032268 EXP18.2(27/315) P 0.02614 regulation of cellular protein metabolic process
GO:0032269 EXP5.66(11/98) P 0.02567 negative regulation of cellular protein metabolic process
Metabolic Process
GO:0051253 EXP13.58(22/235) P 0.01749 negative regulation of RNA metabolic process
GO:0045892 EXP13.29(22/230) P 0.01394 negative regulation of transcription, DNA-dependent
GO:0051248 EXP6.01(12/104) P 0.01668 negative regulation of protein metabolic process
GO:0010605 EXP24.33(35/421) P 0.01922 negative regulation of macromolecule metabolic process
GO:0032259 EXP3.99(8/69) P 0.04471 methylation
GO:0043412 EXP88.94(104/1539) P 0.04728 biopolymer modification
Chromatin/Histone Modification
GO:0016569 EXP3.01(7/52) P 0.02905 covalent chromatin modification
GO:0016570 EXP2.83(7/49) P 0.02163 histone modification
GO:0006468 EXP42.07(55/728) P 0.02422 protein amino acid phosphorylation
GO:0043687 EXP6.79(18/173) P 0.00609 post-translational protein modification
GO:0016575 EXP0.69(3/12) P 0.02857 histone deacetylation
GO:0006479 EXP1.33(5/23) P 0.00896 protein amino acid methylation
GO:0008213 EXP1.33(5/23) P 0.00896 protein amino acid alkylation

set assignments to human gene symbols were obtained from the Molecular Signature Database repository[1]. In total, 645 candidate genes (of 1,420) and 11,054 reference genes (of 25,236) were assigned to at least one C2 term (of 1,891 C2 terms). The enrichment for each C2 term was inferred by a hypergeometric test (one-sided Fisher's Exact Test). For the resulting set of enriched terms a graph is constructed, exported to Cytoscape (http://www.cytoscape.org/) and then manually edited.

In Figure 7.5 candidate genes are shown that correspond to significantly enriched curated gene sets. An enrichment of gene sets derived from studies that investigated the modulation of transcription to UV-C light and 4-nitroquinoline-1-oxide (4NQO) induced DNA damage for different time intervalls . Further an enrichment was found for Hox genes, signaling pathways, cell cylce regulators, autophagy and cell growth. The full table and term descriptions of all enriched C2 dataset terms is shown in the appendix section B.

[1] http://www.broadinstitute.org/gsea/msigdb

Figure 7.3 ***(following page)*:** Map of the GO Molecular Function (MF) Enrichment Analysis. The figure shows in total, 60 significant terms ($p \leq 0.05$) that are arranged in the subfigures (A-F). The terms were processed to subgraphs that are organized in a hierarchical structure, where the more general terms are located at the top and the more specific terms are at the bottom of the graph. The boxes show the GO identifier, the expected number of genes (EXP), and in brackets, the number of significant and annotated genes assigned to the term. The significance level of the p-value (P) is reflected by the box-color ranging from yellow ($p \leq 0.05$) to red ($p \leq 0.001$). A) An enrichment is observed for cytokine binding including interleukin-1 receptor activity and C-C chemokine binding receptor activity. Further, the functions for opioid and vascular endothelial growth factor receptor activity are enriched. B) Molecular functions are enriched that are related to cAMP and GTP binding, where the enrichment is strongest for terms leading to GTP binding. The unconnected terms describe an enrichment for the β adrenergic receptor activity, (Rho) GTPase binding, GTPase activity and GTPase activator activity. C) The subgraph consists of 17 related terms that describe transmembrane transporter activity for ions, amino acids and carbohydrates. In particular terms are enriched in ion transporters for sulfate and cation antiporters, cation symporters for sodium with neurotransmitters, sodium with amino-acids and hydrogen with sugar. D) Shown are enriched terms for transcription regulator activity for transcription repressors and transcription factors. Further, genes for the deacetylation of histones and androgen and chaperone binding are enriched. E,F) A collection of the remaining unconnected enriched GO terms. Terms with only 3 genes for pancreatic ribonuclease activity (endonucleolytic cleavage of RNA), phospatidate phosphatase activity, carbamoyl-phosphate synthase activity and cytoskeletal adaptor activity. Further, an enrichment for glycosaminoglycan and single-stranded DNA binding is shown. For a tablular format of the results see Table A.2.

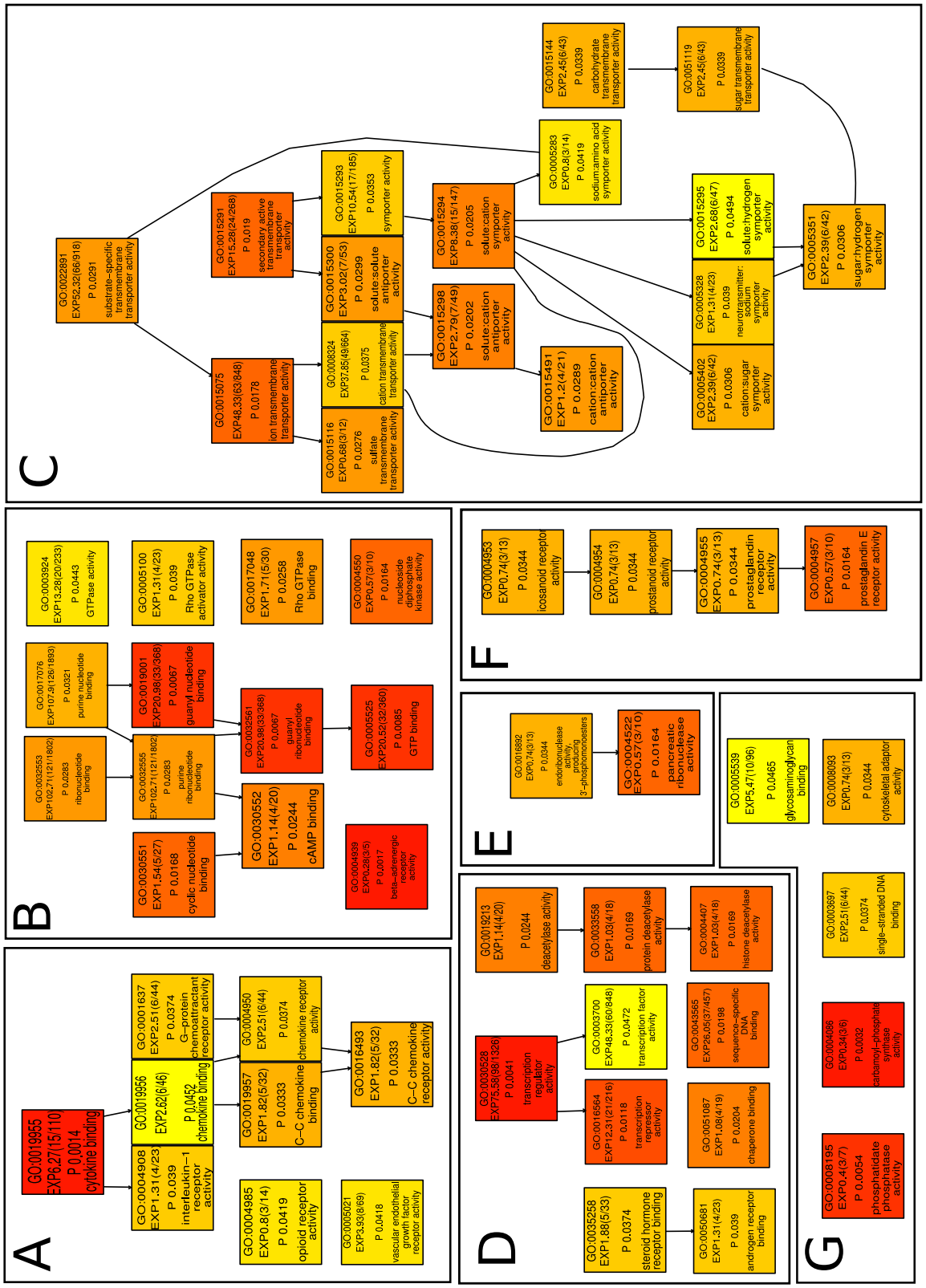
A
GO:0019955
EXP6.27(15/110)
P 0,0014
cytokine binding
GO:0004908
EXP1.31(4/23
P 0.039
interleukin−1
receptor
activity
GO:0019956
EXP2.62(6/46)
P 0,0452
chemokine binding
GO:0001637
EXP2.51(6/44)
P 0.0374
G−protein
chemoattractant
receptor activity
GO:0004985
EXP0.8(3/14)
P 0.0419
opioid receptor
activity
GO:0019957
EXP1.82(5/32)
P 0.0333
C−C chemokine
binding
GO:0004950
EXP2.51(6/44)
P 0.0374
chemokine receptor
activity
GO:0005021
EXP3.33(8/69)
P 0.0418
vascular endothelial
growth factor
receptor activity
GO:0016493
EXP1.82(5/32)
P 0.0333
C−C chemokine
receptor activity
B
GO:0003924
EXP13.28(20/233)
P 0.0443
GTPase activity
GO:0005100
EXP1.31(4/23)
P 0.039
Rho GTPase
activator activity
GO:0017048
EXP1.71(5/30)
P 0.0258
Rho GTPase
binding
GO:0004550
EXP0.57(3/10)
P 0.0164
nucleoside
diphosphate
kinase activity
GO:0017076
EXP107.9(126/1893)
P 0.0321
purine nucleotide
binding
GO:0019001
EXP20.98(33/368)
P 0.0067
guanyl nucleotide
binding
GO:0003553
EXP102.71(121/1602)
P 0.0283
ribonucleotide
binding
GO:0032555
EXP102.71(121/1602)
P 0.0283
purine
ribonucleotide
binding
GO:0032561
EXP20.98(33/368)
P 0.0067
guanyl
ribonucleotide
binding
GO:0005525
EXP20.52(32/360)
P 0.0085
GTP binding
GO:0030551
EXP1.54(5/27)
P 0.0168
cyclic nucleotide
binding
GO:0030552
EXP1.14(4/20)
P 0.0244
cAMP binding
GO:0004939
EXP0.29(3/5)
P 0.0017
beta−adrenergic
receptor
activity
C
GO:0022891
EXP52.32(66/918)
P 0.0291
substrate−specific
transmembrane
transporter activity
GO:0015075
EXP48.33(63/848)
P 0.0178
ion transmembrane
transporter activity
GO:0015291
EXP15.28(24/268)
P 0.019
secondary active
transmembrane
transporter
activity
GO:0015116
EXP0.68(3/12)
P 0.0276
sulfate
transmembrane
transporter activity
GO:0008324
EXP37.85(49/664)
P 0.0375
cation transmembrane
transporter activity
GO:0015300
EXP3.02(7/53)
P 0.0299
solute:solute
antiporter
activity
GO:0015293
EXP10.54(17/185)
P 0.0353
symporter activity
GO:0015294
EXP8.38(15/147)
P 0.0205
solute:cation
symporter
activity
GO:0015298
EXP2.79(7/49)
P 0.0202
solute:cation
antiporter
activity
GO:0015491
EXP1.2(4/21)
P 0.0289
cation:cation
antiporter
activity
GO:0005283
EXP0.8(3/14)
P 0.0419
sodium:amino acid
symporter activity
GO:0015144
EXP2.45(6/43)
P 0.0339
carbohydrate
transmembrane
transporter activity
GO:0005328
EXP1.3(4/23)
P 0.039
neurotransmitter:
sodium
symporter
activity
GO:0015295
EXP2.68(6/47)
P 0.0494
solute:hydrogen
symporter
activity
GO:0005402
EXP2.39(6/42)
P 0.0306
cation:sugar
symporter
activity
GO:0051119
EXP2.45(6/43)
P 0.0339
sugar transmembrane
transporter activity
GO:0005351
EXP2.39(6/42)
P 0.0306
sugar:hydrogen
symporter
activity
F
GO:0004953
EXP0.74(3/13)
P 0.0344
icosanoid receptor
activity
GO:0004954
EXP0.74(3/13)
P 0.0344
prostanoid receptor
activity
GO:0004955
EXP0.74(3/13)
P 0.0344
prostaglandin
receptor
activity
GO:0004957
EXP0.57(3/10)
P 0.0164
prostaglandin E
receptor activity
E
GO:0016892
EXP0.74(3/13)
P 0.0344
endonuclease
activity,
producing
3−phosphomonoesters
GO:0004522
EXP0.57(3/10)
P 0.0164
pancreatic
ribonuclease
activity
GO:0005539
EXP5.47(10/96)
P 0.0465
glycosaminoglycan
binding
GO:0008093
EXP0.74(3/13)
P 0.0344
cytoskeletal adaptor
activity
D
GO:0030528
EXP75.58(99/1326)
P 0.0041
transcription
regulator
activity
GO:0019213
EXP1.14(4/20)
P 0.0244
deacetylase activity
GO:0033558
EXP1.03(4/18)
P 0.0169
protein deacetylase
activity
GO:0004407
EXP1.03(4/18)
P 0.0169
histone deacetylase
activity
GO:0016564
EXP12.31(21/216)
P 0.0118
transcription
repressor
activity
GO:0003700
EXP48.33(60/848)
P 0.0472
transcription factor
activity
GO:0043565
EXP26.05(37/457)
P 0.0198
sequence−specific
DNA
binding
GO:0051087
EXP1.08(4/19)
P 0.0204
chaperone binding
GO:0035258
EXP1.88(5/33)
P 0.0374
steroid hormone
receptor binding
GO:0050681
EXP1.31(4/23)
P 0.039
androgen receptor
binding
G
GO:0008195
EXP0.4(3/7)
P 0.0054
phosphatidate
phosphatase
activity
GO:0004086
EXP0.34(3/6)
P 0.0032
carbamoyl−phosphate
synthase
activity
GO:0003697
EXP2.51(6/44)
P 0.0374
single−stranded DNA
binding

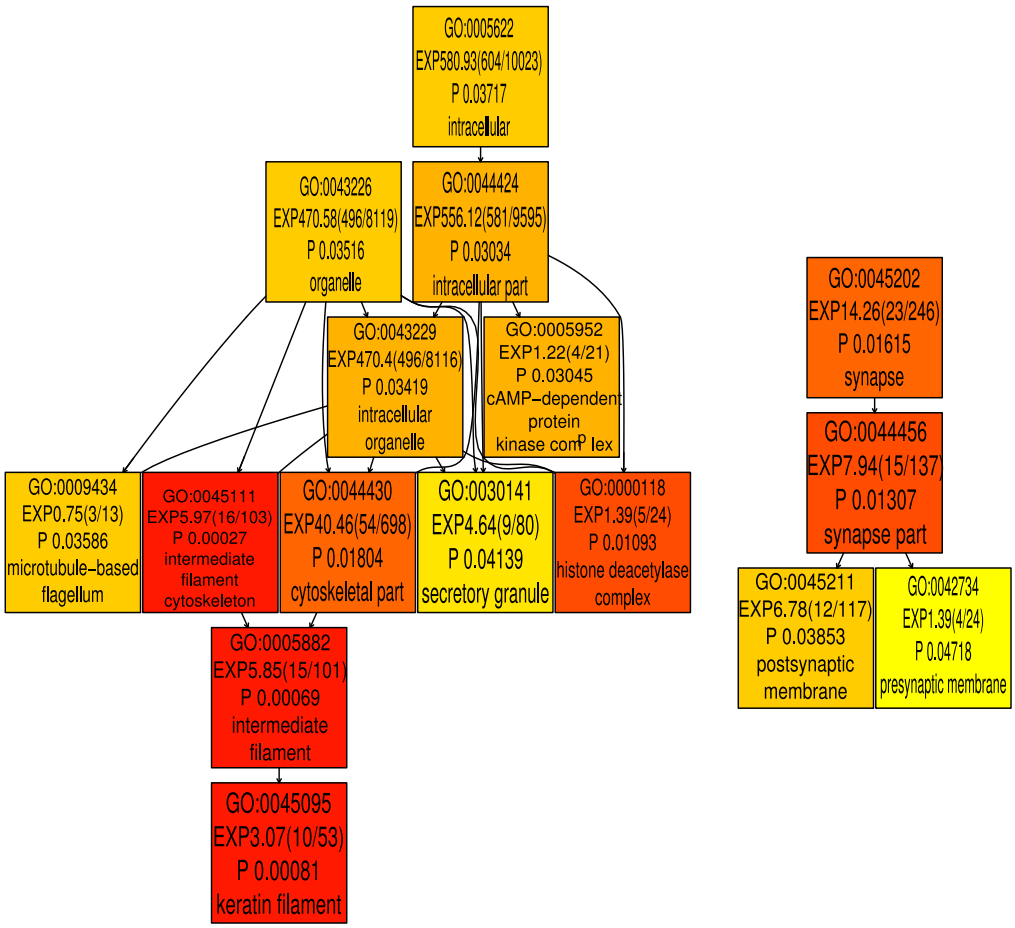

Figure 7.4: Map of the GO Cellular Component (CC) Enrichment Analysis. The figure shows in total, 16 significant terms ($p \leq 0.05$) that are organized in a hierarchical structure, where the more general terms are located at the top and the more specific terms are at the bottom of the graph. The boxes show the GO identifier, the expected number of genes (EXP) and in brackets the number of significant and annotated genes assigned to the term. The significance level of the p-value (P) is reflected by the box-color ranging from yellow ($p \leq 0.05$) to red ($p \leq 0.001$). The following cellular components terms are enriched: the histone deacetylase complex and the keratin filaments that are part of the intermediate filaments of the cytoskeleton. Further, genes related to the cAMP-dependent kinase complex and organelles such as the secretory granule and microtubule-based flagellum are enriched. An enrichment is also found for genes related to the synapse including the pre- and postsynaptic membrane. For a tablular format of the results see Table A.3.

7.3 Discussion

The genome-wide analysis of the transcribed fraction in the human-chimpanzee-rhesus genome alignment identified 565 significant 125 Kb alignment windows, where the ho-

mogeneity of the substitution patterns between human and chimpanzee was rejected and that showed the ∼5% most extreme model difference between both species. The differences of the substitution patterns in the human and chimpanzee models were suggested to result from different extents of transcription-coupled repair in the two species. This provides an initial indicative that the corresponding genes are differentially expressed in the germline of human and chimpanzee. A gene ontology enrichment analysis was conducted to elucidate, whether the identified genes might play a role in embryonic developmental processes that determine the phenotypes of human and chimpanzee.

From the 565 significant alignment windows, a total of 1,420 genes were defined as candidate gene set and 25,236 reference genes overlap with the remaining alignment windows. An enrichment for the three domains of the gene ontology showed that the candidate gene set is enriched in terms related to embryonic developmental processes, such as organ development and neurogenesis, signal transduction, and a variety of regulatory biological processes such as the regulation of replication, transcription, protein translation and post-translational protein modification that modulate gene expression. In summary, the functional annotation of the candidate gene set imply a regulatory role for developmental and morphological processes that could indeed account for the phenotypic differences between human and chimpanzee.

There are several alternative strategies available that could be applied to test for the enrichment of a term vocabulary such as provided by Gene Ontology. Some methods require a weighting measure or statistic that is assigned to each gene, e.g., that was experimentally inferred. The simplest approach is then to compare the distributions of the measures between the candidate and reference genes for each gene set. To assess the significance of the difference between the two distributions a variety of standard statistical methods can be employed, such as the Kolmogorov-Smirnov test (Ben-Shaul *et al.*,

Figure 7.5 ***(following page)*:** Map of the Molecular Signature Database C2 dataset Enrichment Analysis. Shown are the significantly enriched C2 terms with a nominal p-value <= 0.05 (yellow) and the corresponding assigned candidate genes (red). The enrichment for each C2 term was performed using a hypergeometric test. Terms were grouped (in dashed lines) for UVC light modulated transcription studies in fibroblasts (da Costa *et al.*, 2005; Gentile *et al.*, 2003; Kyng *et al.*, 2005), Hox genes and Hox related gene sets (da Costa *et al.*, 2005; Gentile *et al.*, 2003; Kyng *et al.*, 2005). Other enriched gene sets are related to Cytomegalovirus (CMV) and Reovirus infection response, cell communication, autophagy, signalling and cell growth.

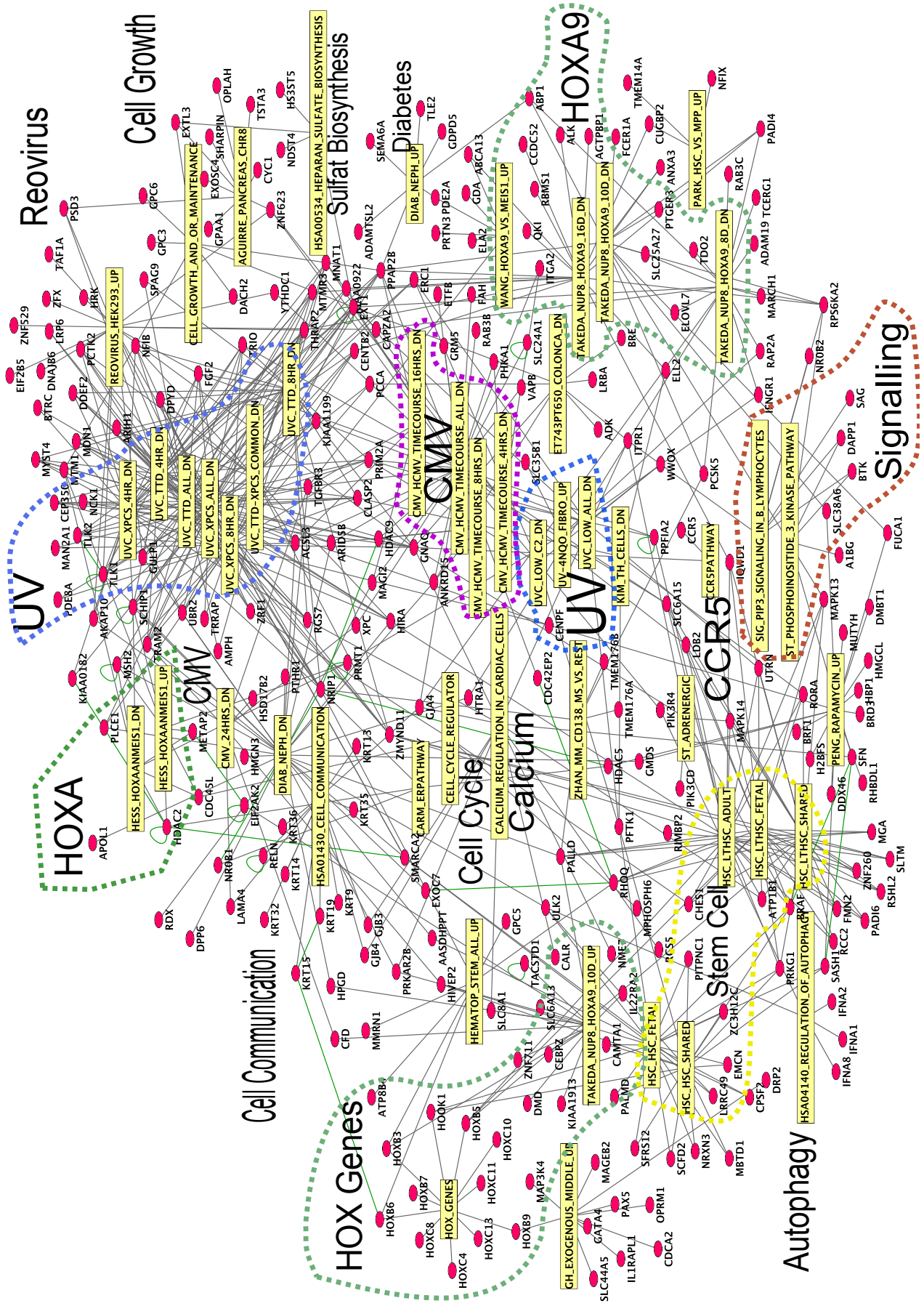
Reovirus
Cell Growth
Sulfat Biosynthesis
Diabetes
HOXA9
Signalling
UV
HOXA
CMV
CMV
Cell Cycle
Calcium
UV
CCR5
Cell Communication
Stem Cell
HOX Genes
Autophagy
REOVIRUS_HEK293_UP
CELL_GROWTH_AND_OR_MAINTENANCE
AGUIRRE_PANCREAS_CHR8
HSA00534_HEPARAN_SULFATE_BIOSYNTHESIS
DIAB_NEPH_UP
WANG_HOXA9_VS_MEIS1_UP
TAKEDA_NUP8_HOXA9_16D_DN
TAKEDA_NUP8_HOXA9_10D_DN
TAKEDA_NUP8_HOXA9_8D_DN
PARK_HSC_VS_MPP_UP
UVC_TTD_4HR_DN
UVC_TTD_ALL_DN
UVC_XPCS_4HR_DN
UVC_XPCS_ALL_DN
UVC_XPCS_8HR_DN
UVC_TTD_XPCS_COMMON_DN
UVC_TTD_8HR_DN
CMV_HCMV_TIMECOURSE_16HRS_DN
CMV_HCMV_TIMECOURSE_ALL_DN
CMV_HCMV_TIMECOURSE_8HRS_DN
CMV_HCMV_TIMECOURSE_4HRS_DN
UVC_LOW_ALL_DN
UVC_LOW_C2_DN
UV_4NQO_FIBRO_UP
ET743PT650_COLONCA_DN
KIM_TH_CELLS_DN
HESS_HOXAANMEIS1_UP
HESS_HOXAANMEIS1_DN
CMV_24HRS_DN
DIAB_NEPH_DN
CELL_CYCLE_REGULATOR
CALCIUM_REGULATION_IN_CARDIAC_CELLS
ZHAN_MM_CD138_MS_VS_REST
ST_ADRENERGIC
CCR5PATHWAY
ST_PHOSPHOINOSITIDE_3_KINASE_PATHWAY
SIG_PIP3_SIGNALING_IN_B_LYMPHOCYTES
PENG_RAPAMYCIN_UP
HSA01430_CELL_COMMUNICATION
ARM_ERPATHWAY
HEMATOP_STEM_ALL_UP
HSC_LTHSC_ADULT
HSC_LTHSC_FETAL
HSC_LTHSC_SHARED
HSC_HSC_FETAL
HSC_HSC_SHARED
HOX_GENES
GH_EXOGENOUS_MIDDLE_DN
HSA04140_REGULATION_OF_AUTOPHAGY

2005), the student t-test (Boorsma *et al.*, 2005) and the Wilcoxon rank test (Barry *et al.*, 2005). Recently introduced methods, the so called gene set enrichment analysis (GSEA) method (Mootha *et al.*, 2003) has the advantage not to require a predefined candidate and reference gene list. The method computes a summary statistic for each gene set from the weighting measures that are assigned to each gene. The null distribution of the summary statistic is computed for each term repeatedly from random permutations of the score assignments of all individual genes. The statistics commonly used are rank statistics, e.g., Kolmogorov-Smirnov score (Subramanian *et al.*, 2005) or summary statistics (Tian *et al.*, 2005; Jiang and Gentleman, 2007). The latter described methods are appropriate when only subtle changes are expected in an experiment, e.g., by a coordinated change of a geneset that are not detected with the conventional methods, such as by a hyper-geometric test (Mootha *et al.*, 2003).

Chapter 8

Outlook

In this thesis a set of candidate genes has been identified showing species-specific substitution patterns. It was shown that the underlying changes in the substitution patterns agree with what would be expected when the genes are subject to species-specific extents of transcription-coupled-repair. This implies that these genes are presumably differentially expressed in the germline of humans and chimpanzees. Interestingly, a Gene Ontology enrichment analysis revealed that the candidate genes play a role in major developmental processes, which are capable to account for different anatomical and behavioral phenotypes of humans and chimpanzees. The proposed gene expression changes are in-silico predictions and are difficult to confirm by experimental analyses. An experimental evaluation of differential gene expression during early embryonic developmental stages between humans and chimpanzees is not feasible due to ethical reasons as embryonic tissue samples would be required. For human and chimpanzee only gene expression data from adult tissues are available. It will therefore remain difficult to find strong correlations of strand-specific substitution patterns detected in this study to actual gene expression levels. Choosing species for an analysis as described here that are more accessible to experimental research, e.g., the species pair Mus Musculus and Mus spretus (Dejager *et al.*, 2009) would facilitate a wet-lab analysis to confirm in-silico predicted gene expression changes. In mammalian species the transcription signature in the substitution patterns of transcribed genomic regions is expected to be same (Green, 2003). Mus musculus and Mus spretus for example have a similar sequence divergence compared to the sequence divergence between humans and chimpanzees (Dejager *et al.*, 2009). The analysis to test for the homogeneity of the substitution patterns could be conducted between Mus musculus and Mus spretus using Rattus norvegicus as outgroup.

However, this analysis is not possible since the genome sequence of Mus spretus is not yet available.

For the use of other eukaryotic model organisms it would be first necessary to elucidate the explicit substitution patterns in transcribed and non-transcribed genomic regions. The observed strand asymmetries in transcribed genomic regions are likely to differ between vertebrates, invertebrates and plant species (Touchon *et al.*, 2004). This could be performed by a genome-wide analysis as described in chapter 4 for different eukaryotic species using the Likelihood-Ratio-Test for strand symmetry.

The factors driven by transcription-related processes that affect genomic DNA sequences are also used for the identification of novel transcribed genomic regions in the human genome (Glusman *et al.*, 2006). In Glusman *et al.* (2006), "transcription footprints" are detected by scoring for strand asymmetry measured by G+T excess, substitution patterns between interspersed repeats, repeat orientations and polyadenylation sites along the human genome. The modular approach from Glusman *et al.* (2006) could also consider branch-specific substitution patterns estimated from a multiple genome alignment to complement and improve predictions of genomic regions that are transcribed in the germline.

The branch-specific substitution model described by (Baake, 1998) that is used in the Single-Branch-Test assumes reversibility of the substitution process. This assumption does not allow to distinguish between the $A \rightarrow G$ and $G \rightarrow A$ rate and between the $T \rightarrow C$ and $C \rightarrow T$ rate. Only few studies consider the use of non-reversible branch-specific (non-homogeneous) substitution models (e.g., Lake, 1997; Barry and Hartigan, 1987). In Chang (1996) an example is shown, where different sets of substitution matrices for the branches of a tree can correspond to the same observed sequences in an alignment. This might be a problem for methods that require a closed-form solution (Lake, 1997) or for iterative optimization methods that converge to local optima (Barry and Hartigan, 1987). In Oscamou *et al.* (2008) the error in the estimation of non-reversible non-homogeneous substitution models was evaluated and shown to allow accurate estimates. The error was measured by the mean distance between the true substitution matrix used for a simulation of 3 taxon alignments and the inferred substitution matrices. However, the accuracy of such methods could also be measured by estimating the variations between branches from simulated data generated using a homogeneous compared to non-homogeneous substitution model. A variety of statistics can be applied to

measure the differences of the substitution patterns when more than two branches are considered (Weiss and von Haeseler, 2003; Hamady *et al.*, 2006). Further evaluations might provide a better understanding when such methods to estimate non-reversible non-homogeneous models give accurate estimates and when they fail.

It will be a challenge to identify the explicit factors that lead to differential gene expression patterns that explain phenotypic variations between different species. Gene expression differences might result from changes in the regulatory stages of gene expression starting from the regulation of DNA transcription to the regulation of post-translational processes. Sequence changes in regulatory genomic regions such as gene promotors, silencers, insulators and enhancers might alter binding specificity of transcription-factors and modify the control of transcriptional initiation, enhancement or repression (Donaldson and Gottgens, 2006). Differences in the RNA processing can alter the stability of the transcribed mRNA (e.g., increased by polyadenylation) and processing of alternative splice forms (Calarco *et al.*, 2007). Another factor is changes of DNA methylation patterns, where transcription is generally repressed in genomic regions that are methylated (Irvine *et al.*, 2002). Changes on the chromatin structure e.g., via histone modifications or chromatin-remodeling enzymes alter the accessibility of the DNA for transcriptional activity (Li *et al.*, 2007). The positioning of chromosomes in the nuclear matrix can also influence transcriptional activity of genomic regions (Lanctot *et al.*, 2007). Another factor is genomic rearrangements that can cause a change of the genomic neighboring environment of a gene. This might have a direct or indirect influence on the expression patterns of a gene (Marques-Bonet *et al.*, 2004). Gene duplications and gene losses observed between or within mammalian species lead to gene copy number variations (CNV) (Perry *et al.*, 2006). CNVs are suggested to affect gene expression by gene dosage effects, by affecting the chromatin structure or changes of the neighboring genomic regulatory sequences (Kleinjan and van Heyningen, 2005). Another suggested regulatiory mechanism for transcription is processes involved in stalling or pausing the RNA polymerase at the stage of early elongation (Tamkun, 2007). However, the explicit factors that would explain differential gene expression patterns between humans and chimpanzees are speculative and unclear to date.

The substitutional changes derived from transcription-coupled-repair denoted as transcription signature are thought to be neutral and assumed to reflect the strength of gene expression. The identified set of candidate genes that showed a different extend of the

transcription signature between human and chimpanzee might affect changes in the regulatory network of the metabolome, transcriptome and proteome. It would therefore be useful to study the role of the candidate genes in the protein-protein interaction network to identify new key regulators of developmental processes. This might help to find new signaling pathways during development and might help to understand related human diseases leading to e.g., developmental anomalies, intellectual impairment or growth retardation.

Bibliography

Alexa, A., Rahnenfuhrer, J. and Lengauer, T. (2006) Improved scoring of functional groups from gene expression data by decorrelating GO graph structure. *Bioinformatics*, **22**, 1600–7.

Ashburner, M., Ball, C., Blake, J., Botstein, D., Butler, H., Cherry, J., Davis, A., Dolinski, K., Dwight, S., Eppig, J., Harris, M., Hill, D., Issel-Tarver, L., Kasarskis, A., Lewis, S., Matese, J., Richardson, J., Ringwald, M., Rubin, G. and Sherlock, G. (2000) Gene ontology: tool for the unification of biology. The Gene Ontology Consortium. *Nat Genet*, **25**, 25–9.

Baake, E. (1998) What can and what cannot be inferred from pairwise sequence comparisons? *Math Biosci*, **154**, 1–21.

Bailey, N., Bailey, A. and Bailey, L. (1990) *The Elements of Stochastic Processes with Applications to the Natural Sciences*. John Wiley and Sons.

Barry, D. and Hartigan, J. (1987) Asynchronous distance between homologous DNA sequences. *Biometrics*, **43**, 261–76.

Barry, W., Nobel, A. and Wright, F. (2005) Significance analysis of functional categories in gene expression studies: a structured permutation approach. *Bioinformatics*, **21**, 1943–9.

Beissbarth, T. and Speed, T. (2004) GOstat: find statistically overrepresented Gene Ontologies within a group of genes. *Bioinformatics*, **20**, 1464–5.

Ben-Shaul, Y., Bergman, H. and Soreq, H. (2005) Identifying subtle interrelated changes in functional gene categories using continuous measures of gene expression. *Bioinformatics*, **21**, 1129–37.

Benjamini, Y. and Y., H. (1995) Controlling the false discovery rate: A practical and powerful approach to multiple testing. *Journal of the Royal Statistical Society. Series B (Methodological)*, **57**, 289–300.

Bielawski, J. and Gold, J. (2002) Mutation patterns of mitochondrial H- and L-strand DNA in closely related Cyprinid fishes. *Genetics*, **161**, 1589–97.

Blanchette, M., Kent, W., Riemer, C., Elnitski, L., Smit, A., Roskin, K., Baertsch, R., Rosenbloom, K., Clawson, H., Green, E., Haussler, D. and Miller, W. (2004) Aligning multiple genomic sequences with the threaded blockset aligner. *Genome Res*, **14**, 708–15.

Boorsma, A., Foat, B., Vis, D., Klis, F. and Bussemaker, H. (2005) T-profiler: scoring the activity of predefined groups of genes using gene expression data. *Nucleic Acids Res*, **33**, W592–5.

Caceres, M., Lachuer, J., Zapala, M., Redmond, J., Kudo, L., Geschwind, D., Lockhart, D., Preuss, T. and Barlow, C. (2003) Elevated gene expression levels distinguish human from non-human primate brains. *Proc Natl Acad Sci U S A*, **100**, 13030–5.

Calarco, J., Xing, Y., Caceres, M., Calarco, J., Xiao, X., Pan, Q., Lee, C., Preuss, T. and Blencowe, B. (2007) Global analysis of alternative splicing differences between humans and chimpanzees. *Genes Dev*, **21**, 2963–75.

Carey, V., Gentry, J., Whalen, E. and Gentleman, R. (2005) Network structures and algorithms in Bioconductor. *Bioinformatics*, **21**, 135–6.

Carlton, J., Muller, R., Yowell, C., Fluegge, M., Sturrock, K., Pritt, J., Vargas-Serrato, E., Galinski, M., Barnwell, J., Mulder, N., Kanapin, A., Cawley, S., Hide, W. and Dame, J. (2001) Profiling the malaria genome: a gene survey of three species of malaria parasite with comparison to other apicomplexan species. *Mol Biochem Parasitol*, **118**, 201–10.

Chang, J. (1996) Full reconstruction of Markov models on evolutionary trees: identifiability and consistency. *Math Biosci*, **137**, 51–73.

da Costa, R., Riou, L., Paquola, A., Menck, C. and Sarasin, A. (2005) Transcriptional profiles of unirradiated or UV-irradiated human cells expressing either the cancer-

prone XPB/CS allele or the noncancer-prone XPB/TTD allele. *Oncogene*, **24**, 1359–74.

CSAC (2005) Initial sequence of the chimpanzee genome and comparison with the human genome. *Nature*, **437**, 69–87.

Dejager, L., Libert, C. and Montagutelli, X. (2009) Thirty years of Mus spretus: a promising future. *Trends Genet*, **25**, 234–41.

Donaldson, I. and Gottgens, B. (2006) Evolution of candidate transcriptional regulatory motifs since the human-chimpanzee divergence. *Genome Biol*, **7**, R52.

Dubchak, I., Poliakov, A., Kislyuk, A. and Brudno, M. (2009) Multiple whole-genome alignments without a reference organism. *Genome Res*, **19**, 682–9.

Duret, L. and Arndt, P. (2008) The impact of recombination on nucleotide substitutions in the human genome. *PLoS Genet*, **4**, e1000071.

Durinck, S., Moreau, Y., Kasprzyk, A., Davis, S., De Moor, B., Brazma, A. and Huber, W. (2005) BioMart and Bioconductor: a powerful link between biological databases and microarray data analysis. *Bioinformatics*, **21**, 3439–40.

Ebersberger, I., Metzler, D., Schwarz, C. and Paabo, S. (2002) Genomewide comparison of DNA sequences between humans and chimpanzees. *Am J Hum Genet*, **70**, 1490–7.

Ebersberger, I. and Meyer, M. (2005) A genomic region evolving toward different GC contents in humans and chimpanzees indicates a recent and regionally limited shift in the mutation pattern. *Mol Biol Evol*, **22**, 1240–5.

Enard, W., Khaitovich, P., Klose, J., Zollner, S., Heissig, F., Giavalisco, P., Nieselt-Struwe, K., Muchmore, E., Varki, A., Ravid, R., Doxiadis, G., Bontrop, R. and Paabo, S. (2002) Intra- and interspecific variation in primate gene expression patterns. *Science*, **296**, 340–3.

Ewing, B. and Green, P. (1998) Base-calling of automated sequencer traces using phred. II. Error probabilities. *Genome Res*, **8**, 186–94.

Eyre-Walker, A. and Hurst, L. (2001) The evolution of isochores. *Nat Rev Genet*, **2**, 549–55.

Felsenstein, J. (2004) *Inferring Phylogenies*. Sinauer Associates, Sunderland, Massachusetts.

Flicek, P., Aken, B., Beal, K., Ballester, B., Caccamo, M., Chen, Y., Clarke, L., Coates, G., Cunningham, F., Cutts, T., Down, T., Dyer, S., Eyre, T., Fitzgerald, S., Fernandez-Banet, J., Graf, S., Haider, S., Hammond, M., Holland, R., Howe, K., Howe, K., Johnson, N., Jenkinson, A., Kahari, A., Keefe, D., Kokocinski, F., Kulesha, E., Lawson, D., Longden, I., Megy, K., Meidl, P., Overduin, B., Parker, A., Pritchard, B., Prlic, A., Rice, S., Rios, D., Schuster, M., Sealy, I., Slater, G., Smedley, D., Spudich, G., Trevanion, S., Vilella, A., Vogel, J., White, S., Wood, M., Birney, E., Cox, T., Curwen, V., Durbin, R., Fernandez-Suarez, X., Herrero, J., Hubbard, T., Kasprzyk, A., Proctor, G., Smith, J., Ureta-Vidal, A. and Searle, S. (2008) Ensembl 2008. *Nucleic Acids Res*, **36**, D707–14.

Francino, M. and Ochman, H. (2001) Deamination as the basis of strand-asymmetric evolution in transcribed Escherichia coli sequences. *Mol Biol Evol*, **18**, 1147–50.

Gardner, M., Hall, N., Fung, E., White, O., Berriman, M., Hyman, R., Carlton, J., Pain, A., Nelson, K., Bowman, S., Paulsen, I., James, K., Eisen, J., Rutherford, K., Salzberg, S., Craig, A., Kyes, S., Chan, M., Nene, V., Shallom, S., Suh, B., Peterson, J., Angiuoli, S., Pertea, M., Allen, J., Selengut, J., Haft, D., Mather, M., Vaidya, A., Martin, D., Fairlamb, A., Fraunholz, M., Roos, D., Ralph, S., McFadden, G., Cummings, L., Subramanian, G., Mungall, C., Venter, J., Carucci, D., Hoffman, S., Newbold, C., Davis, R., Fraser, C. and Barrell, B. (2002) Genome sequence of the human malaria parasite Plasmodium falciparum. *Nature*, **419**, 498–511.

Gentile, M., Latonen, L. and Laiho, M. (2003) Cell cycle arrest and apoptosis provoked by UV radiation-induced DNA damage are transcriptionally highly divergent responses. *Nucleic Acids Res*, **31**, 4779–90.

Gentleman, R., Carey, V., Bates, D., Bolstad, B., Dettling, M., Dudoit, S., Ellis, B., Gautier, L., Ge, Y., Gentry, J., Hornik, K., Hothorn, T., Huber, W., Iacus, S., Irizarry, R., Leisch, F., Li, C., Maechler, M., Rossini, A., Sawitzki, G., Smith, C., Smyth, G., Tierney, L., Yang, J. and Zhang, J. (2004) Bioconductor: open software development for computational biology and bioinformatics. *Genome Biol*, **5**, R80.

Gilad, Y., Oshlack, A., Smyth, G., Speed, T. and White, K. (2006) Expression profiling in primates reveals a rapid evolution of human transcription factors. *Nature*, **440**, 242–5.

Glusman, G., Qin, S., El-Gewely, M., Siegel, A., Roach, J., Hood, L. and Smit, A. (2006) A third approach to gene prediction suggests thousands of additional human transcribed regions. *PLoS Comput Biol*, **2**, e18.

Green, E. (2003) Transcription-associated mutational asymmetry in mammalian evolution. *Nat Genet*, **33**, 514–7.

Green, E., Sidow, A. and Batzoglou, S. (2003) LAGAN and Multi-LAGAN: efficient tools for large-scale multiple alignment of genomic DNA. *Genome Res*, **13**, 721–31.

Hamady, M., Betterton, M. and Knight, R. (2006) Using the nucleotide substitution rate matrix to detect horizontal gene transfer. *BMC Bioinformatics*, **7**, 476.

Hasegawa, M., Kishino, H. and Yano, T. (1985) Dating of the human-ape splitting by a molecular clock of mitochondrial DNA. *J Mol Evol*, **22**, 160–74.

Hubbard, T., Aken, B., Beal, K., Ballester, B., Caccamo, M., Chen, Y., Clarke, L., Coates, G., Cunningham, F., Cutts, T., Down, T., Dyer, S., Fitzgerald, S., Fernandez-Banet, J., Graf, S., Haider, S., Hammond, M., Herrero, J., Holland, R., Howe, K., Howe, K., Johnson, N., Kahari, A., Keefe, D., Kokocinski, F., Kulesha, E., Lawson, D., Longden, I., Melsopp, C., Megy, K., Meidl, P., Ouverdin, B., Parker, A., Prlic, A., Rice, S., Rios, D., Schuster, M., Sealy, I., Severin, J., Slater, G., Smedley, D., Spudich, G., Trevanion, S., Vilella, A., Vogel, J., White, S., Wood, M., Cox, T., Curwen, V., Durbin, R., Fernandez-Suarez, X., Flicek, P., Kasprzyk, A., Proctor, G., Searle, S., Smith, J., Ureta-Vidal, A. and Birney, E. (2007) Ensembl 2007. *Nucleic Acids Res*, **35**, D610–7.

Huvet, M., Nicolay, S., Touchon, M., Audit, B., d'Aubenton Carafa, Y., Arneodo, A. and Thermes, C. (2007) Human gene organization driven by the coordination of replication and transcription. *Genome Res*, **17**, 1278–85.

Irvine, R., Lin, I. and Hsieh, C. (2002) DNA methylation has a local effect on transcription and histone acetylation. *Mol Cell Biol*, **22**, 6689–96.

Jiang, Z. and Gentleman, R. (2007) Extensions to gene set enrichment. *Bioinformatics*, **23**, 306–13.

Jiricny, J., Su, S., Wood, S. and Modrich, P. (1988) Mismatch-containing oligonucleotide duplexes bound by the E. coli mutS-encoded protein. *Nucleic Acids Res*, **16**, 7843–53.

Jukes, T. H. and Cantor, C. R. (1969) Evolution of protein molecules. In Munro, H. N. (ed.), *Mammalian Protein Metabolism*, vol. 3, pages 21–132, Academic Press, New York.

Kanehisa, M. and Goto, S. (2000) KEGG: kyoto encyclopedia of genes and genomes. *Nucleic Acids Res*, **28**, 27–30.

Karaman, M., Houck, M., Chemnick, L., Nagpal, S., Chawannakul, D., Sudano, D., Pike, B., Ho, V., Ryder, O. and Hacia, J. (2003) Comparative analysis of gene-expression patterns in human and African great ape cultured fibroblasts. *Genome Res*, **13**, 1619–30.

Karolchik, D., Hinrichs, A. and Kent, W. (2007) The UCSC Genome Browser. *Curr Protoc Bioinformatics*, **Chapter 1**, Unit 1.4.

Kent, W., Baertsch, R., Hinrichs, A., Miller, W. and Haussler, D. (2003) Evolution's cauldron: duplication, deletion, and rearrangement in the mouse and human genomes. *Proc Natl Acad Sci U S A*, **100**, 11484–9.

Khaitovich, P., Hellmann, I., Enard, W., Nowick, K., Leinweber, M., Franz, H., Weiss, G., Lachmann, M. and Paabo, S. (2005) Parallel patterns of evolution in the genomes and transcriptomes of humans and chimpanzees. *Science*, **309**, 1850–4.

Khaitovich, P., Tang, K., Franz, H., Kelso, J., Hellmann, I., Enard, W., Lachmann, M. and Paabo, S. (2006) Positive selection on gene expression in the human brain. *Curr Biol*, **16**, R356–8.

Khatri, P., Draghici, S., Ostermeier, G. and Krawetz, S. (2002) Profiling gene expression using onto-express. *Genomics*, **79**, 266–70.

Kimura, M. (1980) A simple method for estimating evolutionary rates of base substitutions through comparative studies of nucleotide sequences. *J Mol Evol*, **16**, 111–20.

King, M. and Wilson, A. (1975) Evolution at two levels in humans and chimpanzees. *Science*, **188**, 107–16.

Kleinjan, D. and van Heyningen, V. (2005) Long-range control of gene expression: emerging mechanisms and disruption in disease. *Am J Hum Genet*, **76**, 8–32.

Kumar, S. and Gadagkar, S. (2001) Disparity index: a simple statistic to measure and test the homogeneity of substitution patterns between molecular sequences. *Genetics*, **158**, 1321–7.

Kyng, K., May, A., Stevnsner, T., Becker, K., Kolvra, S. and Bohr, V. (2005) Gene expression responses to DNA damage are altered in human aging and in Werner Syndrome. *Oncogene*, **24**, 5026–42.

Lake, J. (1997) Phylogenetic inference: how much evolutionary history is knowable? *Mol Biol Evol*, **14**, 213–9.

Lamers, M., Perrakis, A., Enzlin, J., Winterwerp, H., de Wind, N. and Sixma, T. (2000) The crystal structure of DNA mismatch repair protein MutS binding to a G x T mismatch. *Nature*, **407**, 711–7.

Lanave, C., Preparata, G., Saccone, C. and Serio, G. (1984) A new method for calculating evolutionary substitution rates. *J Mol Evol*, **20**, 86–93.

Lanctot, C., Cheutin, T., Cremer, M., Cavalli, G. and Cremer, T. (2007) Dynamic genome architecture in the nuclear space: regulation of gene expression in three dimensions. *Nat Rev Genet*, **8**, 104–15.

Li, G., Wang, J., Rossiter, S., Jones, G. and Zhang, S. (2007) Accelerated FoxP2 evolution in echolocating bats. *PLoS One*, **2**, e900.

Lobry, J. (1996) Asymmetric substitution patterns in the two DNA strands of bacteria. *Mol Biol Evol*, **13**, 660–5.

Maere, S., Heymans, K. and Kuiper, M. (2005) BiNGO: a Cytoscape plugin to assess overrepresentation of gene ontology categories in biological networks. *Bioinformatics*, **21**, 3448–9.

Marques-Bonet, T., Caceres, M., Bertranpetit, J., Preuss, T., Thomas, J. and Navarro, A. (2004) Chromosomal rearrangements and the genomic distribution of gene-expression divergence in humans and chimpanzees. *Trends Genet*, **20**, 524–9.

Marvanova, M., Menager, J., Bezard, E., Bontrop, R., Pradier, L. and Wong, G. (2003) Microarray analysis of nonhuman primates: validation of experimental models in neurological disorders. *FASEB J*, **17**, 929–31.

Miller, W., Rosenbloom, K., Hardison, R., Hou, M., Taylor, J., Raney, B., Burhans, R., King, D., Baertsch, R., Blankenberg, D., Kosakovsky Pond, S., Nekrutenko, A., Giardine, B., Harris, R., Tyekucheva, S., Diekhans, M., Pringle, T., Murphy, W., Lesk, A., Weinstock, G., Lindblad-Toh, K., Gibbs, R., Lander, E., Siepel, A., Haussler, D. and Kent, W. (2007) 28-way vertebrate alignment and conservation track in the UCSC Genome Browser. *Genome Res*, **17**, 1797–808.

Moler, C. and Charles, V. L. (2003) Nineteen dubious ways to compute the exponential of a matrix, twenty-five years later. *SIAM Rev.*, **45**, 3–49.

Mootha, V., Lindgren, C., Eriksson, K., Subramanian, A., Sihag, S., Lehar, J., Puigserver, P., Carlsson, E., Ridderstrale, M., Laurila, E., Houstis, N., Daly, M., Patterson, N., Mesirov, J., Golub, T., Tamayo, P., Spiegelman, B., Lander, E., Hirschhorn, J., Altshuler, D. and Groop, L. (2003) PGC-1alpha-responsive genes involved in oxidative phosphorylation are coordinately downregulated in human diabetes. *Nat Genet*, **34**, 267–73.

Mugal, C., von Grunberg, H. and Peifer, M. (2009) Transcription-induced mutational strand bias and its effect on substitution rates in human genes. *Mol Biol Evol*, **26**, 131–42.

Oscamou, M., McDonald, D., Yap, V., Huttley, G., Lladser, M. and Knight, R. (2008) Comparison of methods for estimating the nucleotide substitution matrix. *BMC Bioinformatics*, **9**, 511.

Paten, B., Herrero, J., Beal, K., Fitzgerald, S. and Birney, E. (2008) Enredo and Pecan: genome-wide mammalian consistency-based multiple alignment with paralogs. *Genome Res*, **18**, 1814–28.

Perry, G., Tchinda, J., McGrath, S., Zhang, J., Picker, S., Caceres, A., Iafrate, A., Tyler-Smith, C., Scherer, S., Eichler, E., Stone, A. and Lee, C. (2006) Hotspots for copy number variation in chimpanzees and humans. *Proc Natl Acad Sci U S A*, **103**, 8006–11.

Reinius, B., Saetre, P., Leonard, J., Blekhman, R., Merino-Martinez, R., Gilad, Y. and Jazin, E. (2008) An evolutionarily conserved sexual signature in the primate brain. *PLoS Genet*, **4**, e1000100.

Robinson, M., Grigull, J., Mohammad, N. and Hughes, T. (2002) FunSpec: a web-based cluster interpreter for yeast. *BMC Bioinformatics*, **3**, 35.

Saitou, N. and Nei, M. (1987) The neighbor-joining method: a new method for reconstructing phylogenetic trees. *Mol Biol Evol*, **4**, 406–25.

Salemi, M. and Vandamme, A.-M. (2003) *The Phylogenetic Handbook: A Practical Approach to DNA and Protein Phylogeny Handbook: A Practical Approach to DNA and Protein Phylogeny*. Cambridge University Press.

Schwartz, S., Kent, W., Smit, A., Zhang, Z., Baertsch, R., Hardison, R., Haussler, D. and Miller, W. (2003) Human-mouse alignments with BLASTZ. *Genome Res*, **13**, 103–7.

Shannon, P., Markiel, A., Ozier, O., Baliga, N., Wang, J., Ramage, D., Amin, N., Schwikowski, B. and Ideker, T. (2003) Cytoscape: a software environment for integrated models of biomolecular interaction networks. *Genome Res*, **13**, 2498–504.

Smedley, D., Haider, S., Ballester, B., Holland, R., London, D., Thorisson, G. and Kasprzyk, A. (2009) BioMart–biological queries made easy. *BMC Genomics*, **10**, 22.

Smit, A. (1996) The origin of interspersed repeats in the human genome. *Curr Opin Genet Dev*, **6**, 743–8.

Smit, A., Hubley, R. and Green, P. (1996-2004) Repeatmasker open-3.0. 1996-2004. *http://www.repeatmasker.org*.

Subramanian, A., Tamayo, P., Mootha, V., Mukherjee, S., Ebert, B., Gillette, M., Paulovich, A., Pomeroy, S., Golub, T., Lander, E. and Mesirov, J. (2005) Gene set

enrichment analysis: a knowledge-based approach for interpreting genome-wide expression profiles. *Proc Natl Acad Sci U S A*, **102**, 15545–50.

Sueoka, N. (1995) Intrastrand parity rules of DNA base composition and usage biases of synonymous codons. *J Mol Evol*, **40**, 318–25.

Swofford, D. L., Olsen, G. J., Waddell, P. J. and Hillis, D. M. (1996) Phylogeny reconstruction. In Hillis, D. M., Moritz, C. and Mable, B. K. (eds.), *Molecular Systematics*, pages 407–514, Sinauer Associates, Sunderland, Massachusetts, Second edn..

Tamkun, J. (2007) Stalled polymerases and transcriptional regulation. *Nat Genet*, **39**, 1421–2.

Tamura, K. and Nei, M. (1993) Estimation of the number of nucleotide substitutions in the control region of mitochondrial DNA in humans and chimpanzees. *Mol. Biol. Evol.*, **10**, 512–526.

Taylor, J. R. (1996) *An Introduction to Error Analysis: The Study of Uncertainties in Physical Measurements*. University Science Books, Second edn..

Thomas, P., Campbell, M., Kejariwal, A., Mi, H., Karlak, B., Daverman, R., Diemer, K., Muruganujan, A. and Narechania, A. (2003) PANTHER: a library of protein families and subfamilies indexed by function. *Genome Res*, **13**, 2129–41.

Tian, L., Greenberg, S., Kong, S., Altschuler, J., Kohane, I. and Park, P. (2005) Discovering statistically significant pathways in expression profiling studies. *Proc Natl Acad Sci U S A*, **102**, 13544–9.

Touchon, M., Arneodo, A., d'Aubenton Carafa, Y. and Thermes, C. (2004) Transcription-coupled and splicing-coupled strand asymmetries in eukaryotic genomes. *Nucleic Acids Res*, **32**, 4969–78.

Touchon, M. and Rocha, E. (2008) From GC skews to wavelets: a gentle guide to the analysis of compositional asymmetries in genomic data. *Biochimie*, **90**, 648–59.

Uddin, M., Wildman, D., Liu, G., Xu, W., Johnson, R., Hof, P., Kapatos, G., Grossman, L. and Goodman, M. (2004) Sister grouping of chimpanzees and humans as revealed by genome-wide phylogenetic analysis of brain gene expression profiles. *Proc Natl Acad Sci U S A*, **101**, 2957–62.

Vallender, E. and Lahn, B. (2004) Effects of chromosomal rearrangements on human-chimpanzee molecular evolution. *Genomics*, **84**, 757–61.

Varki, A. and Altheide, T. (2005) Comparing the human and chimpanzee genomes: searching for needles in a haystack. *Genome Res*, **15**, 1746–58.

Venables, W. and Ripley, B. (2002) *Modern Applied Statistics with S. Fourth Edition*. Springer.

Webster, M., Smith, N. and Ellegren, H. (2003) Compositional evolution of noncoding DNA in the human and chimpanzee genomes. *Mol Biol Evol*, **20**, 278–86.

Weiss, G. and von Haeseler, A. (2003) Testing substitution models within a phylogenetic tree. *Mol Biol Evol*, **20**, 572–8.

Wheeler, D., Church, D., Federhen, S., Lash, A., Madden, T., Pontius, J., Schuler, G., Schriml, L., Sequeira, E., Tatusova, T. and Wagner, L. (2003) Database resources of the National Center for Biotechnology. *Nucleic Acids Res*, **31**, 28–33.

Wolfe, K., Sharp, P. and Li, W. (1989) Mutation rates differ among regions of the mammalian genome. *Nature*, **337**, 283–5.

Yang, Z. (1994a) Estimating the pattern of nucleotide substitution. *J Mol Evol*, **39**, 105–11.

Yang, Z. (1994b) Maximum likelihood phylogenetic estimation from DNA sequences with variable rates over sites: approximate methods. *J Mol Evol*, **39**, 306–14.

Yang, Z. (2007) PAML 4: phylogenetic analysis by maximum likelihood. *Mol Biol Evol*, **24**, 1586–91.

Zeeberg, B., Feng, W., Wang, G., Wang, M., Fojo, A., Sunshine, M., Narasimhan, S., Kane, D., Reinhold, W., Lababidi, S., Bussey, K., Riss, J., Barrett, J. and Weinstein, J. (2003) GoMiner: a resource for biological interpretation of genomic and proteomic data. *Genome Biol*, **4**, R28.

Acknowledgement

This thesis would not have been possible without the encouragement and constant support from **Arndt von Haeseler** and **Ingo Ebersberger**. I owe my deepest gratitude to both of you for supervising this project from the very beginning to present time. Thank you for all the fruitful discussions and patience during my Phd. Thank you (especially Ingo Ebersberger) for carefully reading and commenting the chapters and figures and for all your support as supervisor(s) and friend(s). I also want to especially thank Tamara Zoranovic and Josef Penninger that supported the development of the gene ontology enrichment analysis pipeline presented in chapter 7. Thank you Tamara for all the motivation, your patience and all the precious discussions. Also i would like to thank all my other collaborators, like Federica Catalanotti, Manuela Baccarini, Shane Cronin and Yumiko Imai. You sharpened my view on the molecular level. So many people I need to thank at this place. I am sorry that I may not be able to name all of you here. I am indebted to all my colleagues in the CIBIV and the Düsseldorf group, especially to my closest colleagues Tanja Gesell and Minh Bui Quang, which also have read and commented chapter 3. Thank you Tanja for all our conversations and your support. Thank you Martin Grabner for all the discussion we had and all advices about teaching. It was an invaluable experience to be a teaching assistant in your courses that you gave. Thank you Matthias Dehmer for your support and all fruitful discussions. Thank you Heiko Schmidt, Martin Grabner and Wolfgang Fischl, which are responsible for the outstanding computer and backup system at the CIBIV. I also want to thank all visitors of the CIBIV and numerous people I met that discussed my work with me. Thank you Christian Schlötterer for the retreats in the mountains with your group, for very helpful comments on a talk I gave and for providing the opportunity to talk with some of your invited speakers. Also I want to thank the MFPL, IMP and IMBA, who make this international environment possible around the Campus by inviting numerous cutting-edge speakers in their seminars. Thank you also to the WWTF and DFG for financial support. Thank you to all my dear friends. Thank you Sonia, Pedro, Joaquim and Susete for your patience, personal support and your presence.

Appendix A

Gene Ontology Enrichment Analysis - Supplement

A.1 Gene Ontology Biological Process

	GO.ID	Term	Annotated	Significant	Expected	P-value
1	GO:0003002	regionalization	128	23	7.40	0.000001
2	GO:0009952	anterior/posterior pattern formation	93	19	5.37	0.000001
3	GO:0007389	pattern specification process	177	25	10.23	0.000030
4	GO:0048706	embryonic skeletal development	52	12	3.01	0.000031
5	GO:0001501	skeletal development	171	22	9.88	0.000350
6	GO:0051130	positive regulation of cellular component organization and biogenesis	86	14	4.97	0.000380
7	GO:0009653	anatomical structure morphogenesis	988	82	57.10	0.000490
8	GO:0031573	intra-S DNA damage checkpoint	4	3	0.23	0.000740
9	GO:0048856	anatomical structure development	1931	142	111.59	0.001060
10	GO:0001702	gastrulation with mouth forming second	10	4	0.58	0.001750
11	GO:0032502	developmental process	2980	204	172.21	0.002950
12	GO:0007567	parturition	6	3	0.35	0.003370
13	GO:0030838	positive regulation of actin filament polymerization	6	3	0.35	0.003370
14	GO:0045109	intermediate filament organization	6	3	0.35	0.003370
15	GO:0045104	intermediate filament cytoskeleton organization and biogenesis	12	4	0.69	0.003770
16	GO:0048566	embryonic gut development	12	4	0.69	0.003770
17	GO:0048705	skeletal morphogenesis	45	8	2.60	0.003840
18	GO:0050794	regulation of cellular process	5993	382	346.34	0.004030
19	GO:0048704	embryonic skeletal morphogenesis	37	7	2.14	0.004710
20	GO:0001759	induction of an organ	7	3	0.40	0.005640
21	GO:0007439	ectodermal gut development	7	3	0.40	0.005640
22	GO:0010092	specification of organ identity	7	3	0.40	0.005640
23	GO:0031290	retinal ganglion cell axon guidance	7	3	0.40	0.005640
24	GO:0048567	ectodermal gut morphogenesis	7	3	0.40	0.005640
25	GO:0048565	gut development	21	5	1.21	0.005960

26	GO:0043687	post-translational protein modification	1173	88	67.79	0.006090
27	GO:0048513	organ development	1286	95	74.32	0.006780
28	GO:0045103	intermediate filament-based process	14	4	0.81	0.006950
29	GO:0007275	multicellular organismal development	2176	151	125.75	0.007240
30	GO:0007420	brain development	166	18	9.59	0.007450
31	GO:0050789	regulation of biological process	6185	390	357.43	0.007890
32	GO:0031128	induction	8	3	0.46	0.008650
33	GO:0045168	cell-cell signaling during cell fate commitment	8	3	0.46	0.008650
34	GO:0006479	protein amino acid methylation	23	5	1.33	0.008960
35	GO:0008213	protein amino acid alkylation	23	5	1.33	0.008960
36	GO:0032273	positive regulation of protein polymerization	15	4	0.87	0.009050
37	GO:0007154	cell communication	3701	243	213.88	0.009100
38	GO:0048519	negative regulation of biological process	1224	90	70.74	0.009410
39	GO:0048598	embryonic morphogenesis	160	17	9.25	0.011090
40	GO:0009220	pyrimidine ribonucleotide biosynthetic process	16	4	0.92	0.011520
41	GO:0006289	nucleotide-excision repair	54	8	3.12	0.011770
42	GO:0009892	negative regulation of metabolic process	479	40	27.68	0.012080
43	GO:0016477	cell migration	311	28	17.97	0.013250
44	GO:0048523	negative regulation of cellular process	1134	83	65.53	0.013870
45	GO:0045892	negative regulation of transcription, DNA-dependent	230	22	13.29	0.013940
46	GO:0031324	negative regulation of cellular metabolic process	469	39	27.10	0.013950
47	GO:0033043	regulation of organelle organization and biogenesis	114	13	6.59	0.014300
48	GO:0009218	pyrimidine ribonucleotide metabolic process	17	4	0.98	0.014390
49	GO:0048736	appendage development	56	8	3.24	0.014530
50	GO:0060173	limb development	56	8	3.24	0.014530
51	GO:0007205	activation of protein kinase C activity	26	5	1.50	0.015180
52	GO:0051128	regulation of cellular component organization and biogenesis	302	27	17.45	0.016100
53	GO:0051248	negative regulation of protein metabolic process	104	12	6.01	0.016680
54	GO:0048731	system development	1682	117	97.20	0.016980
55	GO:0006183	GTP biosynthetic process	10	3	0.58	0.016990
56	GO:0006228	UTP biosynthetic process	10	3	0.58	0.016990
57	GO:0042278	purine nucleoside metabolic process	10	3	0.58	0.016990
58	GO:0046051	UTP metabolic process	10	3	0.58	0.016990
59	GO:0046128	purine ribonucleoside metabolic process	10	3	0.58	0.016990
60	GO:0007417	central nervous system development	262	24	15.14	0.017190
61	GO:0007411	axon guidance	69	9	3.99	0.017330
62	GO:0051253	negative regulation of RNA metabolic process	235	22	13.58	0.017490
63	GO:0007165	signal transduction	3386	221	195.68	0.017570
64	GO:0033044	regulation of chromosome organization and biogenesis	18	4	1.04	0.017680
65	GO:0032501	multicellular organismal process	3210	210	185.51	0.019150
66	GO:0010605	negative regulation of macromolecule metabolic process	421	35	24.33	0.019220
67	GO:0065007	biological regulation	6631	411	383.21	0.019920
68	GO:0007612	learning	38	6	2.20	0.020690
69	GO:0009790	embryonic development	366	31	21.15	0.021040
70	GO:0000075	cell cycle checkpoint	60	8	3.47	0.021420
71	GO:0007204	elevation of cytosolic calcium ion concentration	60	8	3.47	0.021420
72	GO:0051480	cytosolic calcium ion homeostasis	60	8	3.47	0.021420
73	GO:0008544	epidermis development	133	14	7.69	0.021490

74	GO:0016570	histone modification	49	7	2.83	0.021630
75	GO:0006241	CTP biosynthetic process	11	3	0.64	0.022370
76	GO:0008105	asymmetric protein localization	11	3	0.64	0.022370
77	GO:0009208	pyrimidine ribonucleoside triphosphate metabolic process	11	3	0.64	0.022370
78	GO:0009209	pyrimidine ribonucleoside triphosphate biosynthetic process	11	3	0.64	0.022370
79	GO:0031344	regulation of cell projection organization and biogenesis	11	3	0.64	0.022370
80	GO:0031346	positive regulation of cell projection organization and biogenesis	11	3	0.64	0.022370
81	GO:0046036	CTP metabolic process	11	3	0.64	0.022370
82	GO:0046039	GTP metabolic process	11	3	0.64	0.022370
83	GO:0000902	cell morphogenesis	355	30	20.52	0.023580
84	GO:0032989	cellular structure morphogenesis	355	30	20.52	0.023580
85	GO:0006468	protein amino acid phosphorylation	728	55	42.07	0.024220
86	GO:0007215	glutamate signaling pathway	20	4	1.16	0.025550
87	GO:0032269	negative regulation of cellular protein metabolic process	98	11	5.66	0.025670
88	GO:0042063	gliogenesis	40	6	2.31	0.026120
89	GO:0032268	regulation of cellular protein metabolic process	315	27	18.20	0.026140
90	GO:0010638	positive regulation of organelle organization and biogenesis	30	5	1.73	0.027220
91	GO:0009887	organ morphogenesis	448	36	25.89	0.028030
92	GO:0043283	biopolymer metabolic process	4979	313	287.74	0.028120
93	GO:0051347	positive regulation of transferase activity	151	15	8.73	0.028260
94	GO:0016575	histone deacetylation	12	3	0.69	0.028570
95	GO:0016569	covalent chromatin modification	52	7	3.01	0.029050
96	GO:0021510	spinal cord development	21	4	1.21	0.030160
97	GO:0060255	regulation of macromolecule metabolic process	2653	174	153.32	0.031200
98	GO:0006874	cellular calcium ion homeostasis	101	11	5.84	0.031220
99	GO:0045934	negative regulation of nucleobase, nucleoside, nucleotide and nucleic acid metabolic process	351	29	20.28	0.033270
100	GO:0017148	negative regulation of translation	22	4	1.27	0.035220
101	GO:0055074	calcium ion homeostasis	103	11	5.95	0.035360
102	GO:0022008	neurogenesis	324	27	18.72	0.035550
103	GO:0009119	ribonucleoside metabolic process	13	3	0.75	0.035580
104	GO:0045740	positive regulation of DNA replication	13	3	0.75	0.035580
105	GO:0048265	response to pain	13	3	0.75	0.035580
106	GO:0048547	gut morphogenesis	13	3	0.75	0.035580
107	GO:0007611	learning and/or memory	66	8	3.81	0.035640
108	GO:0006275	regulation of DNA replication	43	6	2.48	0.035900
109	GO:0007398	ectoderm development	143	14	8.26	0.037020
110	GO:0048667	neuron morphogenesis during differentiation	143	14	8.26	0.037020
111	GO:0048812	neurite morphogenesis	143	14	8.26	0.037020
112	GO:0006928	cell motility	443	35	25.60	0.037060
113	GO:0051674	localization of cell	443	35	25.60	0.037060
114	GO:0022604	regulation of cell morphogenesis	55	7	3.18	0.038040
115	GO:0035107	appendage morphogenesis	55	7	3.18	0.038040
116	GO:0035108	limb morphogenesis	55	7	3.18	0.038040
117	GO:0000904	cellular morphogenesis during differentiation	157	15	9.07	0.038090
118	GO:0032147	activation of protein kinase activity	67	8	3.87	0.038510
119	GO:0045860	positive regulation of protein kinase activity	144	14	8.32	0.038920
120	GO:0010001	glial cell differentiation	33	5	1.91	0.039380

121	GO:0031327	negative regulation of cellular biosynthetic process	33	5	1.91	0.039380
122	GO:0031570	DNA integrity checkpoint	33	5	1.91	0.039380
123	GO:0048568	embryonic organ development	33	5	1.91	0.039380
124	GO:0030030	cell projection organization and biogenesis	270	23	15.60	0.040230
125	GO:0006221	pyrimidine nucleotide biosynthetic process	23	4	1.33	0.040750
126	GO:0051495	positive regulation of cytoskeleton organization and biogenesis	23	4	1.33	0.040750
127	GO:0007409	axonogenesis	132	13	7.63	0.041660
128	GO:0032990	cell part morphogenesis	271	23	15.66	0.041670
129	GO:0048858	cell projection morphogenesis	271	23	15.66	0.041670
130	GO:0033674	positive regulation of kinase activity	146	14	8.44	0.042940
131	GO:0019932	second-messenger-mediated signaling	215	19	12.42	0.043000
132	GO:0001708	cell fate specification	14	3	0.81	0.043390
133	GO:0009147	pyrimidine nucleoside triphosphate metabolic process	14	3	0.81	0.043390
134	GO:0016202	regulation of striated muscle development	14	3	0.81	0.043390
135	GO:0030968	endoplasmic reticulum unfolded protein response	14	3	0.81	0.043390
136	GO:0034620	cellular response to unfolded protein	14	3	0.81	0.043390
137	GO:0048546	digestive tract morphogenesis	14	3	0.81	0.043390
138	GO:0048634	regulation of muscle development	14	3	0.81	0.043390
139	GO:0050920	regulation of chemotaxis	14	3	0.81	0.043390
140	GO:0006816	calcium ion transport	160	15	9.25	0.043830
141	GO:0032259	methylation	69	8	3.99	0.044710
142	GO:0010639	negative regulation of organelle organization and biogenesis	57	7	3.29	0.044940
143	GO:0016055	Wnt receptor signaling pathway	121	12	6.99	0.046920
144	GO:0043412	biopolymer modification	1539	104	88.94	0.047280
145	GO:0006875	cellular metal ion homeostasis	108	11	6.24	0.047370
146	GO:0032011	ARF protein signal transduction	46	6	2.66	0.047750
147	GO:0032012	regulation of ARF protein signal transduction	46	6	2.66	0.047750
148	GO:0050673	epithelial cell proliferation	46	6	2.66	0.047750
149	GO:0031323	regulation of cellular metabolic process	2739	177	158.29	0.047890
150	GO:0009890	negative regulation of biosynthetic process	363	29	20.98	0.048010
151	GO:0018958	phenol metabolic process	70	8	4.05	0.048040
152	GO:0007173	epidermal growth factor receptor signaling pathway	35	5	2.02	0.049050
153	GO:0010558	negative regulation of macromolecule biosynthetic process	349	28	20.17	0.049130

A.2 Gene Ontology Molecular Function

	GO.ID	Term	Annotated	Significant	Expected	P-value
1	GO:0019955	cytokine binding	110	15	6.27	0.001400
2	GO:0004939	beta-adrenergic receptor activity	5	3	0.28	0.001700
3	GO:0004086	carbamoyl-phosphate synthase activity	6	3	0.34	0.003200
4	GO:0030528	transcription regulator activity	1326	98	75.58	0.004100
5	GO:0008195	phosphatidate phosphatase activity	7	3	0.40	0.005400
6	GO:0019001	guanyl nucleotide binding	368	33	20.98	0.006700
7	GO:0032561	guanyl ribonucleotide binding	368	33	20.98	0.006700
8	GO:0005525	GTP binding	360	32	20.52	0.008500
9	GO:0016564	transcription repressor activity	216	21	12.31	0.011800
10	GO:0004522	pancreatic ribonuclease activity	10	3	0.57	0.016400
11	GO:0004550	nucleoside diphosphate kinase activity	10	3	0.57	0.016400
12	GO:0004957	prostaglandin E receptor activity	10	3	0.57	0.016400
13	GO:0030551	cyclic nucleotide binding	27	5	1.54	0.016800
14	GO:0004407	histone deacetylase activity	18	4	1.03	0.016900
15	GO:0033558	protein deacetylase activity	18	4	1.03	0.016900
16	GO:0015075	ion transmembrane transporter activity	848	63	48.33	0.017800
17	GO:0015291	secondary active transmembrane transporter activity	268	24	15.28	0.019000
18	GO:0043565	sequence-specific DNA binding	457	37	26.05	0.019800
19	GO:0015298	solute:cation antiporter activity	49	7	2.79	0.020200
20	GO:0051087	chaperone binding	19	4	1.08	0.020400
21	GO:0015294	solute:cation symporter activity	147	15	8.38	0.020500
22	GO:0019213	deacetylase activity	20	4	1.14	0.024400
23	GO:0030552	cAMP binding	20	4	1.14	0.024400
24	GO:0017048	Rho GTPase binding	30	5	1.71	0.025800
25	GO:0015116	sulfate transmembrane transporter activity	12	3	0.68	0.027600
26	GO:0032553	ribonucleotide binding	1802	121	102.71	0.028300
27	GO:0032555	purine ribonucleotide binding	1802	121	102.71	0.028300
28	GO:0015491	cation:cation antiporter activity	21	4	1.20	0.028900
29	GO:0022891	substrate-specific transmembrane transporter activity	918	66	52.32	0.029100
30	GO:0015300	solute:solute antiporter activity	53	7	3.02	0.029900
31	GO:0005351	sugar:hydrogen symporter activity	42	6	2.39	0.030600
32	GO:0005402	cation:sugar symporter activity	42	6	2.39	0.030600
33	GO:0017076	purine nucleotide binding	1893	126	107.90	0.032100
34	GO:0016493	C-C chemokine receptor activity	32	5	1.82	0.033300
35	GO:0019957	C-C chemokine binding	32	5	1.82	0.033300
36	GO:0015144	carbohydrate transmembrane transporter activity	43	6	2.45	0.033900
37	GO:0051119	sugar transmembrane transporter activity	43	6	2.45	0.033900
38	GO:0004953	icosanoid receptor activity	13	3	0.74	0.034400
39	GO:0004954	prostanoid receptor activity	13	3	0.74	0.034400
40	GO:0004955	prostaglandin receptor activity	13	3	0.74	0.034400
41	GO:0008093	cytoskeletal adaptor activity	13	3	0.74	0.034400

A.3 Gene Ontology Cellular Component

	GO.ID	Term	Annotated	Significant	Expected	P-value
1	GO:0019955	cytokine binding	110	15	6.27	0.001400
2	GO:0004939	beta-adrenergic receptor activity	5	3	0.28	0.001700
3	GO:0004086	carbamoyl-phosphate synthase activity	6	3	0.34	0.003200
4	GO:0030528	transcription regulator activity	1326	98	75.58	0.004100
5	GO:0008195	phosphatidate phosphatase activity	7	3	0.40	0.005400
6	GO:0019001	guanyl nucleotide binding	368	33	20.98	0.006700
7	GO:0032561	guanyl ribonucleotide binding	368	33	20.98	0.006700
8	GO:0005525	GTP binding	360	32	20.52	0.008500
9	GO:0016564	transcription repressor activity	216	21	12.31	0.011800
10	GO:0004522	pancreatic ribonuclease activity	10	3	0.57	0.016400
11	GO:0004550	nucleoside diphosphate kinase activity	10	3	0.57	0.016400
12	GO:0004957	prostaglandin E receptor activity	10	3	0.57	0.016400
13	GO:0030551	cyclic nucleotide binding	27	5	1.54	0.016800
14	GO:0004407	histone deacetylase activity	18	4	1.03	0.016900
15	GO:0033558	protein deacetylase activity	18	4	1.03	0.016900
16	GO:0015075	ion transmembrane transporter activity	848	63	48.33	0.017800
17	GO:0015291	secondary active transmembrane transporter activity	268	24	15.28	0.019000
18	GO:0043565	sequence-specific DNA binding	457	37	26.05	0.019800
19	GO:0015298	solute:cation antiporter activity	49	7	2.79	0.020200
20	GO:0051087	chaperone binding	19	4	1.08	0.020400
21	GO:0015294	solute:cation symporter activity	147	15	8.38	0.020500
22	GO:0019213	deacetylase activity	20	4	1.14	0.024400
23	GO:0030552	cAMP binding	20	4	1.14	0.024400
24	GO:0017048	Rho GTPase binding	30	5	1.71	0.025800
25	GO:0015116	sulfate transmembrane transporter activity	12	3	0.68	0.027600
26	GO:0032553	ribonucleotide binding	1802	121	102.71	0.028300
27	GO:0032555	purine ribonucleotide binding	1802	121	102.71	0.028300
28	GO:0015491	cation:cation antiporter activity	21	4	1.20	0.028900
29	GO:0022891	substrate-specific transmembrane transporter activity	918	66	52.32	0.029100
30	GO:0015300	solute:solute antiporter activity	53	7	3.02	0.029900
31	GO:0005351	sugar:hydrogen symporter activity	42	6	2.39	0.030600
32	GO:0005402	cation:sugar symporter activity	42	6	2.39	0.030600
33	GO:0017076	purine nucleotide binding	1893	126	107.90	0.032100
34	GO:0016493	C-C chemokine receptor activity	32	5	1.82	0.033300
35	GO:0019957	C-C chemokine binding	32	5	1.82	0.033300
36	GO:0015144	carbohydrate transmembrane transporter activity	43	6	2.45	0.033900
37	GO:0051119	sugar transmembrane transporter activity	43	6	2.45	0.033900
38	GO:0004953	icosanoid receptor activity	13	3	0.74	0.034400
39	GO:0004954	prostanoid receptor activity	13	3	0.74	0.034400
40	GO:0004955	prostaglandin receptor activity	13	3	0.74	0.034400
41	GO:0008093	cytoskeletal adaptor activity	13	3	0.74	0.034400

Appendix B

C2 Dataset Enrichment Analysis - Supplement

	C2 Term(Curated Gene Set)	Fraction(Significant)	Annotated	Significant	Expected	P.value(Hypergeometric)	Description
1	UVC_TTD_8HR_DN	0.15	149	23	8.69	0.00001647	Down-regulated at 8 hours following treatment of XPB/TTD fibroblasts with $3J/m^2$ UVC
2	UVC_XPCS_4HR_DN	0.13	211	28	12.31	0.00003746	Down-regulated at 4 hours following treatment of XPB/CS fibroblasts with $3J/m^2$ UVC
3	HOX_GENES	0.24	46	11	2.68	0.00005008	HOX genes related to hematopoiesis
4	UVC_TTD_ALL_DN	0.11	325	35	18.96	0.00032400	Down-regulated at any timepoint following treatment of XPB/TTD fibroblasts with $3J/m^2$ UVC
5	UVC_XPCS_ALL_DN	0.10	428	42	24.97	0.00062190	Down-regulated at any timepoint following treatment of XPB/CS fibroblasts with $3J/m^2$ UVC
6	WANG_HOXA9_VS_MEIS1_UP	0.27	22	6	1.28	0.00128600	Genomic signature of progenitors immortalized by Hoxa9 versus Hoxa9 plus Meis1 Increased expression in Hoxa9-immortalized progenitors
7	HEMATOP_STEM_ALL_UP	0.23	31	7	1.81	0.00171200	Up-regulated in populations of human hematopoietic stem cells (CD34+/CD38-/Lin-) from bone marrow, umbilical cord blood, and peripheral blood stem-progenitor cells, compared to the stem cell-depleted population (CD34+/[CD38/Lin++])
8	AGUIRRE_PANCREAS_CHR8	0.18	49	9	2.86	0.00186000	Genes on chromosome 8 with copy-number-driven expression in pancreatic adenocarcinoma.
9	UVC_TTD_4HR_DN	0.10	269	28	15.70	0.00207500	Down-regulated at 4 hours following treatment of XPB/TTD fibroblasts with $3J/m^2$ UVC
10	ET743PT650_COLONCA_DN	0.19	43	8	2.51	0.00302900	Downregulated by both Et-743 and Pt-650 in HCT116 cells (Fig. 6 A)
11	HSA04140_REGULATION_OF_AUTOPHAGY	0.24	21	5	1.23	0.00620000	Genes involved in regulation of autophagy
12	CMV_HCMV_TIMECOURSE_4HRS_DN	0.20	30	6	1.75	0.00687300	Down-regulated in fibroblasts following infection with human cytomegalovirus (at least 3-fold, with Affymetrix change call, in at least two consectutive timepoints), with maximum change at 4 hours
13	SIG_PIP3_SIGNALING_IN_B_LYMPHOCYTES	0.19	32	6	1.87	0.00950300	Genes related to PIP3 signaling in B lymphocytes

14	PENG_RAPAMYCIN_UP	0.11	133	15	7.76	0.01061000	Genes upregulated in response to rapamycin starvation
15	KIM_TH_CELLS_DN	0.25	16	4	0.93	0.01190000	Genes downreguated in human germinal center helper-T (Th) cells versus other CD4+ T-cell types such as naive T cells (from which the others originate), CXCR5+ CCR7+ central memory cells, and CCR7- effector memory cells.
16	HSC_HSC_FETAL	0.10	199	20	11.61	0.01227000	Up-regulated in mouse hematopoietic stem cells from fetal liver (HSC Shared + Fetal)
17	HSC_LTHSC_FETAL	0.10	226	22	13.19	0.01266000	Up-regulated in mouse long-term functional hematopoietic stem cells from fetal liver (LT-HSC Shared)
18	HSC_LTHSC_SHARED	0.10	226	22	13.19	0.01266000	Up-regulated in mouse long-term functional hematopoietic stem cells from both adult bone marrow and fetal liver (Cluster i, LT-HSC Shared)
19	TAKEDA_NUP8_HOXA9_16D_DN	0.10	174	18	10.15	0.01289000	Effect of NUP98-HOXA9 on gene transcription at 16 d after transduction Down
20	HSA01430_CELL_COMMUNICATION	0.12	113	13	6.59	0.01430000	Genes involved in cell communication
21	HSC_HSC_SHARED	0.10	189	19	11.03	0.01437000	Up-regulated in mouse hematopoietic stem cells from both adult bone marrow and fetal liver (Cluster ii, HSC Shared)
22	UVC_XPCS_8HR_DN	0.09	367	32	21.41	0.01475000	Down-regulated at 8 hours following treatment of XPB/CS fibroblasts with $3J/m^2$ UVC
23	CCR5PATHWAY	0.30	10	3	0.58	0.01743000	CCR5 is a G-protein coupled receptor expressed in macrophages that recognizes chemokine ligands and is targeted by the HIV envelope protein GP120.
24	TAKEDA_NUP8_HOXA9_8D_DN	0.10	167	17	9.74	0.01778000	Effect of NUP98-HOXA9 on gene transcription at 8 d after transduction Down
25	CELL_CYCLE_REGULATOR	0.22	18	4	1.05	0.01824000	Obsolete by GO - was not defined before being made obsolete
26	UVC_LOW_C2_DN	0.22	18	4	1.05	0.01824000	Down-regulated at 6-12 hours following treatment of WS1 human skin fibroblasts with UVC at a low dose 10 J/m^2 (cluster c2)
27	UVC_TTD-XPCS_COMMON_DN	0.11	131	14	7.64	0.02046000	Down-regulated at any timepoint following treatment of both XPB/CS and XPB/TTD fibroblasts with 3 J/m^2 UVC
28	CMV_HCMV_TIMECOURSE_16HRS_DN	0.21	19	4	1.11	0.02207000	Down-regulated in fibroblasts following infection with human cytomegalovirus (at least 3-fold, with Affymetrix change call, in at least two consectutive timepoints), with maximum change at 16 hours
29	HSA00534_HEPARAN_SULFATE_BIOSYNTHESIS	0.21	19	4	1.11	0.02207000	Genes involved in heparan sulfate biosynthesis
30	CMV_HCMV_TIMECOURSE_ALL_DN	0.09	340	29	19.84	0.02551000	Down-regulated in fibroblasts following infection with human cytomegalovirus (at least 3-fold, with Affymetrix change call, in at least two consectutive timepoints)
31	HESS_HOXAANMEIS1_DN	0.14	51	7	2.98	0.02761000	Genes downregulated in Hoxa9/Meis1 transduced cells vs control
32	HESS_HOXAANMEIS1_UP	0.14	51	7	2.98	0.02761000	Genes upregulated in Hoxa9/Meis1 transduced cells vs control

33	CALCIUM_REGULATION_IN_CARDIAC_CELLS	0.10	124	13	7.24	0.02865000	
34	DIAB_NEPH_DN	0.08	330	28	19.26	0.02952000	Downregulated in the glomeruli of cadaver kidneys from patients with diabetic nephropathy, compared to normal controls
35	UVC_LOW_ALL_DN	0.13	52	7	3.03	0.03036000	Down-regulated at any timepoint following treatment of WS1 human skin fibroblasts with UVC at a low dose (10 J/m^2) (clusters c1-c5)
36	ST_ADRENERGIC	0.16	31	5	1.81	0.03207000	Adrenergic receptors respond to epinephrine and norepinephrine signaling.
37	TAKEDA_NUP8_HOXA9_10D_UP	0.10	139	14	8.11	0.03211000	Effect of NUP98-HOXA9 on gene transcription at 10 d after transduction UP
38	CELL_GROWTH_AND_OR_MAINTENANCE	0.13	53	7	3.09	0.03329000	The processes pertinent to the integrated function of a cell.
39	ST_PHOSPHOINOSITIDE_3_KINASE_PATHWAY	0.16	32	5	1.87	0.03625000	The phosphoinositide-3 kinase pathway produces the lipid second messenger PIP3 and regulates cell growth, survival, and movement.
40	CMV_HCMV_TIMECOURSE_8HRS_DN	0.23	13	3	0.76	0.03646000	Down-regulated in fibroblasts following infection with human cytomegalovirus (at least 3-fold, with Affymetrix change call, in at least two consectutive timepoints), with maximum change at 8 hours
41	REOVIRUS_HEK293_UP	0.09	196	18	11.44	0.03759000	Up-regulated at any timepoint up to 24 hours following infection of HEK293 cells with reovirus strain T3Abney
42	TAKEDA_NUP8_HOXA9_10D_DN	0.10	116	12	6.77	0.03784000	Effect of NUP98-HOXA9 on gene transcription at 10 d after transduction Down
43	DIAB_NEPH_UP	0.13	55	7	3.21	0.03970000	Upregulated in the glomeruli of cadaver kidneys from patients with diabetic nephropathy, compared to normal controls
44	CMV_24HRS_DN	0.12	56	7	3.27	0.04318000	Downregulated at 24hrs following infection of primary human foreskin fibroblasts with CMV
45	GH_EXOGENOUS_MIDDLE_UP	0.11	93	10	5.43	0.04410000	Up-regulated at middle time points (6-8 hours) following treatment of mammary carcinoma cells (MCF-7) with exogenous human growth hormone
46	HSC_LTHSC_ADULT	0.08	299	25	17.45	0.04421000	Up-regulated in mouse long-term functional hematopoietic stem cells from adult bone marrow (LT-HSC Shared + Adult)
47	PARK_HSC_VS_MPP_UP	0.21	14	3	0.82	0.04445000	Genes differentially expressed in mouse cells with low rhodamine-123 staining, which implies status as self-renewing hematopoietic stem cells (HSCs).
48	ZHAN_MM_CD138_MS_VS_REST	0.15	34	5	1.98	0.04558000	50 top ranked SAM-defined over-expressed genes in each subgroup_MS
49	CARM_ERPATHWAY	0.17	24	4	1.40	0.04812000	Methyltransferase CARM1 methylates CBP and co-activates estrogen receptors via Grip1.
50	UV-4NQO_FIBRO_UP	0.17	24	4	1.40	0.04812000	Up-regulated at any timepoint by treatment of human fibroblasts with UV light or 4-NQO, but not by gamma radiation

Appendix C

Zusammenfassung

Vergleichende Genexpressionsanalysen zwischen Mensch und Schimpanse ermöglichen die Identifizierung von Kandidaten-Genen, die für die phänotypischen Unterschieden zwischen den beiden Arten verantwortlich sein können. Unterschiede in der Genexpression in frühen Stadien der Ontogenese spielen eine potentielle Schlüsselrolle bei der differentiellen Embryonalentwicklung der beiden Arten. Direkte Genexpressionsvergleiche in diesen Entwicklungsstadien sind allerdings in der Regel möglich, da embryonales Gewebe für solche Versuche weder vom Menschen noch vom Schimpansen zur Verfügung steht. In der vorliegenden Arbeit wird daher ein bioinformatischer Ansatz zur Identifizierung von Genen präsentiert, deren Expression sich in einer artspezifischen Weise verändert hat. Das Substitutionsmuster weist in transkribierten genomischen Regionen eine erhöhte Rate von $A \rightarrow G$ im Vergleich zu $T \rightarrow C$ Substitutionen auf, die auf den Effekt der transkriptions-gekoppelten Reparatur zurueckgeführt wird. Es wurden Gene im Genom von Mensch bzw. Schimpanse gesucht, deren Substitutionsmuster Anzeichen eines unterschiedlichen Ausmaßes an der transkription-gekoppelten Reparatur in den beiden Arten zeigen. Zunächst wurden spezifische Substitutionsmatrizen für 12,596 nichtüberlappende 125 Kb Alignmentfenster in der Fraktion des transkribierten Genoms für Mensch, Schimpansen und Rhesus geschätzt. Anschliessend wurde eine neue Teststatistik verwendet, mit der 717 transkribierte Genomregionen identifiziert wurden, bei denen sich die Substitutionsmatrizen von Mensch und Schimpanse signifikant unterscheiden. Die Substitutionsmatrizen unterscheiden sich hauptsächlich in ihrem relativen Ausmaß von $A \leftrightarrow G$ im Vergleich zu $T \leftrightarrow C$ Substitutionen. Genau ein solcher Unterschied ist zu erwarten, wenn die transkription-gekoppelte Reparatur im unterschiedlichem Maße auf die entsprechenden Gene der beiden Arten wirkt. Diese Beobachtung liefert erste

Hinweise darauf, dass diese Gene während der frühen Stadien der Entwicklung von Mensch und Schimpanse differentiell exprimiert werden. Eine nachfolgende Genontologie Anreicherungsanalyse zeigt daß die entsprechenden Gene hauptsächlich eine Rolle in embryonalen Entwicklungsprozessen wie z.B. anatomische Strukturentwicklung (z.B. Skelett, Rückenmark, Gehirn, Darm), Neurogenese, Signaltransduktion, Transkriptionsregulation, Translation und Replikation spielen.

Appendix D

Curriculum Vitae

Ricardo de Matos Simões

MFPL/CIBIV
Dr. Bohrgasse 9
1030 Vienna
Phone: +43 1 4277 24026
Fax: +43 1 4277 24098
Email: ricardo.de.matos.simoes@univie.ac.at
Homepage: http://www.cibiv.at/∼ricardo

Personal Details

Date of Birth:	25.05.1977
Birthplace:	Rheydt/Mönchengladbach, Germany
Nationality:	Portuguese

Academic Education

2010	Phd Thesis: "Species-specific Evolving Regions in the Human and Chimpanzee Genomes", Supervisor: Prof. Arndt von Haeseler, Dr. Ingo Ebersberger
2006-2010 (WS05/06-SS10)	Phd student (Bioinformatics), University of Vienna, Center for Integrative Bioinformatics Vienna (CIBIV), Max F. Perutz Laboratories (MFPL)
2005-2006 (SS05)	Research assistant, Heinrich-Heine-Universitaet Düsseldorf, Institut fuer Bioinformatik (Prof. Arndt von Haeseler), Sequence analysis of chloroplast DNA from non-photosynthetic *Monotropaceae* plant species, collaboration with Benjamin Killian, Dr. Jens Pahnke, Prof. Dr. William Martin
2005 (WS04/05)	Diploma Thesis "Identifizierung artspezifisch evolvierender Genomregionen im Menschen und Schimpansen", Institut fuer Bioinformatik, Heinrich-Heine-Universitaet Düsseldorf
1999-2005 (WS99-WS04/05)	Study of Biology (Diploma) at the Heinrich-Heine-Universitaet Düsseldorf

Teaching Experience

2010 (WS09/10)	R programming (15 hours), Veterinaermedizinische Universitaet Wien, parallel course to an introductory statistics course for biologist held by Dr. Mareike Fischer
2008 (SS08)	Perl programming lecture (8 hours),Veterinaermedizinische Universitaet Wien, introductory programming lecture with practical exercises
2008 (WS08/09)	Applications in Bioinformatics (8 hours), FH Campus Wien, 2 lectures about alignment methods for biological sequences, methods for phylogenetic analysis, including practical exercises in a unix environment
2007 (WS07/08)	R programming tutorial (8 hours), Veterinaermedizinische Universitaet Wien, lecture and practical exercises in R, parallel course to an introductory statistics course for biologist held by Dr. Steffen Klaere

2007 (WS07/08)	Applications in Bioinformatics (8 hours), FH Campus Wien, 2 lectures about alignment methods for biological sequences, methods for phylogenetic analysis, including practical exercises in unix

Other Employments/Teaching Assistant

2006-2010 (SS2006-SS2010)	EDV-course for molecular biologist, teaching assistant (5 days block course) University Vienna, (Dr. Martin Grabner)
2005 (SS05)	Maintainance of a publication database, Heinrich-Heine-Universitaet Düsseldorf, Institut fuer Informatik (Prof. Dr. Michael Leuschel)
2004 (WS04/05)	Created a custom cDNA clone annotation database, Heinrich-Heine-Universitaet Düsseldorf, BMFZ Biologisch-Medizinisches Forschungszentrum (Dr. Andreas Bayer, Dr. Karl Koehrer)
2004 (SS04)	Informatik II, Tutor for seminal lecture exercises, Heinrich-Heine-Universitaet Düsseldorf, Institut fuer Informatik (Prof. Dr. Martin Mauve)
2004 (SS04)	Bioinformatik II, Tutor for a practical perl programming course, Detecting CpG Islands using HMM (Hidden Markov Models) Heinrich-Heine-Universitaet Düsseldorf, Institut fuer Bioinformatik (Prof. Dr. Arndt von Haeseler, Dr. Ingo Ebersberger)
2004 (SS04)	Bioinformatik I, Teaching assistant for practical exercises, Introductory bioinformatics course about alignment and phylogenetic analysis, Heinrich-Heine-Universitaet Düsseldorf, Institut fuer Botanik III (Prof. Dr. William Martin)

Publications

in preparation (2010)	"Species-specific Evolving Regions in the Human and Chimpanzee Genomes", **de Matos Simoes R.**, von Haeseler A., Ebersberger I.
2010 (phd Thesis)	"Species-specific Evolving Regions in the Human and Chimpanzee Genomes", University of Vienna (2010)
2009 (Journal)	Cronin S.J., Nehme N.T., Limmer S., Liegeois S., Pospisilik J.A., Schramek D., Leibbrandt A., **de Matos Simoes R.**, Gruber S., Puc U., Ebersberger I., Zoranovic T., Neely G.G., von Haeseler A., Ferrandon D., Penninger J.M. **Genome-Wide RNAi Screen Identifies Genes Involved in Intestinal Pathogenic Bacterial Infection.** Science. 2009 Jun 11.
2009 (Abstract)	online poster abstract "Species-specific Evolving Regions in the Human and Chimpanzee Genomes", **de Matos Simoes R.**, von Haeseler A., Ebersberger I., http://www.bioinformatics.ic.ac.uk/masamb/posters.html, MASAMB April (2009)
2009 (Journal)	Catalanotti F., Reyes G., Jesenberger V., Galabova-Kovacs G., **de Matos Simoes R.**, Carugo O., Baccarini M. **A Mek1-Mek2 heterodimer determines the strength and duration of the Erk signal.** Nat. Struct. Mol. Biol. 2009 Mar;16(3):294-303. Epub 2009 Feb 15.
2005	Diploma Thesis, "Identifizierung artspezifisch evolvierender Genomregionen im Menschen und Schimpansen", Heinrich-Heine Universitaet Düsseldorf (2005)